Revealing MCL-1 Regulation of Mitochondrial Dynamics in Human Pluripotent Stem Cell-Derived Systems

By

Megan Loraine Rasmussen

Dissertation

Submitted to the Faculty of the

Graduate School of Vanderbilt University

in partial fulfillment of the requirements

for the degree of

DOCTOR OF PHILOSOPHY

in

Cell and Developmental Biology

February 28th, 2021

Nashville, Tennessee

Approved:

Vivian Gama, Ph.D.

Ian Macara, Ph.D.

Marija Zanic, Ph.D.

Edward Levine, Ph.D.

Ethan Lippmann, Ph.D.

Jeffrey Rathmell, Ph.D.

Dedication

I dedicate this thesis to my parents,

Christy & Justin Smith and Paul & Elizabeth Merolla,

whom without their love and encouragement

completion of this work would not have been possible,

who have been a constant source of

knowledge and support.

Acknowledgements

First and foremost, I would like to thank my mentor, Dr. Vivian Gama, for her unyielding support and guidance throughout my graduate career. Vivian is a caring, innovative, and passionate scientist, and I could not have asked for a better fit for my Ph.D. advisor. She has kept me focused on my goals, both professional and personal, throughout my time in her lab, but she also encouraged me to take scientific risks and explore exciting new opportunities. She has an incredible passion for mentorship and helped me to identify my own strengths and passions. I can only hope to be as good of a mentor one day as Vivian has been to me, and it has been a pleasure to witness her success as the lab has grown and transformed over the years. It is bittersweet to be leaving her lab as I move forward with my next career step, but she will always be a mentor to me, and I know that I can always come to her for advice. Without a doubt, an enormous part of my own success as a graduate student is due to her ability to motivate and inspire me to be the best scientist and person possible.

I would like to thank the current and past members of the Gama laboratory, who have truly made my time at Vanderbilt a wonderful experience. I am forever grateful to Natalya Ortolano for first introducing me to Vivian during her rotation in the lab. Joining a new lab together at the end of our first year did not come without its challenges, but having Natalya there every step of the way made it an enjoyable and rewarding experience. She is a truly unique and passionate person, and I will always remember our long hours of writing in coffee shops and our discussions on science and life. Alejandra Romero-Morales joined the lab a year later. She brought not only technical expertise and extensive knowledge in anatomy and

physiology but also a passion for leadership and mentorship. Her collaborative nature and determination are infectious. Two years later, Gabriella Robertson joined the lab. Gabriella is a one-of-a-kind scientist, who is extremely knowledgeable but also fearless in learning new techniques and exploring new areas of research in the lab. She is extremely kind and passionate about mentoring others, and even though we are years apart in our graduate journey, I still learn from her every day. I would also like to thank Piyush Joshi, who joined the lab during our 4th year. His determination and productivity were inspiring, and our collaboration on BAX and BAK allowed me to explore new imaging techniques in brain organoids. The newest member of the lab, Tierney Baum, has already contributed so much to the lab in the form of productivity, scientific discussion, and friendship. I wish our overlap would have been longer, but I am excited to see how her project develops in the future. In addition to the graduate students of the Gama lab, I would also like to thank our past and present lab managers and undergraduate students, without whom our laboratory would not run smoothly. I thank Kyungho Paul Park, who trained me when I first joined the lab in cell culture and general lab techniques. Thanks also to Anuj Rastogi, who later joined the lab and greatly improved the lab's organization, as well as performed many experiments that augmented several of our projects. Thank you to Caroline Bodnya, an extremely talented former undergraduate, who now manages the lab and provides extensive support for each of our projects. To the undergraduate students who I have had the pleasure of mentoring over the years, Leigh Anne Kline, Katherine Sborov, Stephen Russell, Christin Anthony, Linzheng Shi, and Stellan Riffle, I have become a better scientist and mentor because of each of you, and I wish you the best in your future endeavors. I am truly blessed to have known all these amazing colleagues for the last five and a half years.

My research has benefitted greatly from several collaborations at Vanderbilt. I would like to thank Dr. Kathryn Beckermann and Dr. Jeffrey Rathmell, who have provided continued guidance, expertise, and reagents for metabolic studies throughout my project. Thanks to Dr. Lili Wang from Dr. Björn Knollman's lab – her expertise in cardiomyocyte differentiation and function helped to improve our cardiomyocyte study. I would also like to thank Dr. Nilay Taneja and Abigail Neininger from Dr. Dylan Burnette's lab, with whom I had a long and rewarding collaboration on mitochondrial dynamics in cardiomyocytes. Our collaboration exposed me to several new concepts and imaging techniques and widened my research from various perspectives.

In addition to formal collaborations, I have been fortunate to receive mentorship and support from countless other colleagues in the Cell & Developmental Biology department (CDB) and beyond. My work would not be possible without the contributions from my thesis committee, Dr. Ian Macara, Dr. Marija Zanic, Dr. Edward Levine, Dr. Ethan Lippmann, and Dr. Jeffrey Rathmell, who encouraged me to think critically and suggested new directions for me to follow. I would also like to thank other faculty members, Dr. Dylan Burnette, Dr. Matt Tyska, Dr. Chris Wright, Dr. Kevin Ess, Dr. Kris Burkewitz, Dr. Bill Tansey, Dr. Jose Gomez, Dr. Aaron Bowman, Dr. Rebecca Ihrie, Dr. Jonathan Irish, and Dr. Mark Magnuson for their helpful discussions, generosity with reagents and equipment, and coordination of departmental seminars and courses. Thanks to the members of the Stem and Progenitor Cell Interest Group (SPRING) and the Program in Developmental Biology (PDB), with special thanks to Dr. Chris Wright for providing a rigorous yet supportive space to discuss my research. Dr. Wright's passion for graduate education and developmental biology will continue to inspire me as I continue my scientific career. I also want to thank the late Dr. Steve Hann, former Director of Graduate Studies (DGS), who

taught our first CDB course, guided us through our first years in the department, and threw great departmental retreats and Christmas parties. Many thanks also to Dr. Andrea Page-McCaw, who seamlessly took over the DGS position and has been a great advocate for CDB trainees. I would also like to thank my undergraduate mentor, Dr. Clark Coffman, for his continued mentorship and support even after leaving his lab at Iowa State, and for inspiring me to dream big.

My work would not have been possible without the support of the Vanderbilt core facilities. Thank you to Dr. Jenny Schafer, Dr. Bryan Millis, Kari Seedle, and Dr. Nick Mignemi from the Vanderbilt Cell Imaging Shared Resource (CISR) and the Nikon Center of Excellence (NCoE), who have provided the advanced microscopes and valuable training without which much of this research would not have been accomplished. Thanks also to Dr. Anthony Tharp, Josh Luffman, and Anuj Rastogi for their management of the CDB core facilities. I would like to thank Marc Wozniak, Susan Walker, Kristi Hargrove, Lorie Franklin, and all the CDB POD members for ensuring the department runs smoothly. I am deeply grateful for the financial support of the Interdepartmental Graduate Program (IGP), my mentor's financial support, and the American Heart Association for funding the last two years of my training. I also thank the Graduate School for supporting travel to meetings that have been essential to my scientific and career development.

This work would not have been possible without the incredible support of my family. To my mother, Christy Smith, I thank you for being my biggest advocate and best friend throughout graduate school, and for always providing advice and support when I needed it. To my father, Paul Merolla, I thank you for inspiring my love for nature and interest in how things work, for challenging me to think critically,

and for your continued support and encouragement as I move on to the next step in my career. To my step-parents, Justin Smith and Elizabeth Merolla, having you both as mentors has greatly enriched my perspectives on life, and I am extremely grateful to have you as family. To my sister and first best friend, Shelby Merolla, I am thankful for your constant friendship, humor, and support throughout my life – I am so proud of you. To my brother and sister, Cole and Hailee Smith, I am thankful for the love and laughter you bring to everything you do, and I can't wait to see what you both will accomplish as you grow up. To all my grandparents, extended family, and countless family friends, I thank you for being an incredible support system and always encouraging me to do my best in whatever I set my mind to. Graduate school is a long and challenging journey, and I am forever grateful for the many friendships that have supported me along the way. To all the members of the Gama lab, I am fortunate to call you not only colleagues, but my best friends, and I am thankful to you for providing endless laughs and support throughout my time here. I thank Ashley Ogle, who has been like a sister to me, for always being a shoulder to lean on, listening to my research, and adding invaluable experiences and light to my life. I will dearly miss living in the same city as this amazing friend. To all the incredible friends I have made, both new and old, thank you for making these years exceptionally enjoyable and memorable. Lastly, thanks to my two dogs, Ripley and Ronin, for always being the best listeners and study companions.

Finally, I would like to thank my amazing husband and partner in life, Riley Rasmussen. A constant source of love and encouragement, he has supported my aspirations and passion for science for the last decade from all over the world. He has been incredibly patient and understanding in times of uncertainty that can arise in graduate school. Seeing him progress in his own career during his enlistment in the Marine Corps as well as graduating with honors from Belmont University has been inspiring. Completing my Ph.D. has

certainly not been easy, but having Riley in my life through all the ups and downs has been a blessing, and he constantly motivates me to do my best. I am eager to start this new adventure together as we transition to new roles, and I can't wait to see what the next phases of our life will bring.

Table of Contents

List of Tables

List of Figures

Abbreviations

APAF-1: apoptotic protease activating factor 1

BAD: BCL-2-associated agonist of cell death

BAK1/BAK: BCL-2 antagonist killer 1

BAX: BCL-2 associated X

BCL-2: B cell chronic lymphocytic leukemia/lymphoma 2

BCL-w: BCL-2-like 2

BCL-xL: BCL-2-like 1

BFL-1/A1: BCL-2-related protein A1

BID: BCL-2 interacting domain death agonist

BIK: BCL-2 interacting killer

BIM: BCL-2 interacting mediator of cell death

BMF: BCL-2 modifying factor

BMP4: bone morphogenetic protein 4

BNIP3: BCL-2 and adenovirus E1B 19kDa-interacting protein 3

BOK: BCL-2 ovarian killer

CDK1: cyclin-dependent kinase 1

CHK-1: checkpoint kinase 1

CL: cardiolipin

DNA/RNA: deoxyribonucleic acid/ribonucleic acid

DRP-1: dynamin-related protein 1

EB: embryoid body

ERAD: endoplasmic reticulum-associated protein degradation pathway

ERK1/2: extracellular signal-regulated kinase 1/2

ERMES: endoplasmic reticulum-mitochondria encounter structure

ESCs/hESCs: embryonic stem cells/human embryonic stem cells

ETC: electron transport chain

FIS1: mitochondrial fission protein 1

GFP: green fluorescent protein

GTP/GTPase: guanosine triphosphate/hydrolase enzyme

HRK: Harakiri

ICM: inner cell mass

IMM: inner mitochondrial membrane

IMS: inner membrane space

iPSCs/hiPSCs: induced pluripotent stem cells/human induced pluripotent stem cells

hiPSC-CMs: human induced pluripotent stem cell-derived cardiomyocytes

JNK: c-Jun N-terminal kinase

KLF4: Kruppel-like factor 4

KO: knockout

MAPK: mitogen-activated protein kinase

MCL-1: myeloid cell leukemia 1

MEF: mouse embryonic fibroblast

MERC: mitochondria-ER contact

MFN1/2: mitofusin 1/2

MOMP: mitochondrial outer membrane permeabilization

mtDNA: mitochondrial DNA

NAD: nicotinamide adenine dinucluotide

NANOG: nanog homeobox

NIX: BNIP3-like (BNIP3L)

OCT4: octamer-binding transcription factor 4

OM/OMM: outer mitochondrial membrane

OPA1: optic atrophy 1

OXPHOS: oxidative phosphorylation

PA: phosphatidic acid

PC: phosphatidylcholine

PE: phosphatidylethanolamine

PI(4)P: phosphatidylinositol 4-phosphate

PINK1: PTEN-induced putative kinase

PMAIP1/NOXA: phorbol-12-myristate-13-acetate-induced protein 1

PSCs/hPSCs: pluripotent stem cells (iPSCs & ESCs)/human pluripotent stem

PUMA: P53-upregulated modulator of apoptosis

ROS: reactive oxygen species

SIM: structured illumination microscopy

SIRT2: sirtuin-2

SMAD: mothers against decapentaplegic

STED: stimulated emission depletion

STORM: stochastic optical reconstruction microscopy

SNP: single-nucleotide polymorphism

SOX2: sex-determining region Y-box 2

Chapter 1

INTRODUCTION

Adapted with permission from: Rasmussen, M.L., and Gama, V. (2020). Connecting life and death: The BCL-2 family coordinates mitochondrial network dynamics and stem cell fate. International Review of Cell and Molecular Biology. DOI: 10.1016/bs.ircmb.2019.12.005

Abstract

The B cell CLL/lymphoma-2 (BCL-2) family of proteins control the mitochondrial pathway of cell death, also known as intrinsic apoptosis. Direct binding between members of the BCL-2 family regulates mitochondrial outer membrane permeabilization (MOMP) after an apoptotic signal. The ability of the cell to sense stress and translate it into a death signal has been a major theme of research for nearly three decades (Kerr et al., 1972); however, other mechanisms by which the BCL-2 family coordinates cellular homeostasis beyond its role in initiating cell death are emerging. One developing area of research is understanding how the BCL-2 family of proteins regulate development using pluripotent stem cells as a model system. Understanding BCL-2 family-mediated regulation of mitochondrial homeostasis in cell death and beyond will uncover new facets of stem cell maintenance and differentiation potential.

Regulation of stem cell self-renewal and pluripotency by mitochondrial homeostasis

Stem cells can simulate the earliest stages of development, since they give rise to the three main tissue lineages (Thomson et al., 1998). This capacity to differentiate into ectoderm, mesoderm, and endoderm lineages, is known as pluripotency. Embryonic stem cells (ESCs) and induced pluripotent stem cells (iPSCs) are the two stem cell types that harbor this ability. Adult stem cells, also known as somatic stem cells, are multipotent and can replenish dying cells in case of tissue damage, and include hematopoietic stem cells, mesenchymal stem cells, and hair follicle stem cells (reviewed in (Goodell et al., 2015)). Stem cells also have the capacity of self-renewal, which is the process by which the stem cell pool is maintained indefinitely. These capabilities to regenerate and to give rise to the three germ layers have propelled an entire field of research dedicated to modeling embryonic development in culture by manipulating key signaling pathways and growth factors. The first human ESC (hESC) line was derived in 1998 from the inner cell mass (ICM) of the blastocyst (Evans and Kaufman, 1981; Martin, 1981; Thomson et al., 1998), while the discoveries of reverting both mouse and human somatic cells to iPSCs (known as reprogramming) were published in 2006 and 2007, respectively (Takahashi et al., 2007; Takahashi and Yamanaka, 2006). Reprogramming was achieved by inducing the expression of master pluripotency transcription factors such as OCT4 (Octomer-binding transcription factor 4), SOX2 (SRY (sex-determining region Y)-box 2), KLF4 (Kruppel-like factor 4) and *c*-MYC, collectively known as OSKM), but other methods of attaining iPSCs have been reported (reviewed in (Takahashi and Yamanaka, 2015). The ability of both ESCs and iPSCs to self-renew and differentiate has become an efficient tool to study basic processes of human development and various aspects of human diseases, such as diabetes, cardiomyopathy, and cancer (Assady et al., 2001; Hinson et al., 2015; Smith and Tabar, 2019). During

embryonic development, genomic instability is especially dangerous for the integrity of rapidly dividing stem cells. Thus, not surprisingly, stem cells are capable of executing intricate programs to quickly respond to apoptotic stress and prevent the propagation of deleterious mutations. Along with the primed cell death program, a growing number of studies on the BCL-2 family have shown changes in mitochondrial dynamics and metabolic function and regulation as stem cells differentiate and as somatic cells reprogram into iPSCs (Rinkenberger et al., 2000; Madden et al., 2011; Prigione et al., 2011; Dumitru and Gama et al., 2012; Gama and Deshmukh, 2012; Rasmussen et al., 2018). These topics will be covered in this chapter (Figure 1-1).

The molecular mechanisms controlling the unique signaling pathways underlying the ability of stem cells to self-renew and give rise to other cell types likely involve uncharacterized signaling mediated by intracellular metabolites, mitochondrial morphology changes, redox, and mitochondrial priming. In the following chapter, we will discuss the known fundamental mechanisms involved in these changes, centering on the BCL-2 family, as well as describe areas that are open to more detailed exploration. In addition, many aspects of mitochondrial biology are beginning to emerge as hallmarks of pluripotency and self-renewal (Wanet et al., 2015; Rastogi et al., 2019). The inherent sensitivity to apoptosis, dramatic changes in mitochondrial morphology and localization, and shifting metabolic program all accompany the reprogramming process and have been suggested to be required for pluripotency and differentiation. Furthermore, cellular events such as mitochondrial biogenesis, mitochondrial trafficking and motility, and mitochondrial DNA (mtDNA) transcription could also be important for reprogramming and generation

of specialized tissues. Thus, the unique properties of ESCs and iPSCs make them a valuable model system to illuminate the effects of these processes on self-renewal and differentiation.

The BCL-2 family of proteins in stem cell death

Intrinsic apoptosis

Caspase-dependent apoptosis occurs through both extrinsic and intrinsic pathways, which are mediated by external death ligands and mitochondrial-localized proteins, respectively (Elmore, 2007). The focus of this chapter will be on the intrinsic or mitochondrial pathway of apoptosis; the extrinsic apoptotic pathway is another form of regulated cell death that depends on detection and propagation of extracellular signals, which has been comprehensively reviewed here (Ashkenazi and Dixit, 1998; Mehlen and Bredesen, 2011; Galluzzi et al., 2018). The intrinsic pathway of apoptosis is crucial for embryonic development, tissue homeostasis, and in cellular response to irreversible perturbations. When the proteins that regulate apoptosis are mutated, cells can become cancerous and contribute to tumor formation. The BCL-2 family are the main regulatory proteins that control the intrinsic pathway of cell death (Figure 1-2). The direct binding interactions that occur between pro-apoptotic and anti-apoptotic family members govern their activities, ultimately resulting in MOMP after receiving a death signal (Oltval et al., 1993; Kale et al., 2018). Roughly 30 family members have been identified to belong to the BCL-2 family, which is made up of structurally similar globular proteins that are defined by multiple domains, known as BCL-2 homology (BH) domains (BH1, BH2, BH3, and BH4) (Tsujimoto et al., 1984; Kozopas et al., 1993; Chittenden et al., 1995; Adams and Cory, 1998; Chipuk et al., 2010). Family members with multiple BH

domains are either pro-apoptotic "effectors" (BCL-2 associated X (BAX), BCL-2 antagonist killer 1 (BAK1; known as BAK), BCL-2 ovarian killer (BOK)) or anti-apoptotic/pro-survival (BCL-2 apoptosis regulator (BCL-2), BCL-2-like 1 (known as BCL-xL), BCL-2-like 2 (BCL-w), Myeloid cell leukemia (MCL-1), and BCL-2-related protein A1 (BFL-1/A1)). Another group of family members have only one BH domain, known as the BH3-only proteins. The "activator" pro-apoptotic proteins (BCL-2 interacting mediator of cell death (BIM), BCL-2 interacting domain death agonist (BID), P53-upregulated modulator of apoptosis (PUMA)) and "sensitizer" pro-apoptotic proteins (phorbol-12-myristate-13-acetate-induced protein 1 (PMAIP1, best known as NOXA), BCL-2-associated agonist of cell death (BAD), BCL-2 interacting killer (BIK), BCL-2 modifying factor (BMF), and Harakiri (HRK)) work to either activate the effector proteins directly or sequester the anti-apoptotic family members from binding the effectors. After activation of BAK, BAX and/or BOK by the BH3-only proteins, they oligomerize to form pores in the outer mitochondrial membrane, initiating MOMP, reducing mitochondrial membrane potential and releasing cytochrome c from the inner membrane space (Kluck et al., 1997, 1999; Kuwana et al., 2002; Kalkavan and Green, 2018; Moldoveanu and Czabotar, 2019). Mechanistically, each of the effector proteins are regulated through slightly different means. While BAK is usually found anchored to the outer mitochondrial membrane, BAX resides in the cytosol in an inactive state and must undergo a conformational change to insert into the outer mitochondrial membrane through its C-terminal domain (Hsu and Youle, 1997; Wolter et al., 1997; Goping et al., 1998; Gavathiotis et al., 2008; Green and Chipuk, 2008; Todt et al., 2015). Less is known about BOK activity and regulation, but it is proposed to have the ability to initiate MOMP independent of BAK or BAX, and it is modulated by the endoplasmic-reticulum-associated protein degradation (ERAD) pathway (Llambi et al., 2016). Cytochrome c release

results in Apoptotic protease activating factor-1 (APAF-1)/Caspase-9 assembly, known as the apoptosome (Kim et al., 2005; Taylor et al., 2008; Inoue et al., 2009), which activates the caspase cascade, leading to the extensive cleavage and destruction of critical cellular components and proteins (Fuchs and Steller, 2011; Ramirez and Salvesen, 2018). Morphological changes occur, including cell constriction, organelle fragmentation, chromatin condensation, plasma membrane "blebbing" as the cortex ruptures, and finally the break-up of the cell into apoptotic bodies, which are the defining features of apoptosis (Kerr et al., 1972).

There are several proposed models of how the BCL-2 family execute cell death upstream of MOMP (reviewed in (Shamas-Din et al., 2013)): the direct activation model, the displacement model, the embedded together model, and the unified model (Letai et al., 2002; Chen et al., 2005; Leber et al., 2007; García-Sáez et al., 2009; Leber et al., 2010; Llambi et al., 2011). The latter two models highlight the complexity of the mitochondrial cell death pathway. The embedded together model proposes that the specific interactions of the BCL-2 family members are dependent on cellular equilibria, with binding events occurring based on concentration and binding affinities of each protein (Leber et al., 2007). These affinities are also dependent on proximity to the mitochondrial membrane as well as post-translational modifications. The unified model of apoptosis differs in that it proposes that the anti-apoptotic proteins have two "modes": one in binding and sequestering the activator BH3-only proteins, which can be overcome by the sensitizer BH3-only proteins, and the other binding and sequestering BAK/BAX, which results in a more robust inhibition of MOMP (Llambi et al., 2011; Kalkavan and Green, 2018). The

unified model also includes the effects that the BCL-2 family proteins have on mitochondrial dynamics, thus expanding on the embedded together model.

The BCL-2 family in stem cells

The intrinsic apoptosis has been shown to be uniquely regulated in stem cells (Madden et al., 2011; Dumitru and Gama et al., 2012; Gama and Deshmukh, 2012; Liu et al., 2013; Rasmussen et al., 2018). Human PSCs (hPSCs), which comprise both hESCs and hiPSCs, are extremely sensitive to DNA perturbations in a P53-dependent manner. P53 protein expression, however, was not significantly different between hPSCs and differentiated cells, pointing to another mode of action for this rapid apoptotic response. It was found that expression of the BCL-2 family in stem cells is shifted so that pro-apoptotic members are upregulated, while pro-survival members are downregulated, which serves to position them closer to the threshold of apoptosis, a property known as mitochondrial priming (Certo et al., 2006). We showed that BAX aided in this high mitochondrial priming state of hPSCs, since it was found in an activated state in homeostatic conditions but localized at the Golgi until an apoptosis-initiating event occurred (e.g. etoposide-mediated DNA damage), when it would translocate to the mitochondria (Dumitru and Gama et al., 2012). How BAX is maintained at the Golgi in an active state remains elusive, as up to this point active BAX, which is identified by its N-terminal domain (Upton et al., 2007), had only been known to localize at the mitochondrial outer membrane, and furthermore only in dying cells. When hPSCs were differentiated into stem cell aggregates known as embryoid bodies (EBs), BAX was no longer active during homeostasis and retained its mitochondrial localization during

apoptotic stress, indicating a stem cell-specific mechanism of BCL-2 family regulation (Dumitru and Gama et al., 2012). Maintenance of BAX in an active state likely allows for hPSCs and iPSCs to respond rapidly to cell death, thereby preventing potential mutations induced by DNA damage from persisting in the stem cell pool or in the differentiating cell lineage. Conversely, sustaining BAX in an active state would also pose significant risk for spontaneous apoptosis. Thus, isolating BAX at the Golgi could serve to safeguard hPSCs from unnecessary cell death while still allowing for its rapid induction if the cell is antagonized. At the organismal level, this sensitive response may stop the development of abnormal cells in the growing embryo. If constitutive BAX activation is also maintained by other highly proliferative cells in adult tissue, then perhaps it prevents aberrant growth of cancer cells and tumors. Dissection of the mechanisms underpinning BAX activation and localization, both at the Golgi and at the mitochondria, will be necessary to fully elucidate this apoptotic sensitivity as a defining component of PSC homeostasis. As PSCs begin differentiate, they quickly become resistant to DNA damage-mediated apoptosis; this was shown to be facilitated in part by a decrease in mitochondrial priming (Madden et al., 2011). Mitochondrial priming and apoptotic sensitivity have been exploited in recent years to identify dependencies of cancer cells on specific BCL-2 family proteins. This technique is known as BH3 profiling (Montero et al., 2015; Montero and Letai, 2016), and it is useful to measure the different binding affinities between the BCL-2 family members across cell types and patient-derived tumors.

The pro-apoptotic members of the BCL-2 family become activated through several upstream sensing mechanisms. As previously mentioned, PSCs are highly sensitive to DNA damage, which in turn initiates the transcription factor P53 and triggers a repair response and cell cycle arrest (Kruse and Gu, 2009). If

the cell cannot resolve the damage, the BCL-2 family facilitates MOMP and the cell undergoes apoptosis through caspase-mediated degradation. Fluctuations in P53 activation have been shown to determine cell fate (Purvis et al., 2012). During reprogramming of somatic cells back to a pluripotent state, inhibition of P53 greatly improves cell survival due to the bypass of BCL-2 family-mediated cell death (Kawamura et al., 2009; Li et al., 2013). Excellent reviews covering the details of P53 function in stem cells can be found here (Bonizzi et al., 2012; Jain and Barton, 2018). Downstream of BCL-2 family facilitation of MOMP, activity of caspases has been shown to play dual roles in both promoting differentiation and maintaining proper distribution of differentiated cell types, as well as driving reprogramming of somatic cells (Fujita et al., 2008; Li et al., 2010; Fu et al., 2019).

The BCL-2 family in mitochondrial dynamics

The main players of intrinsic apoptosis, the BCL-2 family of proteins, execute their functions at the mitochondria. Beyond being the energy-producing powerhouses of the cell, mitochondria serve as major signaling organelles and constantly fuse and divide in a process known as mitochondrial dynamics (Chan, 2007; Berman et al., 2008; Friedman and Nunnari, 2014). These continuous, energy-consuming events are proposed to occur both in response to various stimuli and to relay signals throughout the cell to other organelles. Emerging studies have also highlighted new links between mitochondrial dynamics machinery, apoptosis and mitochondrial autophagy (mitophagy) (Kageyama et al., 2014; Morciano et al., 2016b; Rasmussen et al., 2018; Fu et al., 2019). Proper equilibrium of mitochondrial dynamics is essential for

cellular and organismal homeostasis, and diseases often manifest when the proteins that regulate fission and fusion are mutated (Chan, 2007; Westermann, 2010; Dorn, 2013; Chan, 2020).

Dynamic movement and fragmentation of the mitochondrial network was first documented in 1915, with various morphological changes described in detailed, hand-drawn illustrations (Lewis and Lewis, 1914). Yet, the notion that mitochondria are static, bean-like organelles has persevered over the decades. The development of more advanced imaging technologies, such as super-resolution microscopy, has allowed for improved observation and tracking of mitochondrial dynamics and motility, which has propelled the field and revealed the remarkable changes that mitochondria initiate (Johnson et al., 1981; Bereiter-Hahn and Vöth, 1994; Rizzuto et al., 1996). Super-resolution microscopy enables the resolution of objects well below the diffraction limit, first described by Ernst Abbe as the minimum distance between two points that can still be distinguished (roughly 200 nm) (1873). Imaging modalities such as stochastic optical reconstruction microscopy (STORM), stimulated emission depletion (STED), and structured illumination microscopy (SIM) have revolutionized the field of cell and organelle biology by allowing researchers to attain imaging resolution of about 10 nm (Figure 1-3) (Wegel et al., 2016; Dlasková et al., 2018). While conventional microscopy techniques are immensely useful for observing large-scale changes in overall mitochondrial network morphology, super-resolution is necessary to resolve distinct mitochondrial compartments, such as the outer and inner mitochondrial membranes, the matrix, cristae folds, and nucleoids that house mitochondrial DNA (mtDNA). Challenges arise when imaging the mitochondria, however, as they are sensitive to cellular conditions and are the center of reactive oxygen species (ROS) generation and apoptotic signaling pathways. Light toxicity is known to cause a rapid increase in mitochondrial fragmentation, making studies in mitochondrial dynamics using live cells

difficult, with PSCs being an even more challenging cell type due to their inherent sensitivity to apoptotic stimuli. Fortunately, this can be overcome by careful optimization of imaging conditions and fluorescent probes. Additionally, new technologies such as light sheet microscopy allow for rapid imaging with greatly reduced levels of photobleaching and toxicity to the sample, improving our ability to capture mitochondrial dynamics with high spatiotemporal resolution in live cells (Chen et al., 2014; Legant et al., 2016). The majority of the imaging data presented in this dissertation was acquired using SIM, but we are currently optimizing our PSC imaging protocols to be used with newly engineered lattice light sheet instruments. Recently described STED nanoscopy modalities will also permit the visualization of individual cristae in live cells (Stephan et al., 2019). These improvements in imaging modalities will allow us to better understand mitochondrial behavior in live PSCs and how perturbations to the BCL-2 family and other mitochondrial proteins affect mitochondrial network morphology, dynamics, motility and behavior.

Mitochondrial fission and fusion

Mitochondrial shape changes drastically depending on the cell type, cell cycle stage, and metabolic state (Chen and Chan, 2017) (Figure 1-4). Differentiated cell types, such as fibroblasts, myocytes, and endothelial cells, generally have elongated, cristae-rich mitochondria that make up complex networks, which promote mtDNA homogenization and energy generation (Kuznetsov et al., 2009). Mitochondrial fission is necessary for distribution of mitochondria to daughter cells during cell division, mitochondrial transport within cells, and isolation of damaged mitochondria for degradation by mitophagy (Nunnari et al., 1997; Pon, 2013; Ganesan et al., 2019). As differentiated cells reprogram and transition into a stem-

like state, mitochondria undergo higher levels of fission and arrange to be more perinuclear (Prieto et al., 2016; Chen and Chan, 2017). The mitochondria of iPSCs are considered more functionally immature, with globular shapes and fewer cristae, contributing to a metabolic profile that is traditionally thought to be more dependent on glycolysis for energy requirements (Facucho-Oliveira and St. John, 2009; Chung et al., 2010). Constitutive activation of the dynamin-related guanosine triphosphates (GTPases) that control fission is likely a major participating factor in maintaining high levels of fragmentation in stem cells (Chung et al., 2010; Prieto et al., 2016).

The large dynamin-related GTPases (DRPs) regulate mitochondrial dynamics by inducing mitochondrial fission (division) and fusion in a highly conserved manner (Praefcke and McMahon, 2004; Hoppins et al., 2007; Chan, 2012). The most well-documented fission-inducing DRP in mammalian cells, Dynamin-related protein 1 (DRP-1) executes its function upon activation by several post-translational modifications, including phosphorylation, ubiquitination, sumoylation, and O-GlcNAcylation (Westermann, 2010). The enzymes that perform this activation of Dynamin-related proteins have not been completely identified, but ERK1/2 and CDK1 have been shown phosphorylate DRP-1 at Serine 616, providing insight into specific pathways that promote increased mitochondrial fragmentation (Taguchi et al., 2007; Prieto et al., 2016). Once DRP-1 is activated, it is translocated from the cytosol to the outer mitochondrial membrane, where it hydrolyzes GTP and self-assembles around the mitochondria, constricting both membranes until the organelle is divided in two (Hoppins et al., 2007; Pon, 2013; Antonny et al., 2016; Francy et al., 2017). The structural domains and mechanistic details of action for DRP-1 have been described in several studies and reviews (Hoppins et al., 2007; Meglei and

McQuibban, 2009; Chappie et al., 2010; Gao et al., 2010; van der Bliek and Payne, 2010; Mears et al., 2011; Francy et al., 2017); however, whether or not DRP-1 activation is differentially regulated in pluripotent stem cells, which have a more fragmented mitochondrial network, has not been elucidated. It has been shown that DRP-1 function in mitochondrial fission is required for proper achievement of pluripotency early on in the reprogramming process (Prieto et al., 2016). As DRP-1 is also involved in the mitochondrial fragmentation observed during apoptosis (Frank et al., 2001), and iPSCs are highly sensitive to apoptotic stimuli, these cells are likely highly dependent on DRP-1 beyond its role in homeostatic conditions.

As stem cells differentiate and become more mature, the mitochondrial network transforms to support the changing needs of the differentiating cell. Mitochondrial fusion is required for the proper maturation of several tissue types, and it is necessary for mtDNA homogenization and assembly of the electron transport chain (ETC) (Chan, 2012).The specific activity of DRP family members that control mitochondrial fusion is not well understood, but *in vitro* studies have shown that inner and outer mitochondrial fusion are mechanistically distinct processes (Legros et al., 2002; Meeusen et al., 2004).The large GTPases that govern the process of mitochondrial fusion are Mitofusin 1 (MFN1), Mitofusin 2 (MFN2), and Optic Atrophy 1 (OPA1) (Alexander et al., 2000; Delettre et al., 2000; Chen et al., 2003). MFN1 and MFN2 are localized to the outer mitochondrial membrane, where they facilitate outer membrane fusion by homo- or hetero-dimerizing with MFNs on adjacent mitochondria and actively fusing the outer membranes. While the MFN paralogs are highly similar, they are not completely redundant and are both required for mitochondrial fusion (Escobar-Henriques and Joaquim, 2019).

Depletion of MFN1 in mouse embryonic fibroblasts (MEFs) leads to increased fragmentation of individual mitochondria, resulting in small fragments, while MFN2 depletion results in larger fragments of aggregated mitochondria (Chen et al., 2003). Interestingly, MFN2 depletion also results in placental defects in mice that were not observed in MFN1 mutants.

Once outer membrane fusion occurs, the inner membrane is fused through the activity of OPA1. OPA1 regulation is complicated, as it has eight different splice isoforms that lead to the formation of two proteolytically cleaved proteins, designated as long OPA1 (OPA1-L) and short OPA1 (OPA1-S), which serve several distinct and overlapping purposes (Mishra et al., 2014; Del Dotto et al., 2017). OPA1-L is anchored in the inner membrane with its GTPase domain exposed to the inner membrane space. It coordinates the active process of inner membrane fusion by forming dimers with OPA1-L proteins on the opposite target membrane. OPA-1S is proposed to provide a more passive, structural role at the mitochondrial matrix in cristae formation and maintenance, while combinations of both long and short forms work together to fine-tune mitochondrial morphology and function (Del Dotto et al., 2018). The OPA1-S form has also been implicated in fission of the inner membrane (Anand et al., 2014). These studies were performed in MEFs, but it would be interesting to probe if the homeostatic balance of OPA1 isoforms is differentially regulated in stem cells and over the course of differentiation. Disproportionate levels of either mitochondrial fusion or fission results in profound pathological abnormalities. These include embryonic lethality at mid-gestation in mice deficient in any of the DRPs (i.e. MFN1, MFN2, OPA1, and DRP1) (Chen et al., 2003; Davies et al., 2007; Alavi et al., 2007; Ishihara et al., 2009; MacVicar and Langer, 2016), as well as neurodegenerative diseases such as Charcot-Marie-Tooth

syndrome and dominant optic atrophy (Züchner et al., 2004; Alavi et al., 2007; Davies et al., 2007; Waterham et al., 2007) caused by mutations in MFN2 and OPA1, respectively.

Mitochondrial dynamics also change during apoptosis; mitochondrial fusion is thought to protect against mitochondrial pore formation (Estaquier and Arnoult, 2007; Jahani-Asl et al., 2010), while mitochondrial fission has been shown occur concurrently with BAK/BAX-mediated cell death (Frank et al., 2001a; Youle and Bliek, 2012). Parallel to this, studies have shown that pro-apoptotic BAK and BAX must be inactivated for mitochondrial fusion to occur, and BAX has been shown to modulate fusion through interactions with the Mitofusins (Karbowski et al., 2006; Brooks et al., 2007; Hoppins et al., 2007, 2011). Additionally, other BCL-2 family members have recently been associated with the maintenance of mitochondrial dynamics in various cell types (Chen et al., 2011; Hardwick and Soane, 2013). In adult neurons, the anti-apoptotic protein BCL-xL is enriched in the mitochondria, where it promotes proper mitochondrial length and size, as well as localization of the mitochondria to the highly energetic synapses (Berman et al., 2008; Li et al., 2008). BCL-xL is required for normal brain development (Chen et al., 2011), and it is likely that its function in neuronal connectivity and communication is partially responsible. Another anti-apoptotic family member, MCL-1, has been shown to also function in the regulation of mitochondrial dynamics in hPSCs. MCL-1 is expressed at high levels in hPSCs, and its depletion causes mitochondrial elongation in stem cells that coincides with the loss of expression of pluripotency markers OCT4 and NANOG (Rasmussen et al., 2018). The changes in mitochondrial morphology are likely due to MCL-1's interaction with DRP-1, but the details of the state of DRP-1 activation are still unknown. Interestingly, MCL-1 was also shown to interact with OPA1, an association that likely occurs through

MCL-1's matrix-localized form (Rasmussen et al., 2018). These non-apoptotic interactions further implicate MCL-1, and perhaps other BH domain proteins, in the modulation of mitochondrial dynamics and homeostasis beyond their roles in cell death. Another study showed that BID, a pro-apoptotic BH3-only protein, also imports into the mitochondrial matrix where it regulates cristae morphology and organization (Salisbury-Ruf et al., 2018). As BID is a known binding protein of MCL-1, it would be interesting to test if these two family members work in concert at the matrix to maintain mitochondrial dynamics as well as pluripotent/self-renewal capacities in stem cells. Understanding the regulation of cell fate from the perspective of mitochondrial dynamics and the BCL-2 family of proteins could shed light on the intricacies of cell signaling and organelle biology.

As previously mentioned, extensive remodeling of the mitochondrial network occurs during apoptosis. These changes result in the release of cytochrome c and other caspase-inducing proteins from the inner membrane space (Goldstein et al., 2000; Garrido et al., 2006; Galluzzi et al., 2018). Mitochondrial fragmentation during apoptosis takes place through two synchronized, but independent, events: dissociation of cristae junctions, where pools of cytochrome c are housed, and BAK/BAX oligomerization and pore formation at the outer membrane (Gao et al., 2001; Lee et al., 2004; Ow et al., 2008; Sheridan et al., 2008; Montessuit et al., 2010; Sinibaldi et al., 2013). A growing number of studies show that DRP-1 acts in response to apoptotic signals, consistent with the idea that mitochondrial fission occurs along with MOMP. DRP-1 has been shown promote BAX translocation to the mitochondria (Wang et al., 2015), and it also localizes to BAX/BAK pores (Frank et al., 2001a; Tanaka and Youle, 2008) where it promotes extensive mitochondrial network fission. DRP-1 depletion prevents mitochondrial fission

during apoptosis, and overexpression of the DRP-1 mutant K38A, which inhibits GTP binding by DRP-1, prevents apoptosis-induced mitochondrial fission (Smirnova et al., 2001; Sugioka et al., 2004; Estaquier and Arnoult, 2007). BAK and BAX have also been reported to localize at fission sites along with DRP-1 and MFN2, providing further evidence that MOMP is associated with the fission regulators (Karbowski et al., 2002; Hoppins et al., 2011).

Summary

As discussed throughout this chapter, the BCL-2 family of proteins regulate the mitochondrial pathway of apoptosis and are thereby seated at the center of several essential signaling pathways. The mitochondrial network is responsible for the regulation of apoptosis, oxidative phosphorylation, coordination of neighboring organelles, and they provide the machinery needed to generate key metabolites that serve the bioenergetic and biosynthetic needs of the cell (Fu et al., 2019). The crosstalk between the pathways of BCL-2 family-mediated cell death, mitochondrial dynamics, and mitophagy must be explored further in PSCs, as it will likely provide important details into how cells navigate the differentiation and reprogramming processes. The role of reactive oxygen species on stem cell maintenance is also an intriguing area of study, since multiple redox-sensitive pathways also control apoptosis and mitochondrial dynamics (e.g. MAPK, ERK1/2, JNK) (Bigarella et al., 2014).

Many questions remain; for example: 1) How do the signaling pathways that converge at the mitochondria intersect to regulate cell fate? 2) How are the changes in mitochondrial network, mitochondrial turnover, and mitochondrial connectivity to other organelles regulated as cells undergo differentiation and

reprogramming? 3) How do changes in mitochondrial morphology contribute to adaptations in metabolic state? 4) How do metabolite levels modulate the activity of epigenetic enzymes ultimately affecting gene expression? Answering these questions would open the opportunity to advance the fields of stem cell biology and apoptosis as well as to rationalize new therapies, as shown by the emergence of pharmacological inhibitors of the BCL-2 family.

Limitations

Up until the last decade or so, ESCs were the only well-studied source of pluripotent stem cells, and they still represent the "gold standard" for stem cell research. The advent of iPSCs from both mouse and human sources has revolutionized the field and allowed for exciting new research programs to arise. However, reprogramming efficiency of somatic cells is still relatively low, and the use of iPSCs in human cell therapy remains challenging due to the ectopic expression of stem cell factors OCT4, SOX2, KLF4, and c-MYC, since these factors are also associated with tumor development. Another issue that must be addressed with *in vitro* PSC research is the proper recapitulation of differentiated adult cell types and disease phenotypes. Despite these limitations, promising clinical studies are still underway for the use of iPSC and ESC derivatives in treatment of several diseases and injuries, including macular degeneration, spinal cord injury, type I diabetes, myocardial infarction, and Parkinson's disease (Trounson and DeWitt, 2016; Mandai et al., 2017; Doi et al., 2020).

Figures and Legends

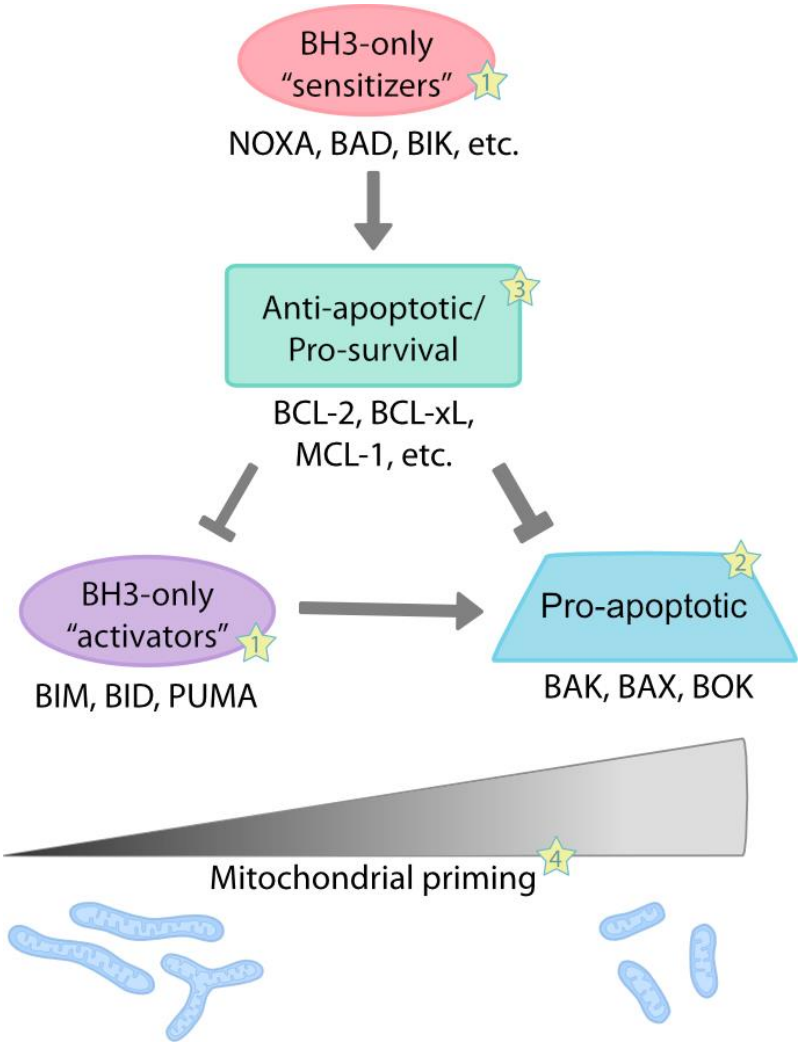

Figure 1-1: The BCL-2 family regulates mitochondrial cell death and homeostasis in stem cells. This schematic depicts the canonical pathways of mitochondrial apoptosis and priming. Highlighted are the reported changes in PSC regulation of these pathways: 1) High levels of pro-apoptotic proteins. 2) BAX is maintained in an active state at the Golgi. 3) High levels of MCL-1, which is important for pluripotent maintenance and mitochondrial fission. 4) Increased fragmentation of the mitochondrial network and higher dependence on glycolytic metabolism.

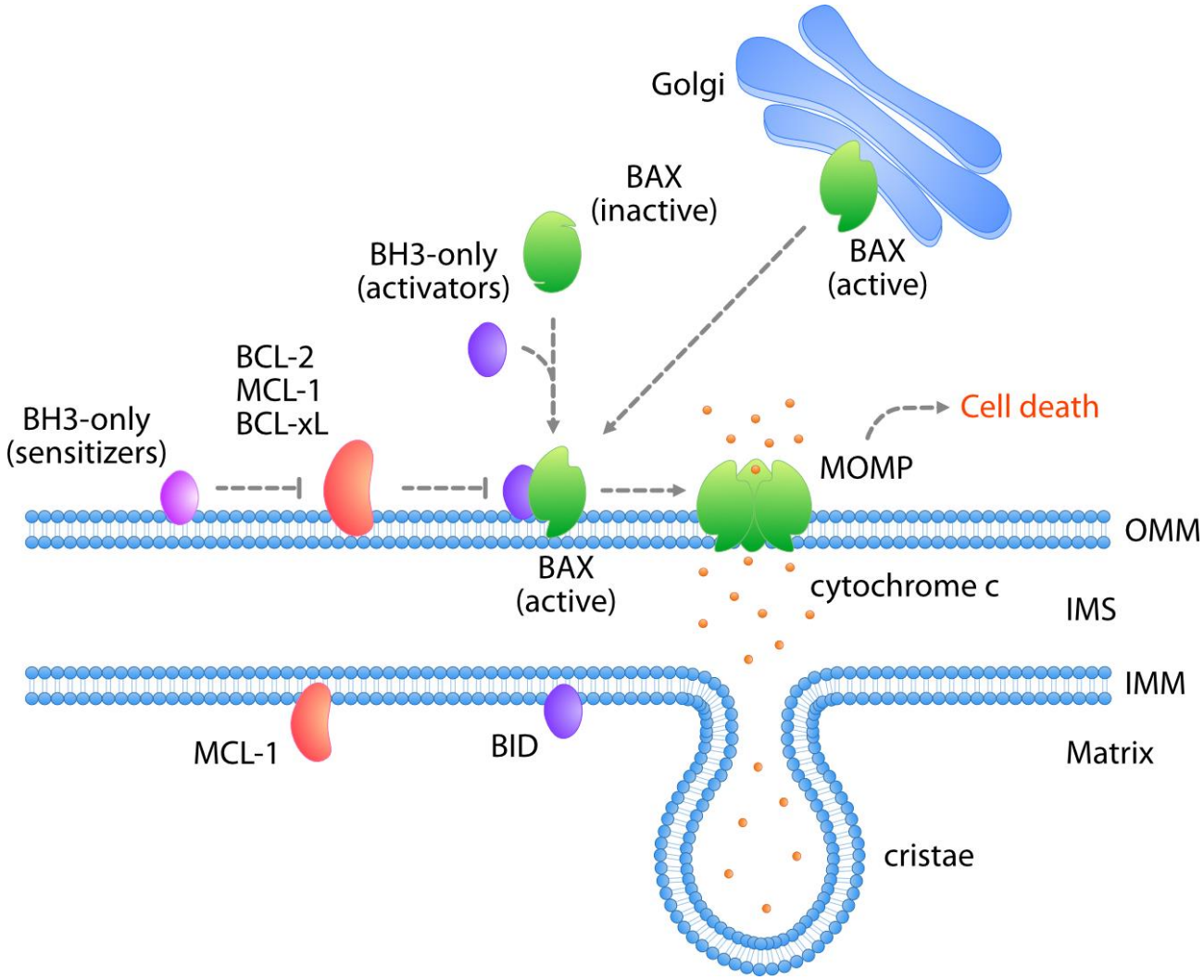

Figure 1-2: The BCL-2 family regulates the mitochondrial pathway of apoptosis. When cells receive an intrinsic death signal, BAX becomes activated by the BH3-only activators, undergoes a conformational change, and translocates to the outer mitochondrial membrane (OMM). BAX (in addition to BAK and BOK) then oligomerize and form pores in the OMM, causing MOMP and the release of cytochrome c into the cytosol. BAX activation can be prevented by sequestration of the activator BH3-only proteins through the pro-survival proteins BCL-2, MCL-1, BCL-xL, etc, which are inhibited by the sensitizer BH3-only family members. In human embryonic stem cells, BAX can be maintained in an active state at the Golgi, which confers quick translocation to the OMM in case of a death signal. Additionally, MCL-1 has been found to reside at the matrix in stem cells, where it is proposed to interact with OPA1.

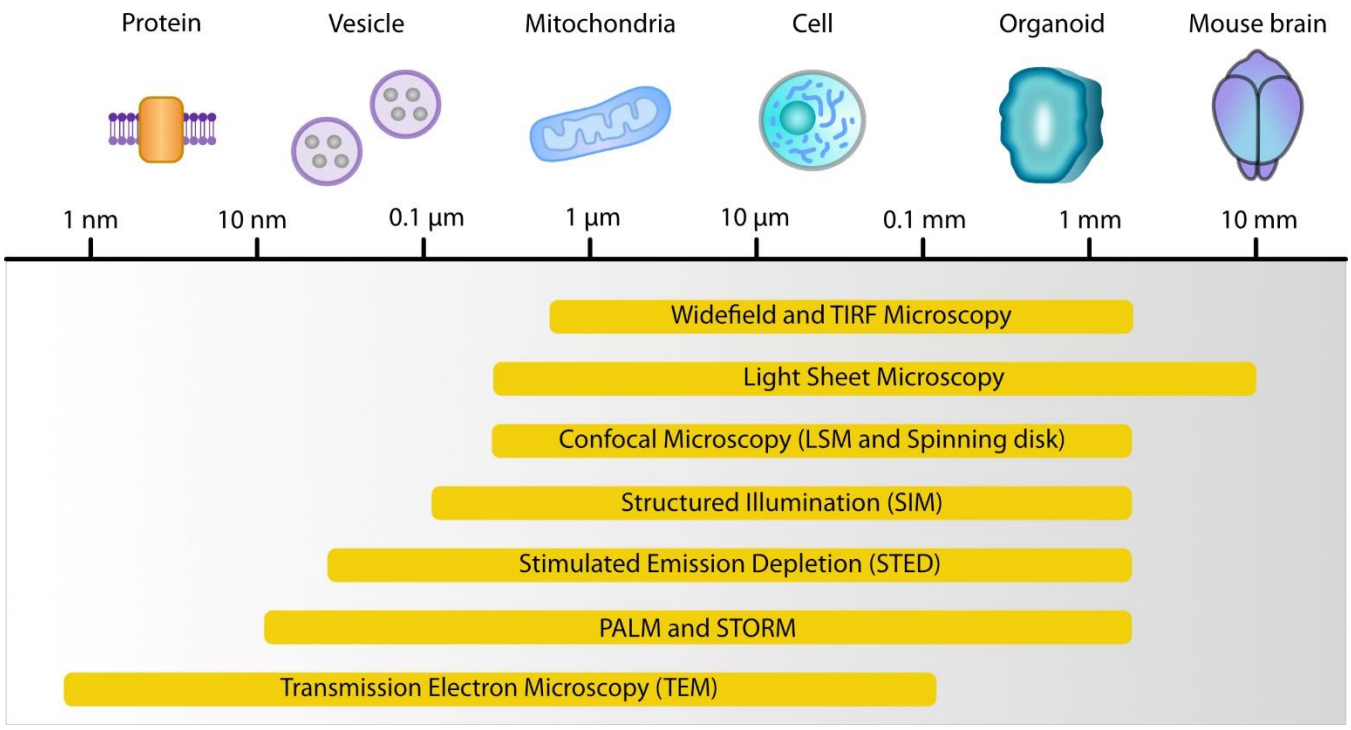

	TEM	PALM and STORM	STED	SIM	Confocal	Light Sheet	Widefield and TIRF
Concept	Transmission electron microscopy (negative staining)	Localization with photoswitching	Stimulated emission depletion	Structured illumination – sinusoidal patterned illumination	Laser scanning or spinning disk; May include modified detectors (e.g. Airyscan)	Planar light sheet illumination (most often in an orthogonal direction); various modalities	Widefield illumination; TIRF: Total internal reflection fluorescence
Speed	Very low	Low (s – min)	High (ms – s)	Medium (ms – s) Sequential multi-frame	High (ms – s) esp. Spinning disk	Very high (ms)	High (ms – s)
Advantages	Good SNR; Relatively simple sample preparation	Excellent lateral and axial resolution	Excellent lateral resolution; Purely physical 2D/3D images	Conventional probes and dyes; Resolution beyond diffraction limit	Conventional probes and dyes; Low phototoxicity	Low phototoxicity; Large samples	Conventional probes and dyes
Disadvantages	Structural artifacts due to staining and dehydration; No live cells	Data processing; Specialized fluorophores; Over/underlabelling artifacts	Photobleaching; STED-capable probes	Photobleaching; Sample thickness; Image reconstruction artifacts	Resolution is diffraction-limited	Data processing; Sample preparation (optical clearing)	Low lateral and axial resolution; Phototoxicity; TIRF: Imaging close to coverslip only
Application	Mitochondrial membrane and cristae topology	Individual protein localization at mitochondrial membranes	Visualization and quantification of individual mitochondrial compartments	Mitochondrial morphology; improved resolution allows for quantification of individual mitochondria	General morphology in thin/thick samples; Spinning disk: mito dynamics in live cells	Lattice light sheet: mito dynamics in live cells; SOPI: whole mount organoids	General morphology in thin samples

Figure 1-3: Microscopy tools for the study of mitochondrial dynamics, morphology, and motility. Many different imaging modalities may be used for the study of mitochondrial processes within cells and tissues. Highlighted here are conventional widefield and confocal techniques, as well as super-resolution and electron microscopy approaches.

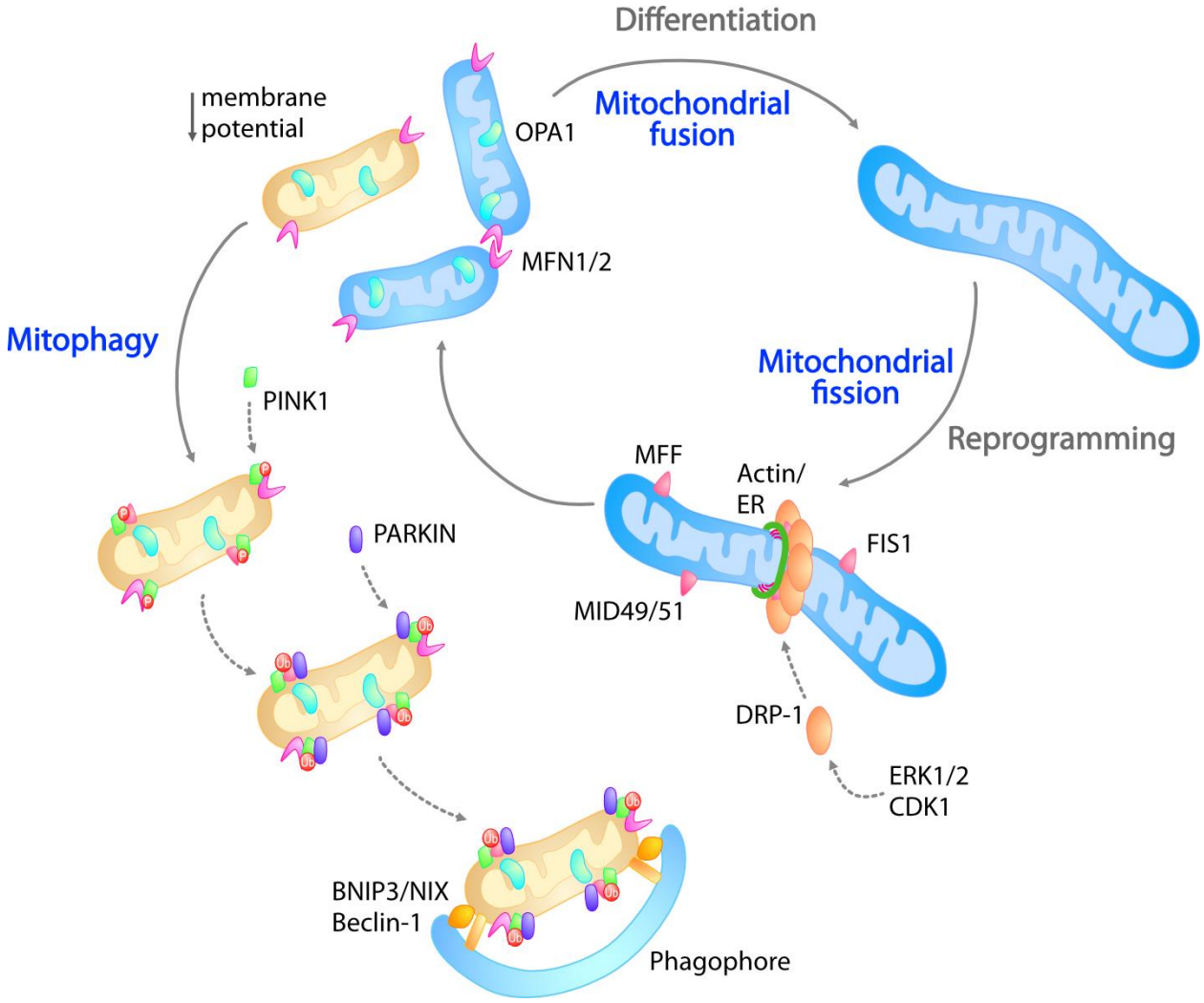

Figure 1-4: The dynamic cycle of mitochondrial morphology and quality control. In homeostasis, differentiation, reprogramming, and during stress, the mitochondrial network undergoes rounds of fusion and fission. During fission, DRP-1 is activated and recruited to pre-constricted regions of mitochondria (facilitated by actin and ER tubules) by its receptors (MFF, MID49/51, FIS1). Mitochondrial fusion is achieved by the activity of MFNs, which dimerize with MFNs on adjacent mitochondria to fuse the OMM. This is followed by OPA1-mediated fusion of the inner mitochondria membrane (IMM). If mitochondria are damaged (i.e. low membrane potential), PINK1 is stabilized at the mitochondria and phosphorylates proteins on the OMM. This phosphorylation triggers Parkin-mediated ubiquitination of OMM proteins, causing recruitment of various adapter proteins and receptors associated with the phagophore. The damaged mitochondrion is then engulfed by the mature mitophagophore, which fuses with the lysosome for degradation.

Chapter 2

MCL-1 PROMOTES PLURIPOTENCY AND MODULATES MITOCHONDRIAL DYNAMICS IN HUMAN PLURIPOTENT STEM CELLS

Adapted with permission from: Rasmussen, M.L., Kline L.A., Park, K.P., Ortolano, N.A., Romero-Morales, A.I., Anthony, C.A., Beckermann, K.E., Gama, V. (2018) A non-apoptotic function of MCL-1 in promoting stem cell pluripotency and modulating mitochondrial dynamics in stem cells. Stem Cell Reports. DOI: 10.1016/j.stemcr.2018.01.005

Abstract

Human pluripotent stem cells (hPSCs) maintain a highly fragmented mitochondrial network, but the mechanisms regulating this phenotype remain unknown. In this Chapter, I describe a non-cell death function of the anti-apoptotic protein, MCL-1, in regulating mitochondrial dynamics and promoting pluripotency of stem cells. MCL-1 expression increases upon reprogramming, and its inhibition or knockdown induces striking changes to the mitochondrial network, which corresponds to a loss of the key pluripotency transcription factors, NANOG and OCT-4. MCL-1 is distinct from other anti-apoptotic BCL-2 family members in that it also resides at the mitochondrial matrix in pluripotent stem cells. Mechanistically, we find MCL-1 to associate with DRP-1 and OPA1, two large GTPases responsible for remodeling the mitochondrial network. MCL-1 knockdown compromised the expression and mitochondrial fission/fusion activity of these key regulators of mitochondrial dynamics. Our findings

uncover an unexpected, non-apoptotic function for MCL-1 in the maintenance of mitochondrial structure and stemness.

Introduction

Considerable efforts have been made to identify the gene networks that regulate the pluripotent state and control the first steps of differentiation, when cells start to acquire a cell-lineage-specific identity. These studies have identified key transcriptional regulatory networks that determine the pluripotent state (Kumar et al., 2014). In contrast, we know relatively little about how different organelles, such as mitochondria, adapt to the changing environments they encounter during differentiation and reprogramming. While increased mitochondrial fragmentation is a fundamental feature of reprogramming (Prieto et al., 2016), the molecular mechanisms underlying this phenomenon are not fully understood.

The mitochondrial dynamics machinery is comprised of dynamin superfamily GTPases that have roles in either fission (division) or fusion of mitochondria. Dynamin-related protein 1 (DRP-1) is required for mitochondrial fission. DRP-1 activation is mediated in part by phosphorylation, ubiquitination, and sumoylation, which allow for increased recruitment to various receptors (*e.g.* FIS1) (Wai and Langer, 2016). However, these mechanisms of enhanced DRP-1 recruitment to the outer mitochondrial membrane are not well characterized in pluripotent stem cells, where they appear to be constitutively active. Once activated, DRP-1 forms oligomers and assembles into rings that constrict around the mitochondria, dividing the organelle into separate entities (Westermann, 2010). Fusion is mediated through the activity of the Optic atrophy type 1 (OPA1) GTPase at the inner mitochondrial membrane

and of mitofusins (MFN1 and MFN2) at the outer mitochondrial membrane (Chen and Chan, 2017). Mitochondrial dynamics is beginning to emerge as a crucial factor regulating cell fate (Martinou and Youle, 2011; Archer, 2013; Khacho et al., 2016).

Many connections between the mitochondrial dynamics machinery and apoptosis have been made. Apoptosis is mediated by the BCL-2 family of proteins (Llambi et al., 2011). When cells are subjected to stress, the mitochondrial network has been shown to undergo DRP-1- and FIS1-mediated fragmentation in a process involving BAX translocation and co-localization with DRP-1 and endophilin B1 (Karbowski et al., 2002; Sheridan et al., 2008; Friedman and Nunnari, 2014). Previous reports suggested that BAX and BAK could also influence MFN2 function in healthy cells (Karbowski et al., 2006). The data shown in this report demonstrate that an anti-apoptotic protein belonging to the BCL-2 family, Myeloid cell leukemia 1 (MCL-1), is a fundamental regulator of mitochondrial dynamics in human pluripotent stem cells, independent of its role in apoptosis. MCL-1 is essential for embryonic development and for the survival of various cell types (Rinkenberger et al., 2000). Interestingly, recent studies have proposed that MCL-1 may also drive changes in cancer cell metabolic profiles to promote the biosynthesis of substrates needed for proliferation (Andersen and Kornbluth, 2012; Opferman, 2016).

To examine the function of MCL-1 in both undifferentiated and differentiated cells, we took advantage of various features of the hPSC model, including: 1) high expression of MCL-1, 2) a predominantly fragmented mitochondrial network, and 3) the ability to induce differentiation into early progenitor stages. This model provided an ideal system to examine not only the potential role of MCL-1 in mitochondrial structure, but also its effects on cell fate. Here we report MCL-1 as a modulator of mitochondrial

dynamics in PSCs, and demonstrate the value of the stem cell model to study the plasticity of the mitochondrial network during reprogramming and differentiation.

Results and Discussion

Human pluripotent stem cells downregulate MCL-1 upon differentiation

We previously reported that human embryonic stem cells (hESCs) become resistant to DNA damage as differentiation is engaged (Dumitru and Gama et al., 2012). This resistance is in part associated with changes in the activation status of BAX, as well as mitochondrial priming (Dumitru and Gama et al., 2012; Liu et al., 2013). We first sought to probe the status of the apoptotic machinery by measuring levels of various BCL-2 family members during differentiation, when this apoptotic resistance is acquired. hESC colonies were grown in suspension in the absence of a matrix layer as aggregates, also known as embryoid bodies (EBs) (Odorico et al., 2001). We compared protein expression between hESCs and three-day EBs by Western blot analysis. Since differentiation causes apoptotic resistance, we expected to detect an overall increase in the expression of anti-apoptotic proteins, and a decrease in the expression of pro-apoptotic proteins. As expected, the pluripotency transcription factor NANOG was downregulated in EBs, and Sirtuin-2 (SIRT2), a NAD+-dependent deacetylase, which is induced upon differentiation (Ramalho-Santos et al., 2002), was upregulated. BAX and BCL-XL showed no detectable changes in expression during differentiation, and BCL-2 was significantly upregulated. In stark contrast, MCL-1 was significantly downregulated after only 3 days of differentiation (Figure 2-1A). MCL-1 downregulation was also detected in mouse ESC-derived EBs (Figure S1A). As reported previously, these

results indicate that BCL-2 may be critical mediator of cell death resistance in early differentiation (Liu et al., 2013). Counterintuitively, MCL-1 does not a appear to be a major determinant of the apoptotic resistance characteristic of EBs (Dumitru and Gama et al., 2012).

To determine whether downregulation of MCL-1 was not a particular trait of EB formation, we differentiated hESCs into trophoblast-like cells by addition of BMP4, and to neural progenitor cells using dual SMAD inhibition, as previously reported (Chambers et al., 2009; Amita et al., 2013) (Figure S1B-F). Differentiation to both lineages was accompanied by a significant downregulation of MCL-1 (Figure S1C-D), mimicking the EB formation results. This was unexpected, since EBs, trophoblast-like cells and neural progenitor cells are more resistant to apoptosis than undifferentiated stem cells (Figure S1E-F).

To probe whether the downregulation of MCL-1 had a functional role in maintaining pluripotency, we examined the effect of inhibiting MCL-1 in hESCs. Cell permeable, selective small molecule antagonists of BCL-2, BCL-XL and MCL-1, known as BH3 mimetics, have been identified (Chonghaile and Letai, 2008). We first used the pan-BCL-2 inhibitor GX15-070 (Chiappori et al., 2012), which inhibits BCL-2, BCL-XL and MCL-1, and compared it to the BH3-only mimetic ABT-737 (Oltersdorf et al., 2005), which only inhibits BCL-2 and BCL-XL. Since these small molecule inhibitors target the main anti-apoptotic proteins, we expected treatment with etoposide in combination with either inhibitor to accelerate cell death onset compared to treatment with only etoposide. Not surprisingly, treatment with ABT-737, increased the sensitivity of hESCs to etoposide-induced DNA damage (Figure 2-1B). However, rather unexpectedly, treatment with GX15-070 had the opposite effect and resulted in reduced

cell death sensitivity in response to etoposide (Figure 2-1B), pointing to a paradoxical effect of MCL-1 inhibition in mediating apoptotic resistance.

These results, together with the observed reduced MCL-1 expression, suggest that MCL-1 inhibition induces a partial protective effect that resembles the decrease in apoptotic sensitivity engaged during differentiation. Consistent with this hypothesis, treatment of hESCs with GX15-070 reduced the expression of pluripotency markers NANOG and OCT-4, while treatment with ABT-737 did not affect expression of these pluripotency factors (Figure 2-1C-E). To confirm the effect of MCL-1 on pluripotency, we then turned to MIM-1, an MCL-1-specific small molecule inhibitor (Cohen et al., 2012), which caused the significant decrease of both NANOG and OCT-4 expression (Figure 2-1F-H and Figure S1G-H). SOX2 expression was not affected by MCL-1 inhibition, suggesting that hESCs treated with MIM-1 may be differentiating to the default neuroectoderm lineage. These results indicate that MCL-1 may be necessary for hPSC maintenance of pluripotency.

MCL-1 is induced during reprogramming, and its inhibition causes changes in the stem cell mitochondrial network

We next examined whether MCL-1 expression upregulation was also engaged during the transition to pluripotency. We first reprogrammed human fibroblasts by delivering pluripotency factors using the non-integrating Sendai-based vector system (Figure S2A-B). Compared to fibroblasts, MCL-1 is expressed at high levels in human induced PSCs (hiPSCs) (Figure 2-2A) and hESCs (Figure 2-2B), both of which are highly sensitized to cell death (Dumitru and Gama et al., 2012) (Figure S2C). Along with high

expression levels of MCL-1, we also observed that iPSCs have a fragmented mitochondrial network when compared to their parent human fibroblast line (Figure S2D), consistent with previous reports suggesting that mitochondria undergo vast changes during reprogramming in response to overexpression of pluripotency factors (Chen and Chan, 2017).

We next investigated whether MCL-1 has a role in the maintenance of mitochondrial dynamics in pluripotent stem cells. We inhibited MCL-1 in hESCs using MIM-1 and examined its effects on mitochondrial structure. In response to MCL-1 inhibition, the mitochondria appear to fuse and become more elongated, as shown by cytochrome c staining (Figure 2-2C-D). We hypothesized that these changes in mitochondrial shape could be orchestrated through crosstalk between MCL-1 and the proteins involved in mitochondrial dynamics. We first interrogated the expression levels of active DRP-1 in response to MCL-1 inhibition. Phosphorylation of DRP-1 on Serine 616 enhances DRP-1 activity (Taguchi et al., 2007). Cells treated with MIM-1 displayed downregulated DRP-1 phosphorylation (p-DRP-1 S616) compared to vehicle control cells (Figure 2-2E-F), providing evidence for a role of MCL-1 in the regulation of DRP-1 activity.

To confirm that the effects of the small molecule inhibitor MIM-1 were due specifically to MCL-1 inhibition, we performed loss-of-function experiments utilizing an RNAi approach. MCL-1 expression was knocked down in hESCs using siRNA. As seen with the small molecule inhibitors of MCL-1, transmission electron microscopy images confirmed significant elongation of the mitochondria in MCL-1 knockdown hESCs in comparison to scramble siRNA controls (Figure 2-3A). Importantly, OCT4 and p-DRP-1 Ser-616 levels were also significantly decreased upon MCL-1 knockdown (Figure 2-3B-C), as

seen in the presence of MIM-1. Therefore, MCL-1 appears to impact pluripotency, at least in part, through the regulation of DRP-1 activity.

Expression of MCL-1 at the mitochondrial matrix delays differentiation

It has been shown that MCL-1, besides localizing to the outer mitochondrial membrane, also localizes to the mitochondrial matrix in MEFs and some human cancer lines (Perciavalle et al., 2012). The mitochondrial targeting sequence of MCL-1 resides in an N-terminal region that is cleaved from the wild-type form, allowing MCL-1 to be trafficked into the matrix. We investigated the effect of these separate forms of MCL-1 on maintaining pluripotency encoded by three expression vectors (Figure 2-3D) (Perciavalle et al., 2012): wild-type *Mcl-1* (*Mcl-1*^{WT}), mitochondrial outer membrane-located *Mcl-1* (*Mcl-1*^{OM}), and mitochondrial matrix-located *Mcl-1* (*Mcl-1*^{Matrix}). MCL-1^{WT} localizes to both the outer mitochondrial membrane and the matrix. MCL-1^{OM} was obtained by mutating the arginine residues at positions 5 and 6 of MCL-1 to alanine. MCL-1^{OM} localizes to the mitochondrial outer membrane, preserving MCL-1 anti-apoptotic function, but it cannot be imported to the mitochondrial matrix. MCL-1^{Matrix} was obtained by fusing the mitochondrial targeting sequence of matrix-localized ATP-synthase to N-truncated MCL-1 (lacking the first 66 amino acids). MCL-1^{Matrix} localizes exclusively to the mitochondrial matrix.

Ectopic expression of MCL-1^{OM} showed the expected decrease in OCT-4 expression in response to BMP4 (Figure 2-3E). Interestingly both MCL-1^{WT} and MCL-1^{Matrix} caused a delay in differentiation in response to BMP4, as shown by a decrease in OCT-4-negative cells (Figure 2-3E, Figure S3). These

results indicate that MCL-1 may have an alternate function at the mitochondrial matrix in maintaining pluripotency.

MCL-1 interacts with and maintains the stability of DRP-1 and OPA1

To confirm that MCL-1 is in fact localized to the mitochondrial matrix in human pluripotent stem cells, we co-expressed a GFP-tagged *MCL-1* construct (GFP:MCL-1) and a DsRed-mito construct, which encodes a truncated form of cytochrome c oxidase 2 (COX2) that localizes exclusively to the mitochondrial matrix (Figure 2-4A). Line-scan measurements of fluorescence show that MCL-1 co-localizes with the matrix marker, DsRed-mito (Figure 2-4B). The localization of MCL-1 at both the outer mitochondrial membrane and at the matrix in stem cells suggests that MCL-1 could be interacting with DRP-1 (at the outer membrane) to promote mitochondrial fragmentation and/or OPA1 (at the matrix) to repress fusion of the mitochondrial network in hESCs.

To test this possibility, we performed co-immunoprecipitation experiments using both total cell fractions and mitochondrial purifications to pulldown MCL-1 and check for binding to DRP-1 and OPA1 (Figure S4A). Western blot analysis identified a shifted band roughly 20 kDa larger than the expected DRP-1 band (Figure S4B). We speculate that this could be a modified, active form of DRP-1, presumably due to its phosphorylation and sumoylation when in its active state (Chang and Blackstone, 2010; Anderson and Blackstone, 2013). In the total cell fraction, we did not detect binding between MCL-1 and OPA1. However, we detected strong binding in mitochondrial preparations of hESCs (Figure S4B). These *in*

vitro biochemical assays suggest that MCL-1 is binding to both DRP-1 and OPA1 in human embryonic stem cells.

We then used a proximity ligation assay (PLA) to confirm binding of these proteins *in situ* (Figure S4C). We first confirmed MCL-1 interaction to the BH3-only protein, BIM. BIM is known to bind MCL-1 by inserting its BH3 domain into MCL-1's surface groove (Martinou and Youle, 2011). We detected the expected interaction of MCL-1 and BIM, as indicated by red fluorescent puncta (Figure S4D). We then probed for binding of MCL-1 with both OPA1 and DRP-1. Indeed, as seen in the immunoprecipitation experiments, we detected MCL-1 interaction with OPA1 (Figure 2-4C) and DRP-1 (Figure 2-4D). We then used a derivative of a recently reported MCL-1 inhibitor, S63845 (Kotschy et al., 2016), which works by competing for binding to the BH3 domain of MCL-1. We confirmed that S63845 also caused changes to the mitochondrial network (Figure S4E). As expected, S63845 effectively disrupted the interaction between MCL-1 and BIM (Figure S4D). Interestingly, as indicated by the decrease in the number of puncta, S63845 (MCL-1*i*) disrupts interactions with mitochondrial dynamics machinery at both the outer mitochondrial membrane (MCL-1:DRP-1) and the matrix (MCL-1:OPA1) (Figure 2-4C-D). These results suggest that MCL-1 associates with both GTPases through its characteristic hydrophobic binding groove (Billard, 2013).

Previously, we determined that MCL-1 downregulation affected the activity of DRP-1, but not its stability (Figure 2-3B). Interestingly, MCL-1 downregulation did cause a significant decrease in OPA1 expression (Figure 2-4E), indicating that MCL-1 influences OPA1 stability, but not necessarily its function, since the mitochondria in hESCs are still capable of fusing when MCL-1 is inhibited (Figure

2-3A). Mitochondrial fusion is key for efficient assembly of the electron transport chain (ETC). Interestingly, OPA1 has also been implicated in maintaining oxidative phosphorylation in cells. Thus, our results suggest that preventing OPA1 activity (either in fusion or in OXPHOS) could be crucial for maintaining stem cell pluripotency.

Taken together, our findings imply that MCL-1 modulates mitochondrial dynamics and pluripotency through interactions with mitochondrial fission and fusion regulators. Based on our observations, we propose a model in which MCL-1 at the outer mitochondrial membrane regulates cell death, as well as promotes DRP-1 activity and mitochondrial fragmentation (Figure 2-4F). Our results with S63845 (Letai, 2016) suggest that these interactions are modulated through the MCL-1 BH3 binding groove. It would be interesting to test whether there are two pools of MCL-1, one that is binding to the pro-apoptotic proteins and inhibiting apoptosis, and another capable of binding and regulating DRP-1, promoting mitochondrial fragmentation. It will also be necessary to follow up the effects that MCL-1 inhibition-induced mitochondrial changes have on the metabolic state of pluripotent stem cells. In addition, examining the metabolic requirement for MCL-1 during reprogramming could be intriguing in light of recent reports suggesting a multi-stage reprogramming process (Lee et al., 2016).

The process of differentiation into progenitors and committed cells is likely regulated, at least in part, by a shift in dependence to MCL-1 anti-apoptotic activity. It will be crucial to examine MCL-1's function in adult stem cells from different tissues. Likewise, identifying the signaling pathways by which mitochondria-nucleus crosstalk occurs upstream and downstream of MCL-1 in stem cells and their progenitors, as has been shown with murine neural progenitor cells (Khacho et al., 2016), is an important

future direction. By studying the role of MCL-1 in mitochondrial dynamics, we can increase our understanding of the fundamental mechanisms governing pluripotency and self-renewal.

Limitations of the study

There remain several limitations for examining mitochondrial dynamics *in vitro* and *in vivo*. User-based microscopy studies tend to be labor-intensive and low-throughput. The advances of high content imaging strategies will alleviate some of these limitations, but attaining the resolution required to determine fission and fusion events in live cells will still prove to be challenging. Approaches using imaging flow cytometry could allow for measurement of several mitochondrial parameters such as membrane potential, mitochondrial ROS, cell viability, and the degree of fusion activity using two or more distinct mitochondria-targeted fluorescent proteins (Nascimento et al., 2016).

For the experiments outlined in Figure 2-3, the MCL-1 mutant constructs used for rescue of the differentiation phenotype caused by BMP4 were based off the mouse sequence for MCL-1, and we did not control for the presence of endogenous MCL-1. Nevertheless, only overexpression of MCL-1^{Matrix}, not MCL-1^{OM}, was sufficient to prevent OCT4 loss; thus, we are assured the stem cell state of human PSCs is dependent upon MCL-1^{Matrix} expression. We are currently generating human MCL-1 constructs to address these potential issues, and the addition of affinity tags or fluorescent protein tags will aid in our dissection of MCL-1 interacting partners and sub-organellar localization.

Figures and Legends

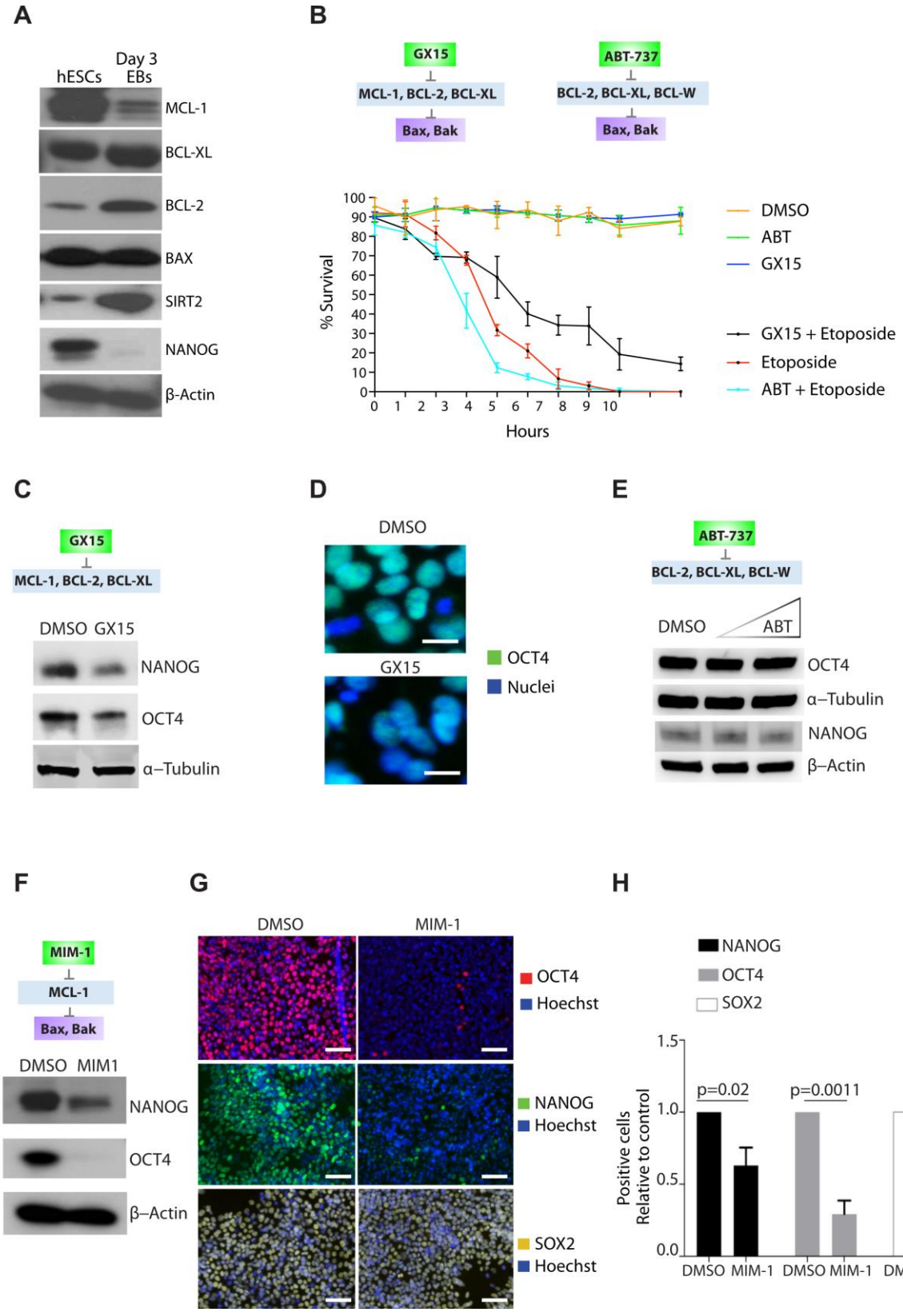

Figure 2-1. hESCs engage rapid apoptosis after DNA damage, which can be reversed upon cell differentiation by MCL-1 inhibition. (A) MCL-1 protein expression is significantly decreased in EBs. **(B)** hESCs were treated with GX15070 or ABT-737 ±20 μM etoposide. Cell survival was quantified each hour after etoposide treatment. **(C)** GX15-070 treatment of hESCs results in decreased expression of NANOG and OCT-4. **(D)** Immunofluorescence images (63X) show decreased staining for OCT-4 (green) when treated with GX15-070. Nuclei: Hoechst 33258; scale: 10 μm. **(E)** In contrast, increasing treatments of ABT-737 do not affect OCT-4 or NANOG protein levels. **(F)** Treatment of hESCs with 500 nM MIM-1 results in lowered expression of NANOG and OCT-4. **(G-H)** Immunofluorescence (20X) shows decreased expression of NANOG and OCT4; scale: 100 μm; error bars represent ±SD for three independent experiments. *See also Figure S2-1.*

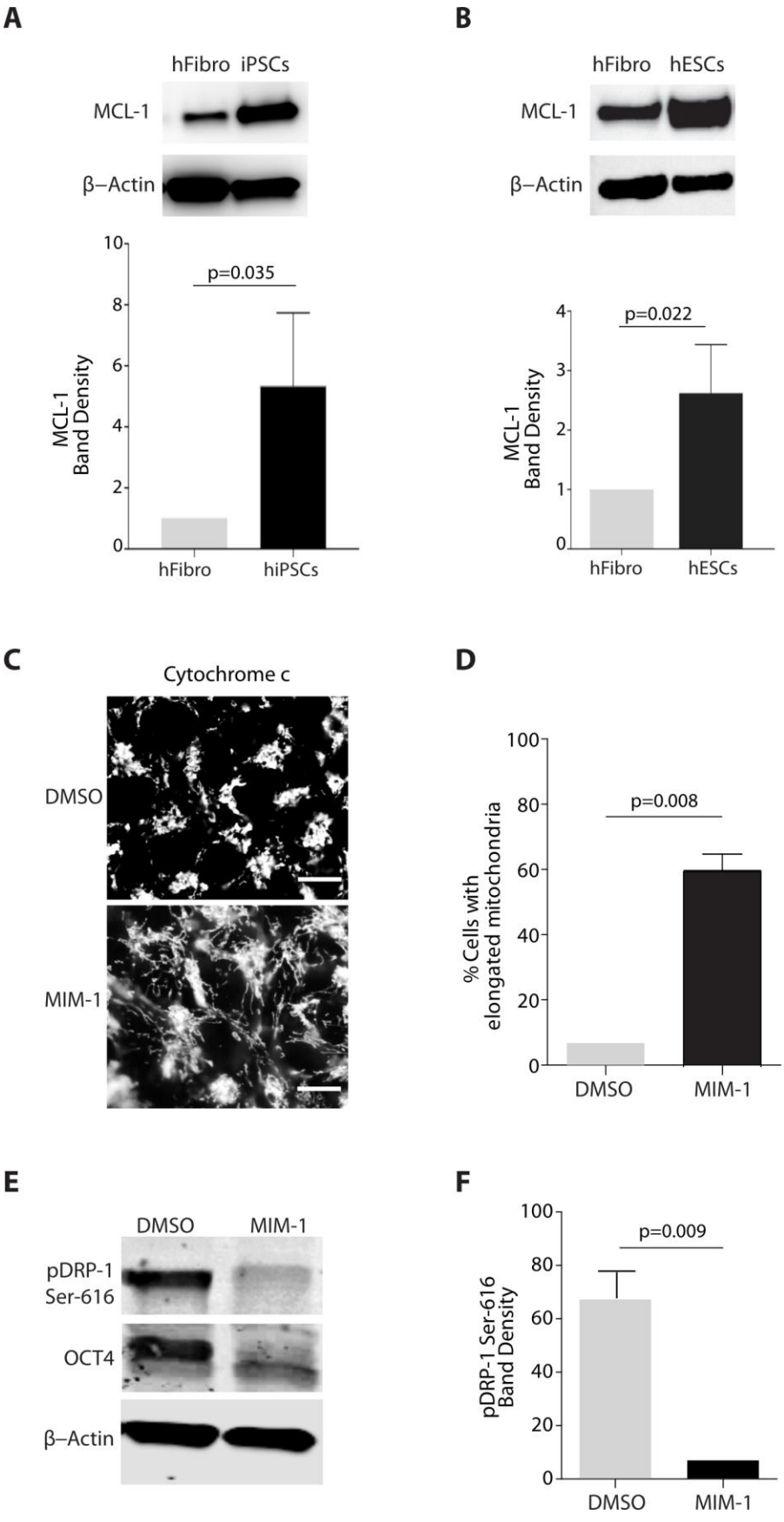
A
hFibro iPSCs
MCL-1
β–Actin
MCL-1 Band Density
p=0.035
hFibro
hiPSCs
B
hFibro hESCs
MCL-1
β–Actin
MCL-1 Band Density
p=0.022
hFibro
hESCs
C
Cytochrome c
DMSO
MIM-1
D
% Cells with elongated mitochondria
p=0.008
DMSO
MIM-1
E
DMSO MIM-1
pDRP-1 Ser-616
OCT4
β–Actin
F
pDRP-1 Ser-616 Band Density
p=0.009
DMSO
MIM-1

Figure 2-2. MCL-1 is highly expressed in hESCs and maintains mitochondrial fission. MCL-1 protein expression is increased in hiPSCs **(A)** and hESCs **(B)** when compared to human fibroblasts (hFibrob). Bar graphs show quantification of band intensity relative to hFibrob beta-actin. **(C)** hESCs were treated with 500 nM MIM-1, inducing mitochondrial elongation. Cytochrome c staining (cyt c) depicts mitochondria (63X); scale: 10 μm. **(D)** Number of cells with elongated mitochondria in panel C. **(E-F)** MIM-1 treatment (500 nM) in hESCs results in p-DRP-1 S616 downregulation; band density was quantified relative to control DMSO. All error bars represent ±SD in at least three independent experiments. *See also Figure S2-2.*

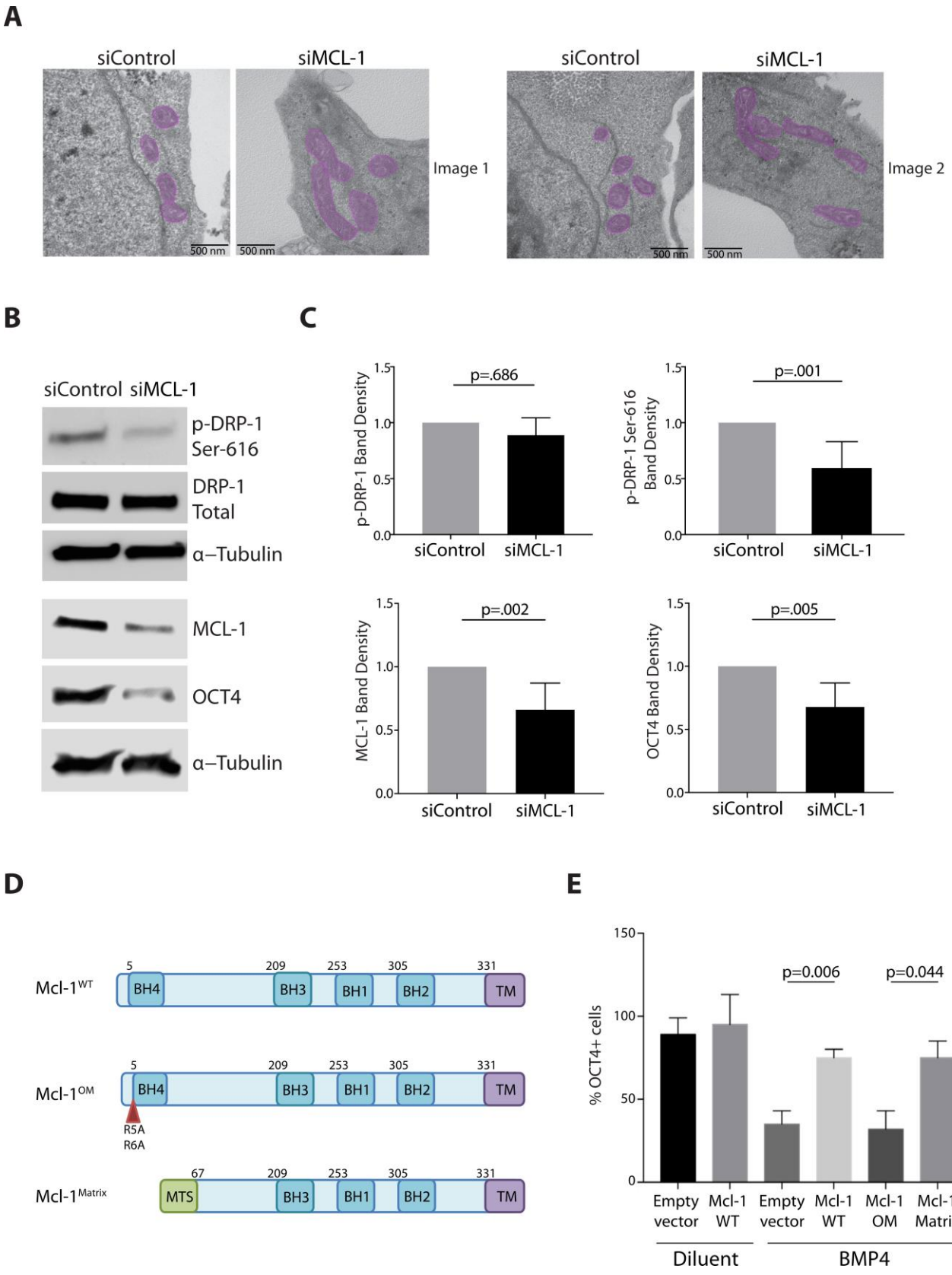
A
siControl
siMCL-1
500 nm
Image 1
Image 2
B
siControl siMCL-1
p-DRP-1 Ser-616
DRP-1 Total
α–Tubulin
MCL-1
OCT4
α–Tubulin
C
p-DRP-1 Band Density
p=.686
p-DRP-1 Ser-616 Band Density
p=.001
MCL-1 Band Density
p=.002
OCT4 Band Density
p=.005
D
Mcl-1WT
Mcl-1OM
Mcl-1Matrix
BH4
BH3
BH1
BH2
TM
MTS
R5A
R6A
E
% OCT4+ cells
p=0.006
p=0.044
Empty vector
Mcl-1 WT
Mcl-1 OM
Mcl-1 Matrix
Diluent
BMP4

Figure 2-3. MCL-1 inhibition results in elongated mitochondria and low expression of active DRP-1. (A) TEM images showing elongated mitochondrial morphology in hESCs after MCL-1 downregulation. Scale: 500 μm. **(B)** Knockdown of MCL-1 results in lowered expression of OCT-4 and p-DRP-1 S616. **(C)** Quantification of Western blots (WBs) in panel B; error bars represent ±SD for at least three separate experiments. **(D)** Representation of murine constructs encoding MCL-1. **(E)** hESCs were treated with BMP4, then transfected with *Mcl-1*^{WT}, *Mcl-1*^{OM} or *Mcl-1*^{Matrix}. OCT4 expression was quantitated; error bars represent ±SD for three independent experiments. *See also Figure S2-3.*

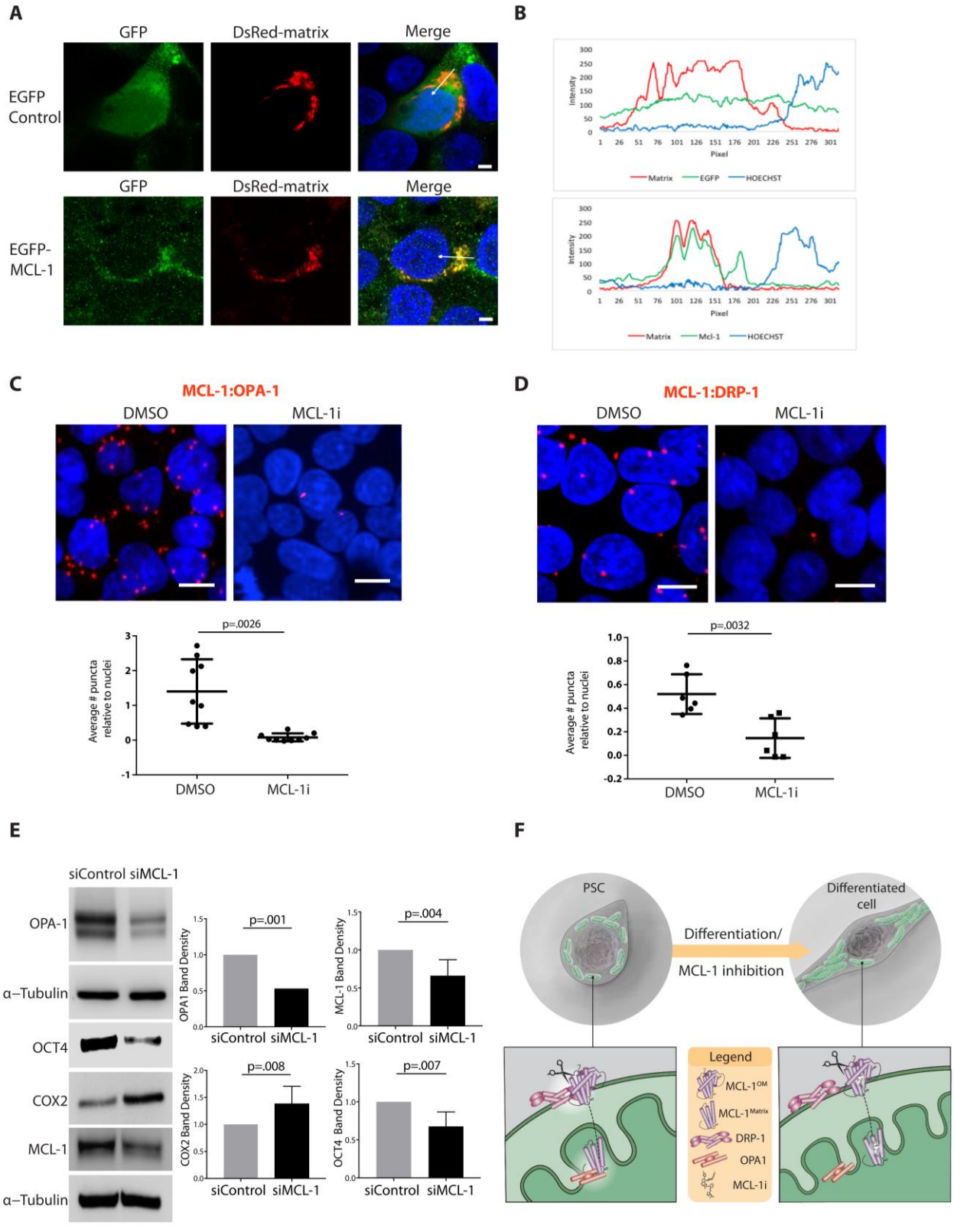
A
GFP
DsRed-matrix
Merge
EGFP Control
EGFP-MCL-1
B
Intensity
Pixel
Matrix
EGFP
HOECHST
Mcl-1
C
MCL-1:OPA-1
DMSO
MCL-1i
p=.0026
Average # puncta relative to nuclei
D
MCL-1:DRP-1
p=.0032
E
siControl siMCL-1
OPA-1
α–Tubulin
OCT4
COX2
MCL-1
p=.001
p=.004
p=.008
p=.007
OPA1 Band Density
MCL-1 Band Density
COX2 Band Density
OCT4 Band Density
F
PSC
Differentiated cell
Differentiation/
MCL-1 inhibition
Legend
MCL-1OM
MCL-1Matrix
DRP-1
OPA1
MCL-1i

Figure 2-4. MCL-1 regulates mitochondrial dynamics through interaction with DRP-1 and OPA1. (**A**) hiPSCs expressing EGFP-MCL-1 or Control EGFP and DsRed-mito. Scale: 2 μm. **(B)** Line intensity plots show co-localization of EGFP-MCL-1 and DsRed-mito. **(C-D)** PLA of cells treated for 6 hours ±100nM S63845 (MCL-1*i*). Representative images are shown. Red = MCL-1:OPA1 **(C)** and MCL-1:DRP-1 **(D)** proximity; blue = Hoechst 33258. Average puncta/cell (±S.D.) was quantitated for at least 300 cells/sample and assessed in three independent experiments, Welch's unpaired 2-tailed T-test. Scale: 10 μm. (**E**) WB of MCL-1 after siRNA-mediated knockdown. At least three independent experiments were quantified; error bars represent ±SD. **(F)** Working model of MCL-1 regulation of mitochondrial dynamics. *See also Figure S2-4.*

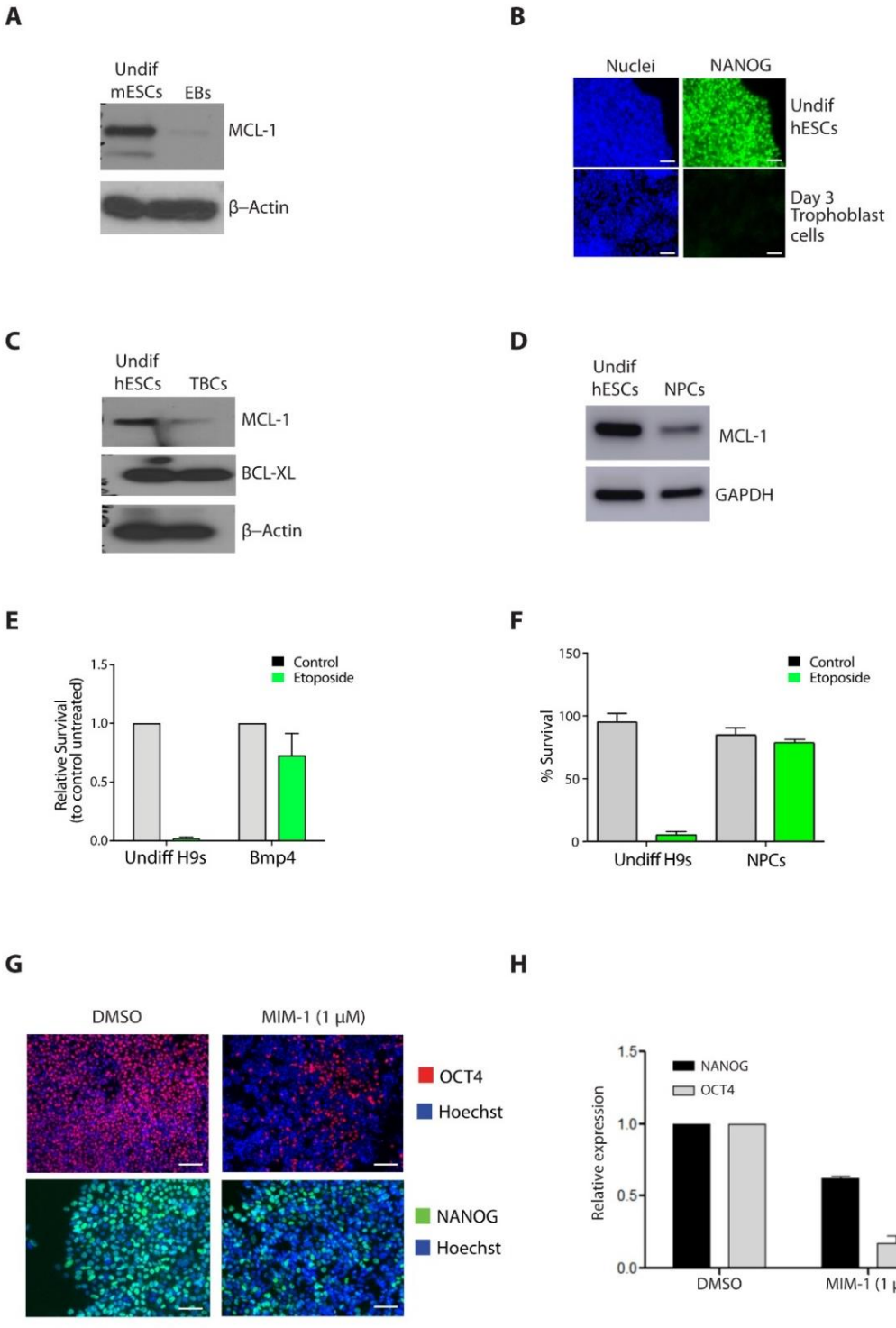
A
Undif mESCs
EBs
MCL-1
β–Actin
B
Nuclei
NANOG
Undif hESCs
Day 3 Trophoblast cells
C
Undif hESCs
TBCs
MCL-1
BCL-XL
β–Actin
D
Undif hESCs
NPCs
MCL-1
GAPDH
E
Relative Survival (to control untreated)
1.5
1.0
0.5
0.0
Control
Etoposide
Undiff H9s
Bmp4
F
% Survival
150
100
50
0
Control
Etoposide
Undiff H9s
NPCs
G
DMSO
MIM-1 (1 μM)
OCT4
Hoechst
NANOG
Hoechst
H
Relative expression
1.5
1.0
0.5
0.0
NANOG
OCT4
DMSO
MIM-1 (1 μM)

Figure S2-1. **(A)** Western blot shows decreased MCL-1 expression after 7 days of differentiation to EBs from mESCs. **(B)** hESCs were treated with BMP4 to induce trophoblast differentiation. After 3 days of treatment, MCL-1 levels are decreased, while immunofluorescence images show expected decrease of NANOG; scale: 100 μm. **(C)** MCL-1 levels decrease upon differentiation to trophoblast-like cells (TBCs). **(D)** Neural progenitor cells (NPCs) were obtained after differentiation of hESCs for 7 days. MCL-1 levels are decreased in NPCs in comparison to undifferentiated hESCs. **(E-F)** hESCs become resistant to etoposide-induced DNA damage upon differentiation to TBCs and NPCs, respectively. **(G-H)** Treatment of hESCs with 1 μM MIM-1 results in decreased OCT-4 and NANOG expression; scale: 100 μm. Error bars represent ±SD for triplicate experiments.

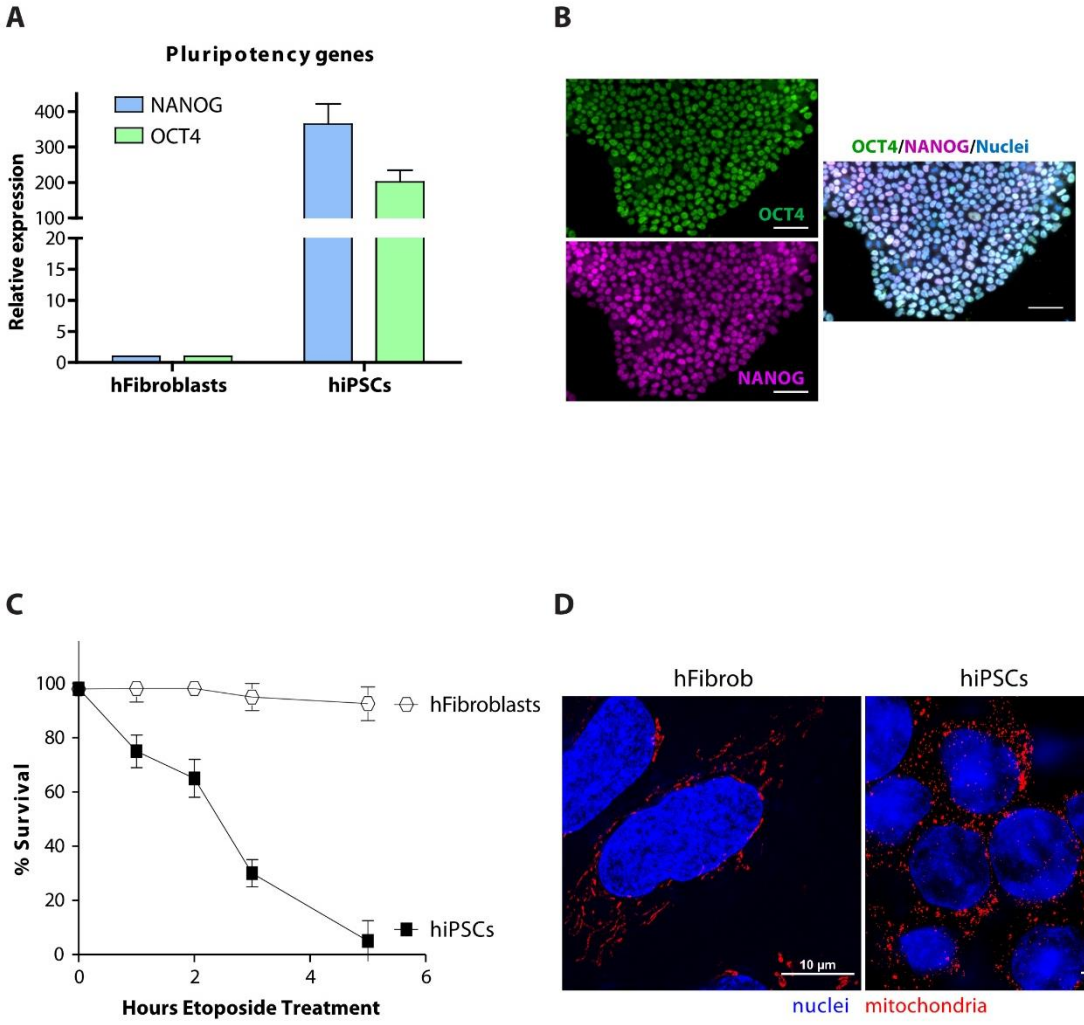
A
Pluripotency genes
NANOG
OCT4
Relative expression
400
300
200
100
20
15
10
5
0
hFibroblasts
hiPSCs
B
OCT4
NANOG
OCT4/NANOG/Nuclei
C
% Survival
100
80
60
40
20
0
0
2
4
6
hFibroblasts
hiPSCs
Hours Etoposide Treatment
D
hFibrob
hiPSCs
10 µm
10 µm
nuclei
mitochondria

Figure S2-2. (A) Human fibroblasts were reprogrammed into iPSCs, and qRT-PCR confirmed expression of NANOG and OCT4. Error bars represent ±SD for three independent experiments. **(B)** Immunofluorescence for NANOG and OCT4 in iPSCs; scale: 100 μm. **(C)** Reprogrammed cells were highly sensitive to DNA damage when compared to the fibroblast parent line. **(D)** Immunofluorescence shows that iPSCs have fragmented, punctate mitochondria when compared to fibroblasts (mitochondria are stained with anti-COX2, DNA is stained with Hoechst); scale: 10 μm.

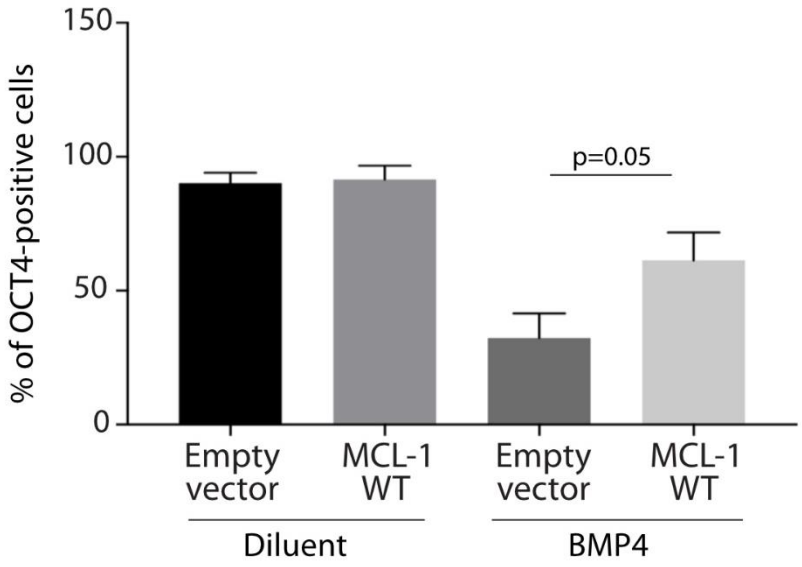

Figure S2-3. Overexpression of human wild-type MCL-1 delayed differentiation of hESCs after BMP4 treatment, partially rescuing expression of OCT-4 in comparison to the empty vector. Error bars represent ±SD for three independent experiments.

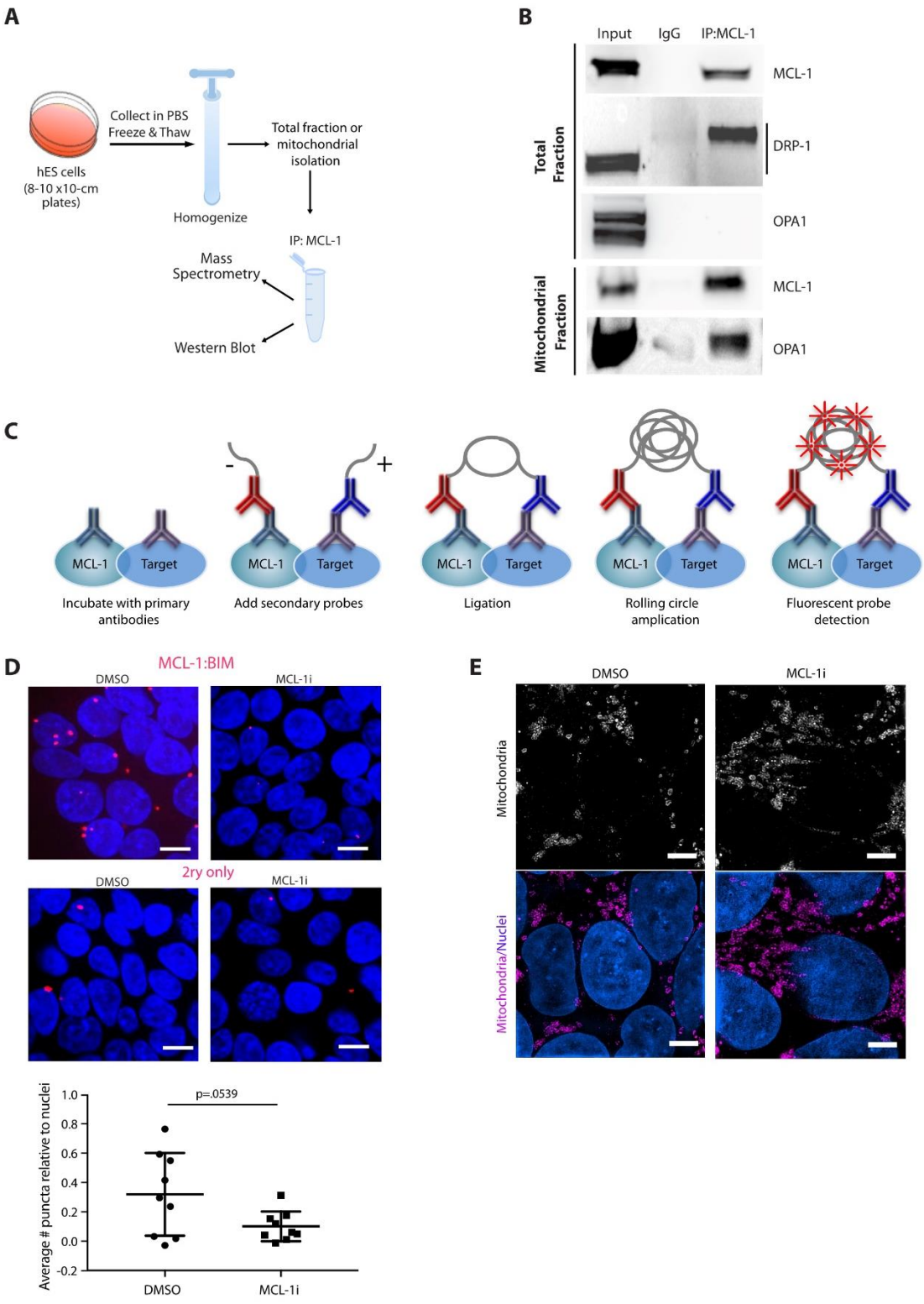
A
hES cells
(8-10 x10-cm
plates)
Collect in PBS
Freeze & Thaw
Homogenize
Total fraction or
mitochondrial
isolation
IP: MCL-1
Mass
Spectrometry
Western Blot
B
Input
IgG
IP:MCL-1
Total
Fraction
MCL-1
DRP-1
OPA1
Mitochondrial
Fraction
MCL-1
OPA1
C
MCL-1
Target
Incubate with primary
antibodies
Add secondary probes
Ligation
Rolling circle
amplication
Fluorescent probe
detection
D
MCL-1:BIM
DMSO
MCL-1i
2ry only
DMSO
MCL-1i
Average # puncta relative to nuclei
1.0
0.8
0.6
0.4
0.2
0.0
-0.2
p=.0539
DMSO
MCL-1i
E
DMSO
MCL-1i
Mitochondria
Mitochondria/Nuclei

Figure S2-4. (A) Protocol for immunoprecipitation of MCL-1 for mass spectrometry and Western blot analyses. **(B)** MCL-1 pull-down assays from hESCs show Western blots from both total lysate and mitochondrial fractions. The anti-DRP-1 antibody detects binding at a higher molecular weight than the native form of DRP-1, indicating that MCL-1 could bind to a modified form of DRP-1. MCL-1:OPA1 binding is only detected in the mitochondrial fraction. **(C)** Schematic of PLA protocol. **(D)** PLA showing MCL-1:BIM binding, which is disrupted by treatment with MCL-1 inhibitor (MCL-1*i*). Incubation with secondary probe-only shows no binding above background level in the control or treatment conditions; scale: 10 μm. Graph shows quantification of MCL-1:BIM puncta. Average puncta/cell (±S.D.) was quantitated for at least 300 cells/sample and assessed in three independent experiments; Welch's unpaired 2-tailed t-test. **(E)** Mitochondrial changes are observed in hESCs after treatment with a derivative of S63845, a potent MCL-1 small molecule inhibitor; scale: 5 μm.

Chapter 3

MCL-1 INHIBITION BY SELECTIVE BH3 MIMETICS DISRUPTS MITOCHONDRIAL DYNAMICS CAUSING LOSS OF VIABILITY AND FUNCTIONALITY OF HUMAN CARDIOMYOCYTES

Adapted with permission from: Rasmussen, M.L., Taneja N., Neininger, A.C., Wang, L., Robertson, G.L., Riffle, S.N., Shi, L., Knollmann, B.C., Burnette, D.T., Gama, V. (2020) MCL-1 inhibition by selective BH3 mimetics disrupts mitochondrial dynamics causing loss of viability and functionality of human cardiomyocytes. iScience. DOI: 10.1016/j.isci.2020.101015

Abstract

MCL-1 is a well characterized inhibitor of cell death that has also been shown to be a regulator of mitochondrial dynamics in human pluripotent stem cells. The goal of the studies described in this Chapter was to use cardiomyocytes derived from human induced pluripotent stem cells (hiPSC-CMs) to uncover whether MCL-1 is crucial for cardiac function and survival. Inhibition of MCL-1 by BH3 mimetics resulted in the disruption of mitochondrial morphology and dynamics as well as disorganization of sarcomeres. Blocking MCL-1 function affects the association of DRP-1 and MCL-1 at the outer mitochondrial membrane, resulting in decreased function of hPSC-CMs as indicated by reduced ATP production, calcium flux, and beat amplitude. Cardiomyocytes display abnormal cardiac performance even after caspase inhibition, indicating a non-apoptotic activity of MCL-1 in hiPSC-CMs. BH3 mimetics targeting MCL-1 are promising anti-tumor therapeutics. Advancement of BCL-2 family inhibitors,

especially targeting MCL-1, depends on understanding not only its canonical function in preventing apoptosis, but also in the maintenance of mitochondrial dynamics and function.

Introduction

Myeloid cell leukemia-1 (MCL-1) was originally identified as an early-induced gene in human myeloid leukemia cell differentiation (Kozopas et al., 1993; Reynolds et al., 1996; Yang et al., 1996). MCL-1 is structurally similar to other anti-apoptotic BCL-2 (B cell lymphoma-2) family proteins (*i.e.* BCL-2, BCL-XL (B cell lymphoma extra-large)) (Chipuk et al., 2010). However, its larger, unstructured N-terminal domain and shorter half-life likely indicated that MCL-1 was not completely functionally redundant with other anti-apoptotic proteins (Perciavalle and Opferman, 2013). Supporting this idea, MCL-1 has been shown to be essential for embryonic development and for the survival of various cell types, including cardiomyocytes, neurons, and hematopoietic stem cells (Rinkenberger et al., 2000; Opferman et al., 2005; Arbour et al., 2008; Weber et al., 2010; Wang et al., 2013; Thomas et al., 2013).

MCL-1 is one of the most amplified genes in human cancers and is frequently associated with resistance to chemotherapy (Beroukhim et al., 2010; Perciavalle and Opferman, 2013). Earlier work demonstrated that *MCL-1* genetic deletion is peri-implantation lethal in embryogenesis, not due to defects in apoptosis, but rather due to a combination of an embryonic developmental delay and an implantation defect (Rinkenberger et al., 2000). However, the non-apoptotic mechanism by which MCL-1 functions in normal and cancerous cells is still unclear. We previously reported that MCL-1 regulates mitochondrial dynamics in human pluripotent stem cells (hPSCs, which refers to both human embryonic stem cells

(hESCs) and induced pluripotent stem cells (hiPSCS)) (Rasmussen et al., 2018). We found that MCL-1 maintains mitochondrial network homeostasis in hPSCs through interactions with Dynamin related protein-1 (DRP-1) and Optic atrophy type 1 (OPA1). In this study, we investigated whether this non-apoptotic role of MCL-1 remains as stem cells differentiate, using cardiomyocytes derived from human induced pluripotent stem cells (hiPSC-CMs).

Mitochondrial fusion promotes elongation of the mitochondrial network, which is key for mitochondrial DNA (mtDNA) homogenization and efficient assembly of the electron transport chain (ETC) (Westermann, 2010; Friedman and Nunnari, 2014). Loss of mitochondrial fusion has been implicated as a mechanism for the onset of dilated cardiomyopathy, and reported to also contribute to hypertrophic cardiomyopathy and other heart diseases (Dorn, 2013; Dorn et al., 2015; Ong et al., 2017). Mitochondrial homeostasis is essential during cardiomyocyte differentiation and embryonic cardiac development (Kasahara et al., 2013; Kasahara and Scorrano, 2014; Cho et al., 2014). However, there is limited information about the mechanisms used by cardiomyocytes to minimize the risks for apoptosis, especially in cells derived from highly sensitive stem cells (Imahashi et al., 2004; Murriel et al., 2004; Gama and Deshmukh, 2012; Dumitru and Gama et al., 2012; Walensky, 2012).

Ultrastructural changes in mitochondria have long been observed in response to alterations in oxidative metabolism (Hackenbrock, 1966; Khacho et al., 2016). It has become increasingly clear that individual mitochondrial shape changes can also have dramatic effects on cellular metabolism (Chan, 2007; Hsu et al., 2016), (Itoh et al., 2013; Burté et al., 2015). Several studies in the heart suggest that alterations in mitochondrial dynamics causes abnormal mitochondrial quality control, resulting in the buildup of

defective mitochondria and reactive oxygen species (ROS) (Galloway and Yoon, 2015; Song et al., 2017). Interestingly, it has been shown that modulating the production of ROS can favor or prevent differentiation into cardiomyocytes (Buggisch et al., 2007; Murray et al., 2014). Thus, specific metabolic profiles controlled by mitochondrial dynamics are likely critical for hiPSC-CMs, since they can influence cell cycle, biomass, metabolite levels, and redox state (Zhang et al., 2012).

It is not completely understood how dynamic changes in metabolism affect cardiomyocyte function. Deletion of MCL-1 in murine heart muscle resulted in lethal cardiomyopathy, reduction of mitochondrial DNA (mtDNA), and mitochondrial dysfunction (Thomas et al., 2013; Wang et al., 2013). Inhibiting apoptosis via concurrent BAK/BAX knockout allowed for the survival of the mice; conversely, the mitochondrial ultrastructure abnormalities and respiratory deficiencies were not rescued. These results indicate that MCL-1 also has a crucial function in maintaining cell viability and metabolic profile in cardiomyocytes. Despite these efforts, the non-apoptotic mechanism by which MCL-1 specifically functions in cardiomyocytes is still unknown. Furthermore, a role for MCL-1 in the regulation of mitochondrial dynamics in cardiac cells has not yet been defined. Here we report that MCL-1 inhibition via BH3 mimetics caused severe contractility defects and impaired long-term survival of hPSC-CMs, due to MCL-1's essential function regulating mitochondrial morphology and dynamics.

Results

MCL-1 inhibition causes severe defects in hiPSC-CM mitochondrial network

Recently published small molecule inhibitors of MCL-1 have been anticipated as potent anti-tumor agents against MCL-1-dependent cancers with limited cardiotoxicity in mouse models (Cohen et al., 2012; Kotschy et al., 2016; Letai, 2016). Thus, we chose to use hiPSC-CMs to examine the effects of MCL-1 inhibition on mitochondrial morphology using the small molecule inhibitor S63845 (Kotschy et al., 2016), combined with structured illumination microscopy (SIM) to observe mitochondria at high-resolution. Cardiomyocytes were imaged after 4 days of treatment with vehicle (DMSO) or MCL-1 inhibitor (S63845) and the caspase inhibitor Q-VD-OPh (QVD) to prevent downstream effects of apoptosis on mitochondrial morphology (Figure 1A-C). Mitochondrial networks in S63845-treated cells were severely disrupted, with individual mitochondria becoming shorter in length and more globular on average, as opposed to elongated networks in control cells. Quantification of SIM images shows a significant reduction in average mitochondrial length (Figure 1D) and a significant increase in mitochondria sphericity (Figure 1E) compared to control cells. In addition to S63845, we also tested two other small molecule MCL-1 inhibitors, AMG-176 (AMG) and AZD5991 (AZD) (Caenepeel et al., 2018; Tron et al., 2018). While we observed mitochondrial defects in both inhibitor conditions (Figure 1F-H), mitochondrial morphology in AMG-treated cells was not significantly different compared to control cells (Figure 1I-J). Quantification of SIM images shows a significant reduction in average mitochondrial length in cells treated with AZD (Figure 1I).

Corresponding with the fragmented mitochondrial phenotypes seen in S63845-treated cells, we also observed impaired mitochondrial respiration as measured by the Seahorse XFe96 analyzer. MCL-1 inhibition significantly lowered the maximum oxygen consumption rate (OCR) after addition of FCCP, an uncoupler of oxidative phosphorylation (OXPHOS) (Figure S1A). ATP production was significantly reduced in S63845-treated cells as calculated from the OCR trace (Figure S1B). QVD was added to account for any effects on metabolism due to downstream apoptosis, but cells displayed similar OCR and ATP production as with S63845 alone (Figure S1C-D).

Recent reports have determined that MCL-1 functions not only as an apoptosis regulator but also as a modulator of mitochondrial morphology and dynamics (Perciavalle et al., 2012; Morciano et al., 2016a; Rasmussen et al., 2018). Thus, we hypothesized that inhibiting MCL-1 with BH3 mimetics would affect the functionality of human cardiomyocytes, due to the disruption of crucial MCL-1 interactions with the mitochondrial dynamics machinery, which will ultimately lead to cell death.

MCL-1 inhibition affects contractility of hiPSC-CMs and myofibril assembly in a caspase-independent manner

Previous studies focused on human cardiomyocytes have suggested an effect of MCL-1 inhibition on mitochondrial morphology and mild effects on overall cardiac function (Guo et al., 2018). However, MCL-1 inhibition by S63845 was shown to have minimal effects on murine ejection fraction (Kotschy et al., 2016). These results are intriguing, considering previous studies reporting that MCL-1 deletion from murine cardiomyocytes has severe effects on mitochondrial morphology and cardiac function, which were

not rescued by co-deletion of BAK and BAX (Wang et al., 2013). We treated hiPSC-CMs with S63845, while inhibiting caspase activity using QVD, and measured spontaneous cardiac beating using the Axion Biosystems analyzer (Clements and Thomas, 2014) (Figure 2A). We also used the BCL-2 inhibitor, Venetoclax (ABT-199) (Souers et al., 2013), to probe whether these cells are also sensitive to BCL-2 inhibition. We observed that only MCL-1 inhibition caused severe defects in cardiomyocyte functionality within 48 hours of treatment (Figure 2B-F). In particular, spike amplitude mean (Figure 2B) and spike slope mean (Figure 2C) were significantly decreased at 20 and 48 hours, while beat period irregularity was significantly increased at 20 hours post-treatment (Figure 2D). BCL-2 inhibition did not cause changes in cardiac beating ability compared to DMSO control in any of the measured parameters (Figure 2B-F), suggesting that the function of hiPSC-CMs is highly dependent on MCL-1, but not BCL-2. S63845-treated cells stopped beating completely at 48 hours, accounting for the decrease in beat period mean and beat period irregularity at this time-point (Figure 2D-E). The field potential duration (FPD) was not detectable after 20 hours of MCL-1 inhibition (Figure 2F). We also observed similar defects in cardiomyocyte functionality in cells treated with AZD5991, but not AMG-176 (Figure S2A-E).

In a previous report, MCL-1 inhibition using RNAi also resulted in mitochondria morphology defects including severe cristae disruption and remarkable vacuolation in the mitochondrial matrix (Guo et al., 2018). In this study, MCL-1 knockdown by siRNA (Figure S2F-G) also caused increased beat period irregularity (Figure S2H), increased delay between beats (Figure S2I), and decreased FPD mean (Figure S2J). These results suggest that MCL-1 inhibition in human cardiomyocytes causes bradycardia- and arrhythmia-like phenotypes.

Since MCL-1 inhibition disrupted hiPSC-CM spike amplitude mean, we decided to probe whether calcium influx was also impaired in these cells. We visualized calcium dynamics using the GCaMP5G calcium reporter in hiPSC-CMs (Figure 2G). In DMSO-treated cells, we measured approximately a 1.9-fold increase in signal intensity (Figure 2H). As a positive control, we treated cells with cadmium chloride ($CdCl_2$), a calcium channel-blocker, which completely disrupted calcium intake, giving a ratio of 1.0. Consistent with our results with the MEA recordings, calcium signal intensity was significantly reduced in hiPSC-CMs treated with S63845 or AZD5991. AMG-176 treatment caused a significant, but less severe reduction in calcium intake. We also measured beating by light microscopy and found that MCL-1 inhibition reduced the proportion of beating cells in a dose dependent manner (Figure 2I).

Intriguingly, we also observed significant changes in the structure of the actin network and subsequent myofibril organization in cells treated with any of the MCL-1 inhibitors (Figure 2J and S2K). hiPSC-CMs treated with MCL-1 inhibitors displayed poor Z-line organization, lower density of F-actin, and increased presence of stress fibers. Blinded quantification of F-actin organization revealed that MCL-1 inhibitor-treated cells had significantly less organized myofibril structure (Figure 2J and S2K).

MCL-1 co-localizes with mitochondrial dynamics proteins in hiPSC-CMs, and S63845 disrupts MCL-1:DRP-1 co-localization

Since MCL-1 inhibition disrupted mitochondrial network integrity in hiPSC-CMs and MCL-1 depletion affects mitochondrial dynamics proteins DRP-1 and OPA1 (Rasmussen et al., 2018), we next examined the effects of MCL-1 inhibition on the expression levels of these proteins in hiPSC-CMs. S63845-treated cells had a significant increase in the expression levels of DRP-1 (Figure 3A-B and S3A-

C) but not in phospho-DRP-1 (pDRP-1 S616) (Figure 3C). MCL-1 expression levels were significantly increased (Figure 3D-E). Previous studies also reported this induction of MCL-1 protein expression upon MCL-1 inhibition (Kotschy et al., 2016). There were no significant changes in OPA1 (Figure 3D-E) or TOM20 (Figure 3D and S3D). We then assessed whether MCL-1 interacts with DRP-1 and OPA1, two GTPases responsible for maintaining mitochondrial morphology and dynamics, using *in situ* proximity ligation assay (PLA). Our data shows that MCL-1 is in close proximity to both DRP-1 and OPA1 (Figure 3G-J). PLA puncta were quantified and normalized to the number of puncta in the control sample (Figure S3E). The co-localization of MCL-1 with DRP-1 (Figure 3G-H), but not OPA1 (Figure 3I-J), was disrupted upon inhibition of MCL-1 with S63845, suggesting that MCL-1 interacts with DRP-1 through its BH3 binding groove.

To further assess the disruption of the mitochondrial network caused by MCL-1 inhibition, we employed an assay using a photo-convertible plasmid (mito-tdEos) to assess connectivity and fusion/motility of mitochondria. After photo-converting an area of the mitochondrial network, we assess the spread of red signal, which we used as a proxy for mitochondrial fusion. We observed that in cells treated with MCL-1 inhibitor, both the initial converted area and the spread of the converted red signal after 20 minutes were significantly decreased, indicating impaired mitochondrial fusion (Figure 4A-D). This phenomenon was DRP-1-dependent, since cells deficient in DRP-1 maintained an elongated network even when treated with S63845 (Figure 4E-F and Figure S4A-B).

MCL-1 inhibition results in hiPSC-CM death

To examine whether hiPSC-CMs treated with MCL-1 inhibitor were undergoing apoptosis, we treated the cells with increasing doses of S63845 and examined the activation of caspase-3 and caspase-7. Cells responded to S63845 in a dose-dependent manner after 48 hours, with 1-2 μM MCL-1*i* inducing the most caspase activity (Figure 5A). We observed a similar dose response with both AMG and AZD (Figure 5B). It is important to note that S63845 and AZD5991, which had more severe effects on cardiomyocytes overall, are of similar chemical structure, whereas AMG-176 was less toxic to hiPSC-CMs (Hird and Tron, 2019). To confirm that cells were undergoing a caspase dependent cell death, we performed long-term live cell imaging in the presence of MCL-1 inhibitors with and without caspase inhibition (Figure S4A-D). These results indicate that hiPSC-CMs are also committing to a caspase-independent cell death in response to MCL-1 inhibition. To assess the type of death caused by MCL-1 inhibition, we treated the cells with IM-54, a known inhibitor of necrosis. Interestingly, IM-54 treatment rescued the toxicity caused by MCL-1 inhibition (Figure 5C).

Previous reports have established that iPSC-derived cardiomyocytes mimic immature progenitor cells. To test the possibility that the effects of the MCL-1 inhibitors were exacerbated by the immature state of hiPSC-CMs, we used a previously published hormone-based method for cardiomyocyte maturation (Figure 6A-B) (Parikh et al., 2017; Gentillon et al., 2019). We tested for caspase-3/7 activation after 24 hours of treatment with increasing doses of S63845 and detected similar effects of MCL-1 inhibition in hormone-matured hiPSC-CMs and vehicle-treated hiPSC-CMs (Figure 6C-D). Importantly, treatment

of these hormone-matured hiPSC-CMs also results in decreased functionality in response to a low dose of MCL-1 inhibitor (100 nM S63845) (Figure 6E-G).

Long-term MCL-1 inhibition, but not BCL-2 inhibition, causes defects in cardiomyocyte functionality

MCL-1 inhibition has significant effects on hiPSC-CM contractility and functionality when used at higher doses. To test if MCL-1 inhibition still affects cardiac functionality at lower doses, we treated hiPSC-CMs for two weeks (with treatments every two days) with 100 nM S63845. We also treated cells with the BCL-2 inhibitor ABT-199 (100 nM) and a combination of S63845 + ABT-199 (100 nM each). MCL-1 inhibition significantly disrupted hiPSC-CM spike amplitude mean and spike slope mean (Figure 7A-B). While there were minimal differences between treatments in the beat period mean or FPD mean (Figure S6A-B), spike slope mean (Figure 7B), conduction velocity mean (Figure 7C), max delay mean (Figure 7D), and propagation consistency (Figure 7E) were significantly lowered in either the S63845 condition or when combined with ABT-199. Cells treated with ABT-199 appeared healthy and were functionally similar to control cells throughout the experiment (Figure 7A-E and Figure S6A-B). Cells displayed mitochondrial network and actin disruption in the S63845-treated condition, and even more severe phenotypes were observed in cells treated with both inhibitors when compared to control cells (Figure 7F-I and Figure S6C-F). BCL-2 inhibition had little effect on mitochondrial network organization and virtually no effect on myofibril organization (Figure 7H and Figure S6E). Our results

further support the idea that MCL-1 is essential for maintaining mitochondrial homeostasis of human cardiomyocytes (Figure S7).

Discussion

Recent studies have implicated MCL-1 in the maintenance of mitochondrial homeostasis in various cell types (Perciavalle and Opferman, 2013; Rasmussen et al., 2018; Senichkin et al., 2019). In this report, we show that MCL-1 inhibition affects human cardiomyocyte functionality potentially due to MCL-1's non-apoptotic role in modulating mitochondrial dynamics. Inhibition of MCL-1 using BH3 mimetics is a promising strategy to treat tumors (Hird and Tron, 2019), since resistance to chemotherapy is often associated with MCL-1 upregulation (Kotschy et al., 2016). To optimize the use of MCL-1 inhibitors, a deeper understanding of the biology of MCL-1 is crucial. Our studies show that MCL-1 inhibition affects human cardiomyocyte functional parameters such as spike amplitude, beat propagation, and conduction velocity, which overlap with disruption of the mitochondrial and actin networks, ultimately leading to cell death.

Cardiomyocytes exposed to MCL-1 inhibitors appear to exhibit bradycardia and arrhythmia phenotypes. Interestingly, these phenotypes were not seen in cells treated with Venetoclax, indicating that hiPSC-CMs are less dependent on BCL-2, and highlighting a potential role for MCL-1 beyond its canonical function in apoptosis. This is further supported by the finding that hiPSC-CMs treated with 100 nM S63845 alone were alive, but not beating, after two weeks of treatment.

We hypothesize that this alternate function of MCL-1 in maintaining mitochondrial homeostasis is due to its interactions with DRP-1 and OPA1, which are essential regulators of mitochondrial morphology and dynamics (Labbé et al., 2014; Nishimura et al., 2018). Treatment of iPSC-CMs with MCL-1 inhibitor caused disruption of the mitochondrial network and significantly decreased MCL-1 proximity to DRP-1 at the mitochondria. Since the interaction with OPA1 was not disturbed, it is possible that MCL-1 interacts with OPA1 either through a different domain, or with a different isoform of OPA1 in hiPSC-CMs than in hPSCs (Rasmussen et al., 2018). Another possibility is that, upon differentiation, the small molecule can no longer penetrate the inner mitochondrial membrane. We also confirmed that the mitochondrial network disruption is dependent on DRP-1, since DRP-1 knockdown prevented the fragmentation caused by MCL-1 inhibition. The recruitment of DRP-1 to the mitochondria has been proposed to be a critical inducer of mitophagy (Lee et al., 2011; Kageyama et al., 2014; Burman et al., 2017). Thus, an interesting possibility is that inhibition of MCL-1 is decreasing clearing of damaged mitochondria in cardiomyocytes. It will be important to test if key proteins involved in mitophagy are affected in the presence of MCL-1 inhibitors.

The photo-conversion experiments in this study did not test for fragmentation directly; thus it is possible that the mitochondrial phenotypes are caused by a lack of fusion or mitochondrial motility. Further studies into the mechanism of MCL-1's interaction with DRP-1 and OPA1 could shed light on this possibility. In contrast to iPSCs (Rasmussen et al., 2018), S63845 did not affect the proximity of MCL-1 with OPA1 at the mitochondria. MCL-1 at the mitochondrial matrix has been proposed to regulate β-oxidation of long-fatty acids through interactions with VLCAD, and deletion of MCL-1 from the matrix caused

hyperactivity of β-oxidation. It is tempting to speculate that inhibiting MCL-1 at the matrix of human cardiomyocytes would result in significant damage to the heart.

We investigated the effects of MCL-1 inhibition on calcium flux using the GCaMP5G calcium reporter. Our data shows a significant decrease in calcium flux with all inhibitors tested. These results could help explain the loss of functionality caused by MCL-1 inhibition. In addition to this loss of cardiomyocyte functionality, MCL-1 inhibition also caused significant disruption of actin networks within hiPSC-CMs. There are many possible mechanisms that could drive this phenotype. One hypothesis is that disruption of actin networks could be a result of decreased calcium flux and resultant loss of cardiomyocyte beating. Indeed, previous studies have shown that the maintenance of proper myofibril organization requires functional calcium channels and cellular contractility (Sharp et al., 1997; Simpson et al., 1993). Future studies should aim to test other potential hypotheses, such as altered metabolism and ROS production. Furthermore, cardiomyocytes treated with BH3 mimetics show a mild dose-dependent activation of caspase-3 that was inhibited by QVD. However, when measuring overall cell viability, the most significant rescue of viability was achieved by the necrosis inhibitor, IM-54. How is inhibition of MCL-1 triggering caspase-independent cell death that is inhibited by necroptosis inhibitor? Mitochondrial disruption induced by BH3 mimetics may cause increased oxidative stress that results in the loss of function and viability of cardiomyocytes. This is in agreement with previous reports (Thomas et al 2013), that demonstrated the induction of necrosis in *Mcl-1* deficient murine hearts. The data in this study show that *Mcl-1* deletion did not result in the massive loss of myocytes due to apoptosis (Thomas et al., 2013). It would be of interest to examine the molecular mechanisms behind this phenotype.

MCL-1 inhibition also caused cardiomyocyte death in hormone-matured cells (Parikh et al., 2017). While apoptosis sensitivity has been shown to decrease throughout development (Wright and Deshmukh, 2006; Sarosiek et al., 2017), these matured cells were more sensitive to S63845 treatment than vehicle-treated cells. It would be of interest to determine whether MCL-1 function in mitochondrial dynamics affects the maturation of iPSC-CMs or heart development *in vivo* (Kasahara et al., 2013; Feaster et al., 2015; Parikh et al., 2017). We speculate that other determinants of mitochondrial homeostasis, including mitochondrial biogenesis and mitophagy, may be affected by MCL-1 deficiency as cardiomyocytes mature. While previous studies reported limited effects of S63845 in mouse heart function, a recent study using a humanized mouse model demonstrated that S63845 binds human MCL-1 with higher affinity than mouse MCL-1 (Kotschy et al., 2016; Brennan et al., 2018). While this study did not report significant effects to the heart of humanized mice treated with S63845, the potential interactions of human MCL-1 with mitochondrial dynamics proteins and VLCAD may be species-specific and not completely recapitulated in this mouse model. Collectively these reports highlight the importance of further research on the effect of MCL-1 on human-specific mitochondrial dynamics and metabolism. These results together with previous work from other groups (Thomas et al., 2013; Wang et al., 2013) suggest that hiPSC-CMs may be an appropriate platform to assess the safety and potential off-target effects of MCL-1 inhibitors on adult human hearts.

Studies from our laboratory suggest that inhibition of MCL-1 induces the differentiation of iPSCs (Rasmussen et al., 2018), which is likely associated with changes in metabolism to support cell-type specific processes (Folmes et al., 2016). Since mitochondrial morphology is tightly coupled to metabolic

adaptations, future studies will aim to investigate whether MCL-1 inhibition may cause a metabolic switch from fatty acid β-oxidation to glycolysis. Cardiac contractions depend on energy from these metabolic pathways, and thus cardiac mitochondria are forced to work constantly and likely require strict quality control mechanisms to maintain a functioning state (Dorn et al., 2015). This quality control process could depend in part on MCL-1. In support of this idea, our studies indicate that MCL-1 activity is essential for hiPSC-CM viability and contractility, which could be linked to MCL-1's non-apoptotic function at the mitochondrial matrix. The eventual apoptotic response detected at later time points could be the result of mitochondrial ROS signaling to trigger translocation and activation of BAX (Chaudhari et al., 2007). The disruption of actin and myofibril morphology could also be explained by heightened ROS induction and downstream ROS-mediated damage. Another important aspect that needs to be evaluated is the prevalence of phenotypically normal genetic variants that could predispose otherwise healthy individuals to stress-related cardiomyopathy (Garcia-Pavia et al., 2019). Our results emphasize the need for a more complete molecular understanding of MCL-1's mechanism of action in human cardiomyocytes, as it may reveal new approaches to prevent potential cardiac toxicities associated with chemotherapeutic inhibition of MCL-1.

Limitations of the study

The protocol for myocyte maturation described in Figure 3-6 involves treatment with both tri-iodo-L-thyronine (T3) and dexamethasone, which leads to the generation of extensive T-tubule network and other functional traits of mature myocytes (Parikh et al., 2017). While effective in generating "matured"

T-tubule structures, we did not fully evaluate other traits of cardiomyocyte maturation. Thus, our study could be complemented by other approaches to achieve myocyte maturation (e.g. altering the metabolic state, co-culturing with mesenchymal stem cells or using three-dimensional approaches) (Machiraju and Greenway, 2019; Karbassi et al., 2020). Collective data, however, suggest that MCL-1 activity is required for normal cardiac myocyte mitochondrial activity. The results reported here further support the validity for testing small molecule MCL-1 inhibitors in human iPSC-derived model systems that could reveal potential toxicity prior to admission in phase 1 clinical trials.

Figures and Legends

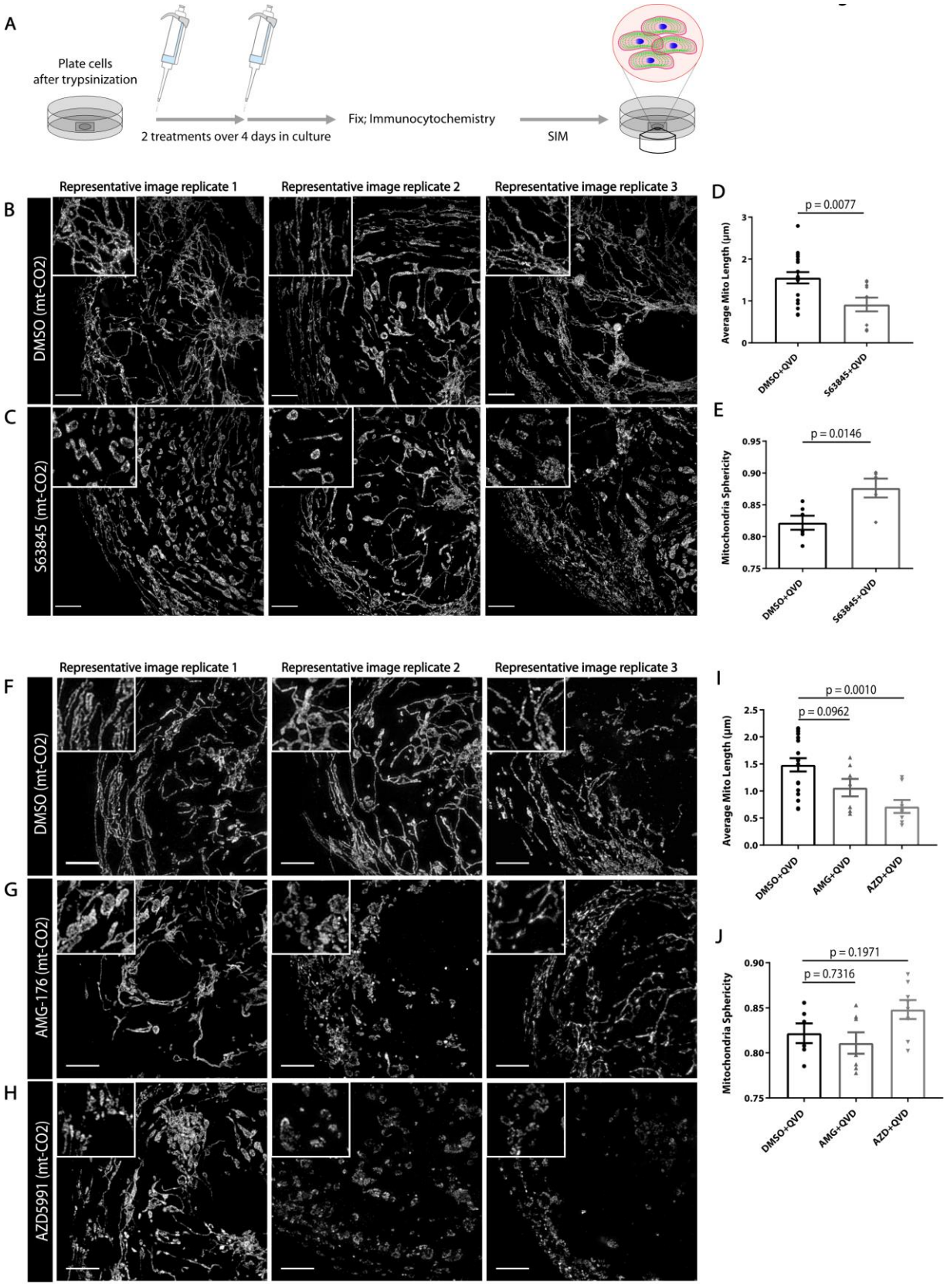

Figure 3-1: MCL-1 inhibition causes mitochondrial fragmentation. (A) Schematic of cell treatment paradigm used throughout this study. Structured Illumination Microscopy (SIM) was used for acquisition of all super-resolution images. hiPSC-CMs were treated with vehicle DMSO **(B)** or 2 μM S63845 **(C)** and Q-VD-Oph (QVD). Quantification of average mitochondrial length **(D)** and mitochondrial sphericity **(E)** are shown, in which a spherical object would have a value of 1.0. hiPSC-CMs were treated with vehicle DMSO **(F)**, 2 μM AMG-176 **(G)**, or 2 μM AZD5991 **(H)** and QVD. Insets show magnification of individual mitochondria morphology. Scale: 5 μm for all mitochondria images. Representative images are shown for all panels. Quantification of mitochondrial length **(I)** and mitochondrial sphericity **(J)** are shown, with AZD5991 treatment significantly decreasing average mitochondrial length. Graphs represent mean ±SEM from at least 3 independent experiments (n > 20 cells per condition). *See also Figure S3-1.*

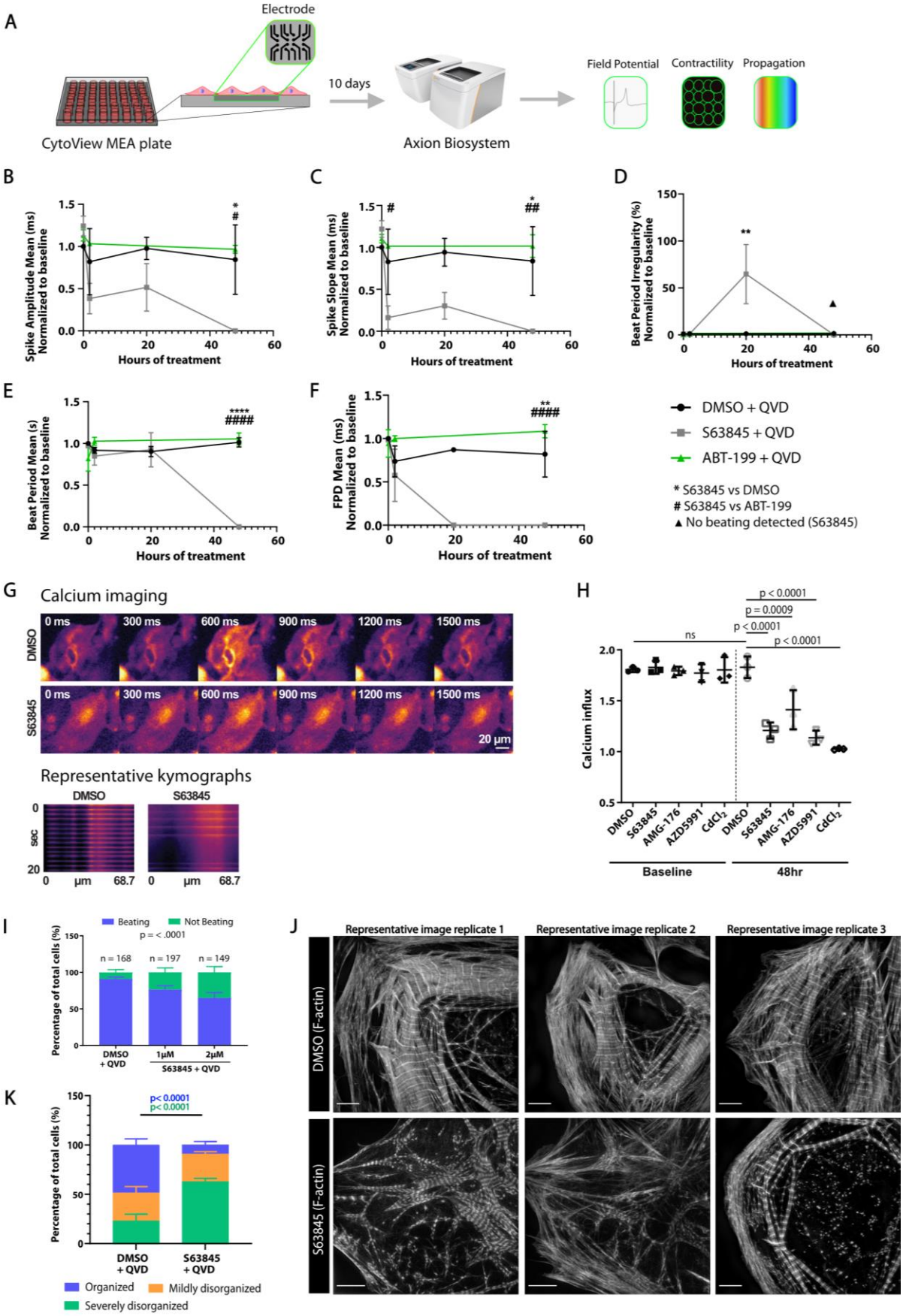
A
Electrode
10 days
Field Potential
Contractility
Propagation
CytoView MEA plate
Axion Biosystem
B
Spike Amplitude Mean (ms) Normalized to baseline
Hours of treatment
C
Spike Slope Mean (ms) Normalized to baseline
Hours of treatment
D
Beat Period Irregularity (%) Normalized to baseline
Hours of treatment
E
Beat Period Mean (s) Normalized to baseline
Hours of treatment
F
FPD Mean (ms) Normalized to baseline
Hours of treatment
DMSO + QVD
S63845 + QVD
ABT-199 + QVD
* S63845 vs DMSO
# S63845 vs ABT-199
▲ No beating detected (S63845)
G
Calcium imaging
DMSO
S63845
0 ms
300 ms
600 ms
900 ms
1200 ms
1500 ms
20 µm
Representative kymographs
DMSO
S63845
sec
µm
68.7
H
Calcium influx
p < 0.0001
p = 0.0009
p < 0.0001
ns
p < 0.0001
DMSO
S63845
AMG-176
AZD5991
CdCl2
Baseline
48hr
I
Beating
Not Beating
p = < .0001
n = 168
n = 197
n = 149
Percentage of total cells (%)
DMSO + QVD
1µM
2µM
S63845 + QVD
J
Representative image replicate 1
Representative image replicate 2
Representative image replicate 3
DMSO (F-actin)
S63845 (F-actin)
K
p< 0.0001
p< 0.0001
Percentage of total cells (%)
DMSO + QVD
S63845 + QVD
Organized
Mildly disorganized
Severely disorganized

Figure 3-2: MCL-1 inhibition causes functional defects and disruption of myofibrils. (A) Schematic of MEA paradigm for recording cardiac performance in live cells. hiPSC-CMs were plated on a CytoView MEA plate (Axion Biosystems) and treated with either vehicle (DMSO), 0.5 μM S63845, or 0.5 μM ABT-199 and QVD. Activity was recorded at baseline (0 hrs), 2 hrs, 20 hrs, and 48 hrs post-initial treatment for 5 minutes each. Spike amplitude mean **(B)**, spike slope mean **(C)**, beat period irregularity **(D)**, beat period mean **(E)**, and field potential duration (FPD) mean **(F)** were recorded. P-values show significance as follows: * = DMSO +QVD vs. S63845 +QVD, # = ABT-199 +QVD vs. S63845 +QVD. One symbol indicates $p < 0.05$, two symbols indicate $p < 0.01$, three symbols indicate $p < 0.001$, and four symbols indicate $p < 0.0001$. P-values were determined by two-way ANOVA. Graphs represent mean ±SEM. **(G)** Representative montage from GCaMP calcium indicator time-lapse imaging in hiPSC-CMs treated with DMSO +QVD or S63845 +QVD (top). Representative kymographs of calcium pulses from individual cells treated with DMSO +QVD or S63845 +QVD (bottom). **(H)** Quantification of calcium influx from hiPSC-CMs treated with QVD and either vehicle DMSO, S63845, AMG-176, or AZD5991, in which a value of 1.0 indicates no change in fluorescence intensity. n=60 cells from 3 independent experiments. Symbols indicate mean and error bars indicate ±SD. **(I)** Proportion of beating vs. not beating hiPSC-CMs in each condition as observed by light microscopy. Significance between beating vs. not beating cells was determined by Chi-square test. Error bars indicate ±SD and percentages were pooled from 3 experiments. **(J)** Vehicle-treated hiPSC-CMs have organized myofibril structure as shown by maximum intensity projections. hiPSC-CMs treated with 2 μM S63845 have myofibrils that are unorganized and poorly defined Z-lines. Scale: 5 μm. Representative images are shown for all panels. **(K)** Quantification of myofibril phenotypes represented in panel I ($n > 20$ cells per condition from 3 separate experiments). Error bars indicate ±SD. *See also Figure S3-2.*

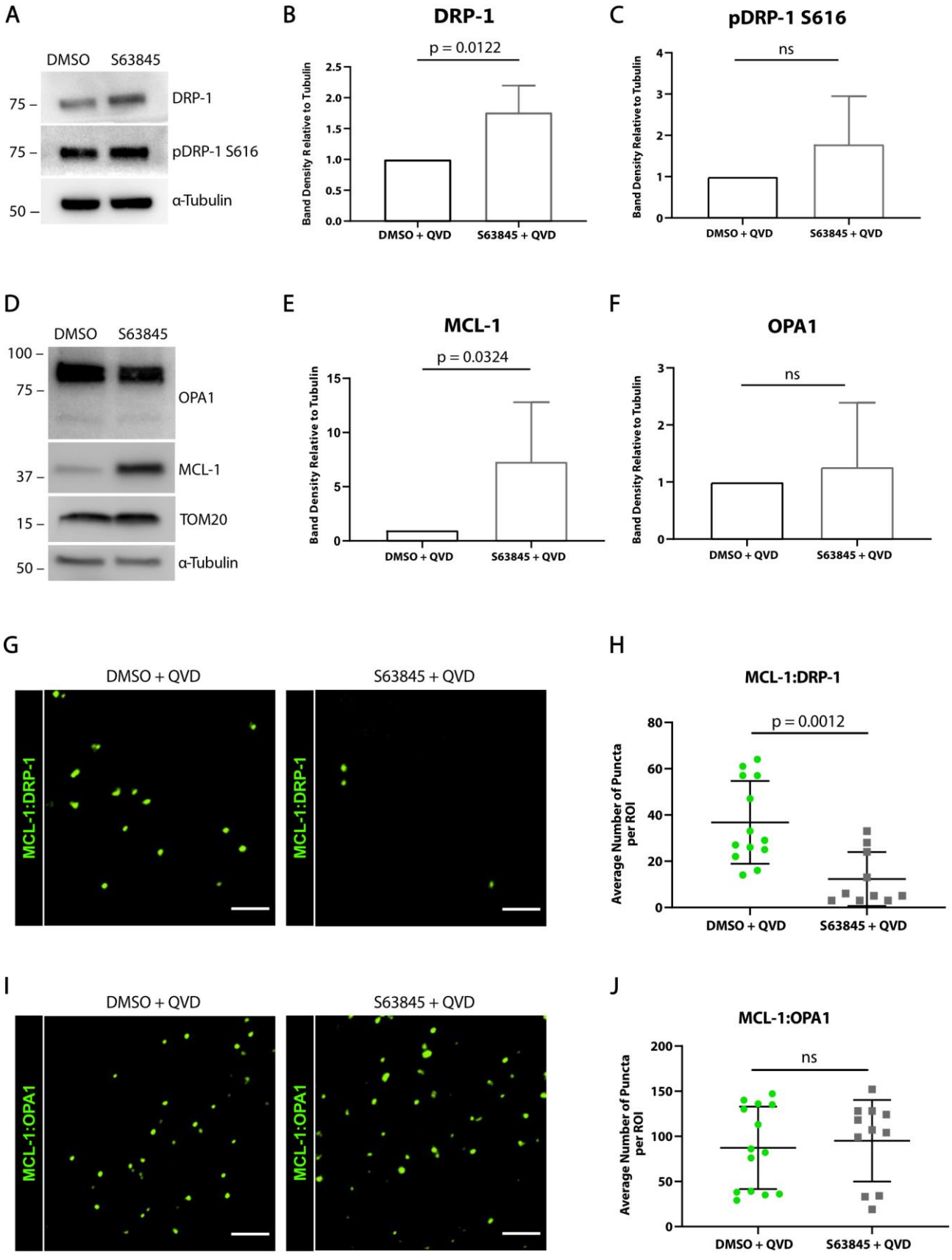
A
DMSO
S63845
75 –
DRP-1
75 –
pDRP-1 S616
50 –
α-Tubulin
B
DRP-1
p = 0.0122
Band Density Relative to Tubulin
DMSO + QVD
S63845 + QVD
C
pDRP-1 S616
ns
Band Density Relative to Tubulin
DMSO + QVD
S63845 + QVD
D
DMSO
S63845
100 –
75 –
OPA1
37 –
MCL-1
15 –
TOM20
50 –
α-Tubulin
E
MCL-1
p = 0.0324
Band Density Relative to Tubulin
DMSO + QVD
S63845 + QVD
F
OPA1
ns
Band Density Relative to Tubulin
DMSO + QVD
S63845 + QVD
G
DMSO + QVD
S63845 + QVD
MCL-1:DRP-1
MCL-1:DRP-1
H
MCL-1:DRP-1
p = 0.0012
Average Number of Puncta per ROI
DMSO + QVD
S63845 + QVD
I
DMSO + QVD
S63845 + QVD
MCL-1:OPA1
MCL-1:OPA1
J
MCL-1:OPA1
ns
Average Number of Puncta per ROI
DMSO + QVD
S63845 + QVD

Figure 3-3: MCL-1 interacts with mitochondrial dynamics proteins. (A) Western blot showing total and phospho- DRP-1 expression in hiPSC-CMs treated with DMSO +QVD or S63845 +QVD. Quantification of DRP-1 **(B)** and pDRP-1 S616 **(C)** band density relative to α-Tubulin (n=3 independent experiments). **(D)** Western blot showing OPA1, MCL-1, and TOM20 levels in hiPSC-CMs treated with S63845 +QVD. Quantification of MCL-1 **(E)** and OPA1 **(F)** band density relative to α-Tubulin (n=3 independent experiments). **(G-J)** Representative ROIs of PLA showing MCL-1:DRP-1 **(G)** or MCL-1:OPA1 **(I)** puncta in vehicle- or S63845-treated hiPSC-CMs. Scale: 5 μm. Quantification of PLA puncta from MCL-1:DRP-1 **(H)** or MCL-1:OPA1 **(J)** interactions (n=10-15 ROIs per condition from 3 independent experiments). All graphs represent mean ±SD. *See also Figure S3-3.*

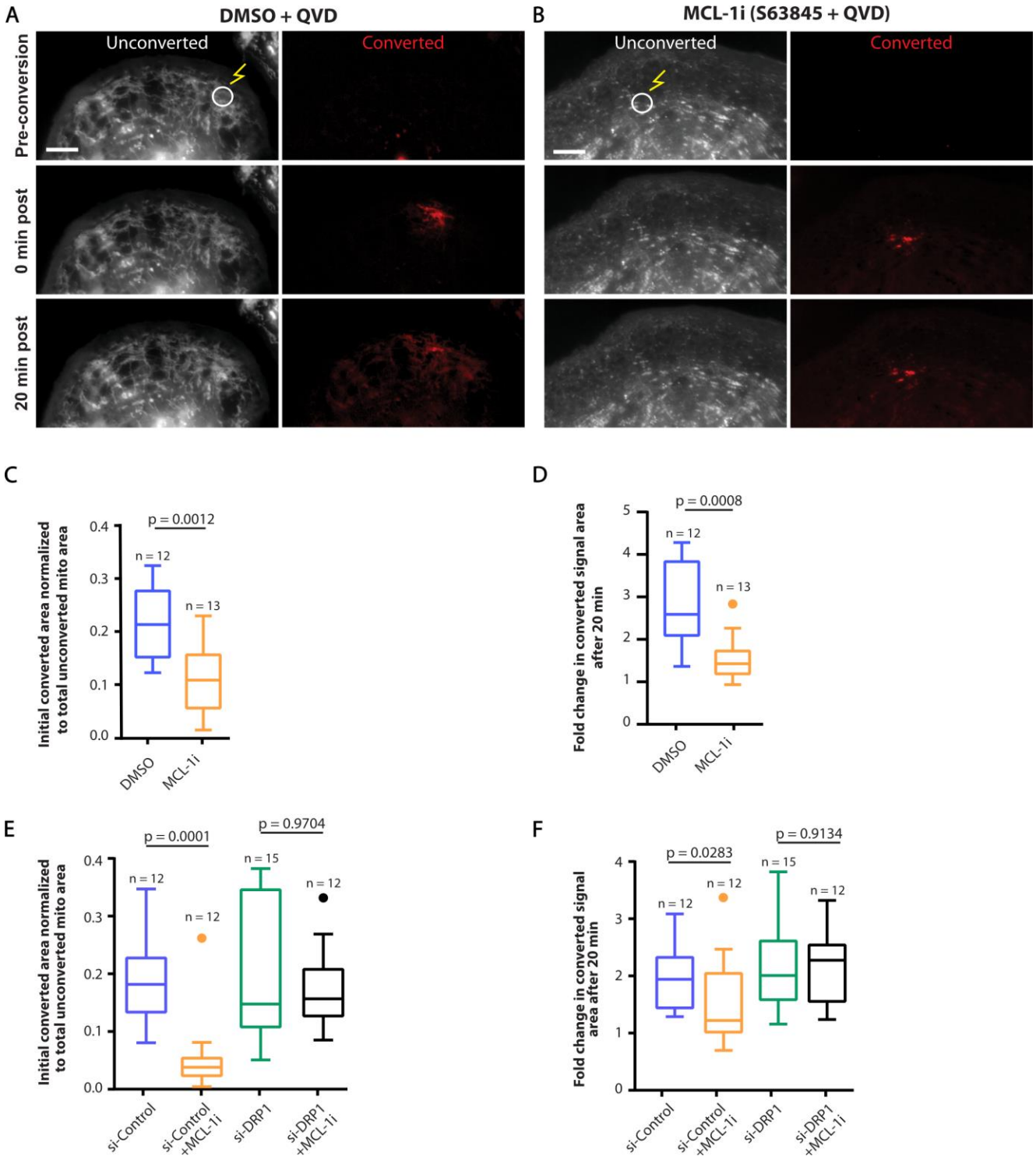
A
DMSO + QVD
Unconverted
Converted
Pre-conversion
0 min post
20 min post
B
MCL-1i (S63845 + QVD)
Unconverted
Converted
C
Initial converted area normalized to total unconverted mito area
p = 0.0012
n = 12
n = 13
DMSO
MCL-1i
D
Fold change in converted signal area after 20 min
p = 0.0008
n = 12
n = 13
DMSO
MCL-1i
E
Initial converted area normalized to total unconverted mito area
p = 0.0001
p = 0.9704
n = 12
n = 12
n = 15
n = 12
si-Control
si-Control +MCL-1i
si-DRP1
si-DRP1 +MCL-1i
F
Fold change in converted signal area after 20 min
p = 0.0283
p = 0.9134
n = 12
n = 12
n = 15
n = 12
si-Control
si-Control +MCL-1i
si-DRP1
si-DRP1 +MCL-1i

Figure 3-4: MCL-1 inhibition results in mitochondrial fragmentation in a DRP-1 dependent manner. (A) Vehicle- and **(B)** S63845-treated hiPSC-CMs were transfected with mito-tdEos and a small area was photo-converted (see methods). Cells were imaged for 20 minutes-post-conversion to assess mitochondrial network connectivity. Scale: 5 μm. Quantification of the initial converted area normalized to total unconverted area **(C)** and fold change in converted area after 20 minutes **(D)** shows decreased initial connectivity and mitochondrial fusion after treatment with 2 μM S63845 and QVD (MCL-1*i*). **(E)** Quantification of initial converted area normalized to total unconverted area in hiPSC-CMs transfected with control siRNA or siRNA targeting DRP-1 ±MCL-1*i* (2 μM S63845) and QVD. **(F)** Quantification of fold change in converted area after 20 minutes in same treatments from Figure 4E. Boxplots represent median of 3 independent experiments and Tukey whiskers. *See also Figure S3-4.*

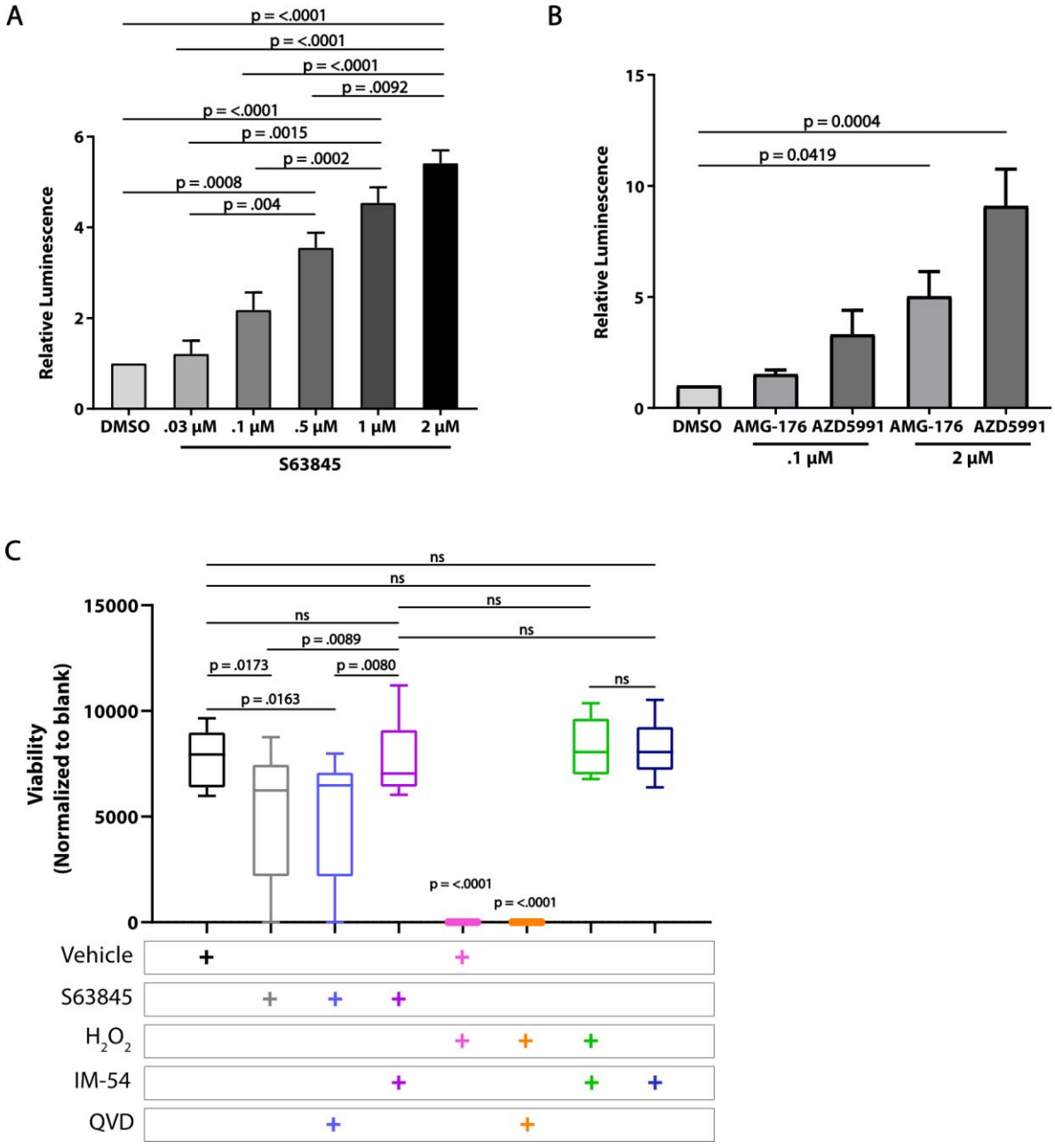
A
p = <.0001
p = <.0001
p = <.0001
p = .0092
p = <.0001
p = .0015
p = .0002
p = .0008
p = .004
Relative Luminescence
0
2
4
6
DMSO
.03 µM
.1 µM
.5 µM
1 µM
2 µM
S63845
B
p = 0.0004
p = 0.0419
Relative Luminescence
0
5
10
15
DMSO
AMG-176
AZD5991
AMG-176
AZD5991
.1 µM
2 µM
C
ns
ns
ns
ns
ns
p = .0089
p = .0173
p = .0080
ns
p = .0163
Viability
(Normalized to blank)
0
5000
10000
15000
p = <.0001
p = <.0001
Vehicle
S63845
H2O2
IM-54
QVD

Figure 3-5: MCL-1 inhibition causes cell death in hiPSC-CMs. hiPSC-CMs were treated with increasing doses of S63845 **(A)** or AMG-176 and AZD5991 **(B)** for 48 hours before caspase activity was measured by CaspaseGlo 3/7 assay (Promega). Quantification shows results from at least 3 independent experiments performed in duplicate and were normalized to DMSO control. Graphs represent mean ±SEM. **(C)** CellTiter-Blue assay (Promega) was used to assess cell viability in hiPSC-CMs. P-values were calculated by one-way ANOVA. Data was quantified from 3 independent experiments performed in triplicate. Boxplots show median with Tukey whiskers. *See also Figure S3-5.*

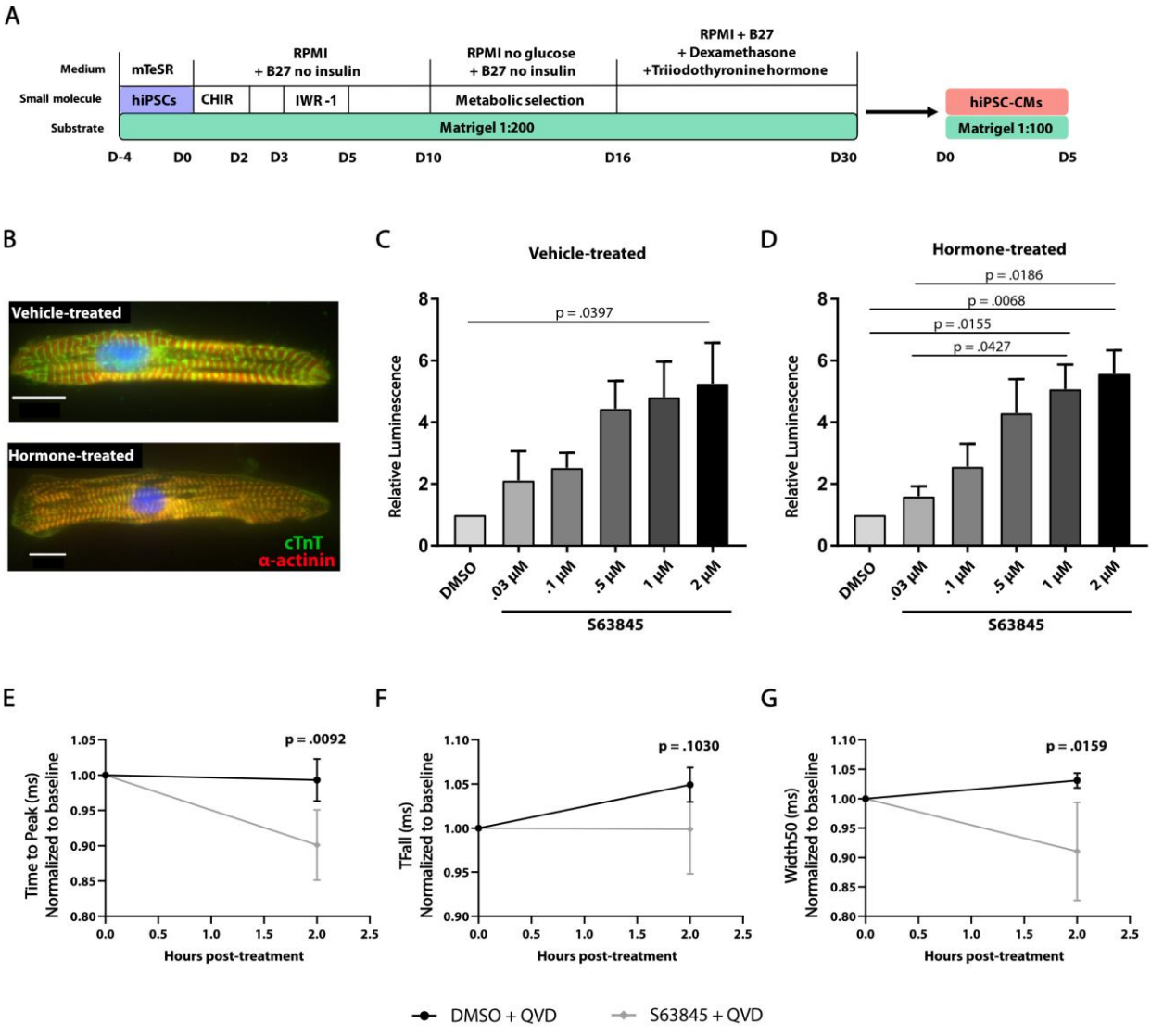
A
Medium
Small molecule
Substrate
mTeSR
RPMI
+ B27 no insulin
RPMI no glucose
+ B27 no insulin
RPMI + B27
+ Dexamethasone
+Triiodothyronine hormone
hiPSCs
CHIR
IWR -1
Metabolic selection
Matrigel 1:200
hiPSC-CMs
Matrigel 1:100
D-4
D0
D2
D3
D5
D10
D16
D30
D0
D5
B
Vehicle-treated
Hormone-treated
cTnT
α-actinin
C
Vehicle-treated
p = .0397
Relative Luminescence
DMSO
.03 μM
.1 μM
.5 μM
1 μM
2 μM
S63845
D
Hormone-treated
p = .0186
p = .0068
p = .0155
p = .0427
Relative Luminescence
DMSO
.03 μM
.1 μM
.5 μM
1 μM
2 μM
S63845
E
p = .0092
Time to Peak (ms)
Normalized to baseline
Hours post-treatment
F
p = .1030
TFall (ms)
Normalized to baseline
Hours post-treatment
G
p = .0159
Width50 (ms)
Normalized to baseline
Hours post-treatment
DMSO + QVD
S63845 + QVD

Figure 3-6: MCL-1 inhibition causes caspase activation and functional defects in mature hiPSC-CMs. (A) Schematic of maturation protocol for hiPSC-CMs using hormone method. **(B)** hiPSC-CMs treated with dexamethasone (Dex) and triiodothyronine (T3) display more mature myofibril phenotype compared to vehicle-treated control cells. Scale: 10 μm. **(C)** Vehicle- or **(D)** Dex+T3-treated hiPSC-CMs were exposed to S63845 at increasing doses for 24 hours. Caspase activity was measured as in Figure 5A-B using the CaspaseGlo 3/7 assay. Quantification was performed from 3 independent maturation experiments in duplicate. Graphs represent mean ±SEM. **(E-G)** CardioExcyte96 recordings show disruption of cardiac activity in Dex+T3-matured hiPSC-CMs when treated with 100 nM S63845. Data was quantified for Time to Peak **(E)** Time to Fall (TFall) **(F)**, and Width50 **(G)**. Quantification was performed from 3 independent maturation experiments for at least 5 wells per condition. P-values were calculated by two-way ANOVA and graphs show mean ±SEM.

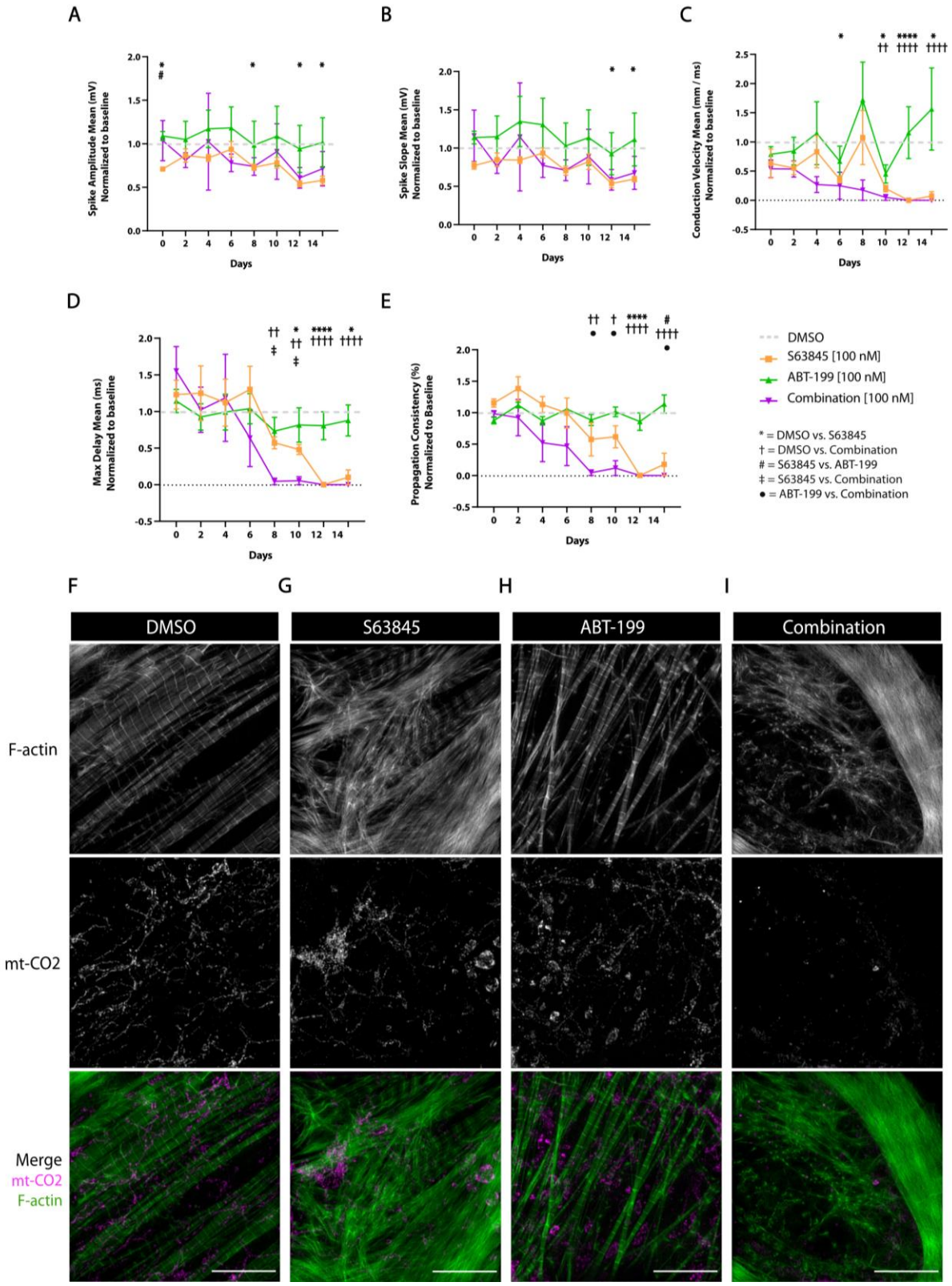
A
B
C
D
E
F
G
H
I
Spike Amplitude Mean (mV) Normalized to baseline
Spike Slope Mean (mV) Normalized to baseline
Conduction Velocity Mean (mm / ms) Normalized to baseline
Max Delay Mean (ms) Normalized to baseline
Propagation Consistency (%) Normalized to Baseline
Days
DMSO
S63845 [100 nM]
ABT-199 [100 nM]
Combination [100 nM]
* = DMSO vs. S63845
† = DMSO vs. Combination
# = S63845 vs. ABT-199
‡ = S63845 vs. Combination
● = ABT-199 vs. Combination
DMSO
S63845
ABT-199
Combination
F-actin
mt-CO2
Merge
mt-CO2
F-actin

Figure 3-7: Chronic inhibition of MCL-1, but not BCL-2, results in cardiac activity defects. hiPSC-CMs were treated every 2 days with DMSO, 100 nM S63845 (orange), 100 nM ABT-199 (green), or both inhibitors (magenta) for 14 days. MEA recordings were taken 2 hours following each treatment for 5 minutes and results were normalized to baseline recording for each respective well, followed by normalization to DMSO (gray dotted line). Results of recordings for spike amplitude mean **(A)**, spike slope mean **(B)**, conduction velocity mean **(C)**, max delay mean **(D)**, and propagation consistency **(E)** are shown. P-values show significance as follows: * = DMSO vs. S63845, † = DMSO vs. Combination, # = S63845 vs. ABT-199, ‡ = S63845 vs. Combination, ● = ABT-199 vs. Combination. One symbol indicates $p < 0.05$, two symbols indicate $p < 0.01$, three symbols indicate $p < 0.001$, and four symbols indicate $p < 0.0001$. P-values were determined by two-way ANOVA. Graphs represent mean ±SEM. **(F-I)** Mitochondria and F-actin were imaged at the end of the treatment paradigm in Figure 6A-E. Representative images are shown of cells treated with DMSO **(F)**, 100 nM MCL-1*i* (S63845) **(G)**, 100 nM ABT-199 **(H)**, and 100 nM S63845 + 100 nM ABT-199 (Combination) **(I)**. Scale: 10 μm. *See also Figure S3-6.*

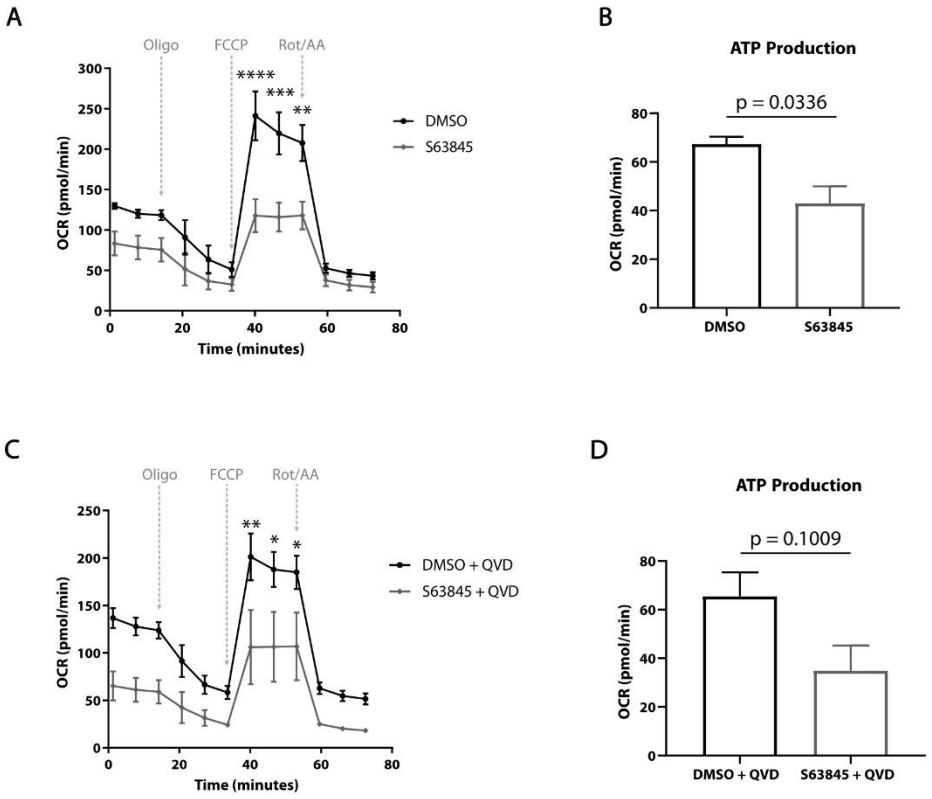

Figure S3-1. Analysis of oxygen consumption in hiPSC-CMs treated with MCL-1 inhibitor. **(A, C)** Oxygen consumption rate (OCR) was measured using the Seahorse Biosciences Mito Stress Test on an XFe96 analyzer. OCR after injection of FCCP was significantly reduced in cells treated with S63845 only **(A)** and S63845 +QVD **(C)** compared to vehicle controls (n = 3 independent experiments done in triplicate). *p < .05, **p <.01, ***p <.001, and ****p <.0001. Error bars indicate ±SEM. **(B, D)** ATP production was calculated from the corresponding OCR traces in panels A and C for each condition. ATP production was reduced in both conditions, with S63845 treatment alone resulting in significant impairment of ATP production compared to vehicle control **(B)**. Graphs represent mean ±SEM and p-values were determined by student's t-test.

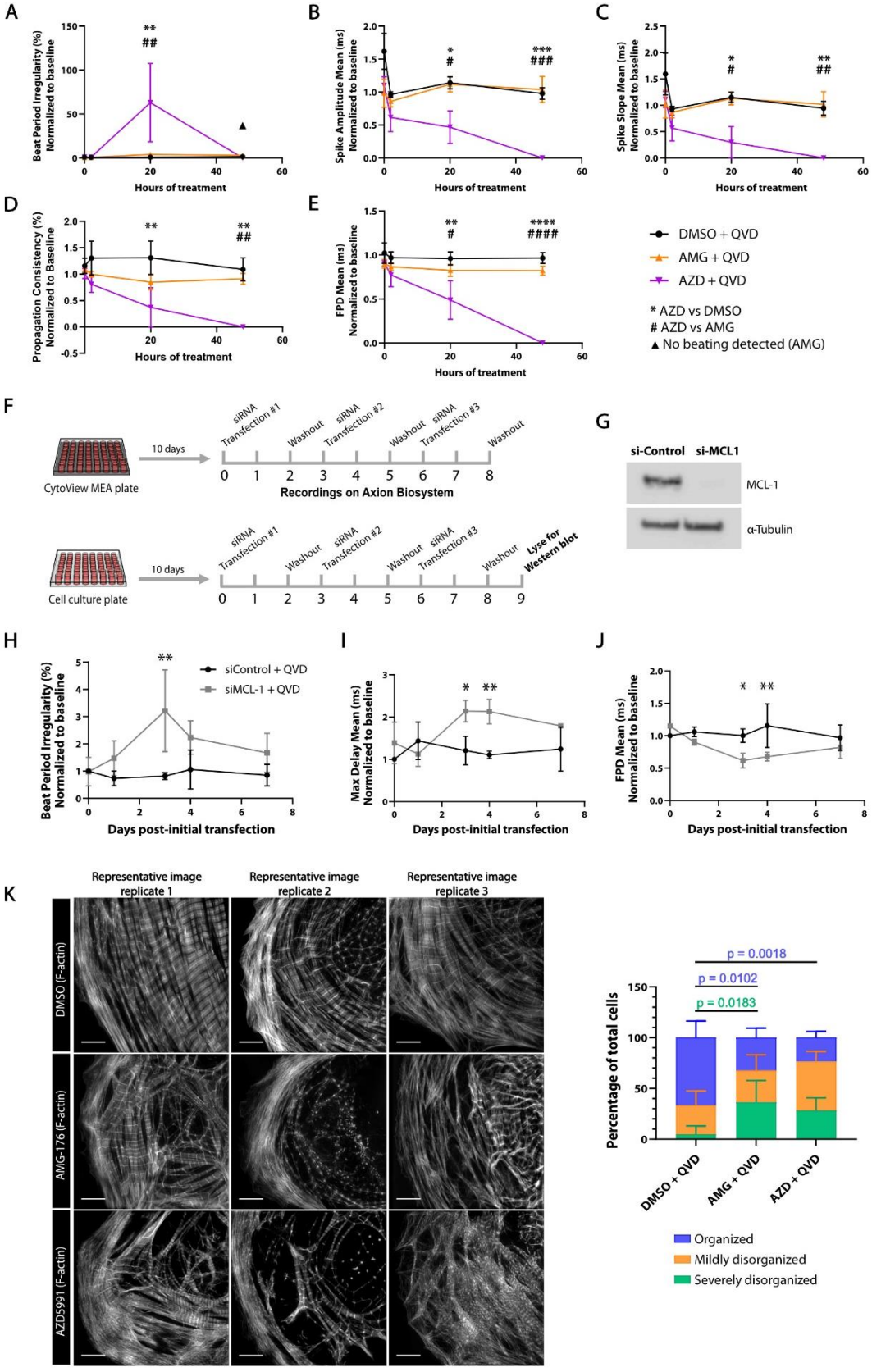
A
Beat Period Irregularity (%) Normalized to baseline
Hours of treatment
B
Spike Amplitude Mean (ms) Normalized to baseline
Hours of treatment
C
Spike Slope Mean (ms) Normalized to baseline
Hours of treatment
D
Propagation Consistency (%) Normalized to Baseline
Hours of treatment
E
FPD Mean (ms) Normalized to baseline
Hours of treatment
DMSO + QVD
AMG + QVD
AZD + QVD
* AZD vs DMSO
# AZD vs AMG
▲ No beating detected (AMG)
F
CytoView MEA plate
10 days
siRNA Transfection #1
Washout
siRNA Transfection #2
Washout
siRNA Transfection #3
Washout
Recordings on Axion Biosystem
Cell culture plate
Lyse for Western blot
G
si-Control
si-MCL1
MCL-1
α-Tubulin
H
siControl + QVD
siMCL-1 + QVD
Beat Period Irregularity (%) Normalized to baseline
Days post-initial transfection
I
Max Delay Mean (ms) Normalized to baseline
Days post-initial transfection
J
FPD Mean (ms) Normalized to baseline
Days post-initial transfection
K
Representative image replicate 1
Representative image replicate 2
Representative image replicate 3
DMSO (F-actin)
AMG-176 (F-actin)
AZD5991 (F-actin)
p = 0.0018
p = 0.0102
p = 0.0183
Percentage of total cells
DMSO + QVD
AMG + QVD
AZD + QVD
Organized
Mildly disorganized
Severely disorganized

Figure S3-2. (A) hiPSC-CMs were plated on a CytoView MEA plate (Axion Biosystems) and treated with QVD and vehicle (DMSO), 0.5 μM AMG-176, or 0.5 μM AZD5991. Live-cell activity was recorded for 5 minutes and results were normalized to baseline recordings for each well. Beat period irregularity **(A)** was increased at 18 hrs in AZD-treated cells before cells stopped beating at 48 hrs, while DMSO and AMG had low levels of beat period irregularity overall. Spike amplitude mean **(B)** and spike slope mean **(C)** were both decreased by 20 hrs and completely reduced by 48 hrs in the AZD condition. Propagation consistency **(D)** and field potential duration (FPD) **(E)** were both significantly reduced in AZD-treated cells at 20 hrs in comparison to DMSO control and AMG-176. P-values were determined by two-way ANOVA and show significance as follows: * = DMSO +QVD vs. AZD5991 +QVD, # = AZD5991 +QVD vs. AMG-176 +QVD. One symbol indicates $p < 0.05$, two symbols indicate $p < 0.01$, three symbols indicate $p < 0.001$, and four symbols indicate $p < 0.0001$. Graphs represent mean ±SEM. **(F)** Schematic of MCL-1 knockdown experiments. hiPSC-CMs were plated from thaw in either the CytoView MEA plate or in a tissue culture-treated 96-well plate and fed regularly for 10 days, followed by three rounds of siRNA transfection. Cells in the 96-well plate were lysed for Western blot following the third round of transfection. **(G)** Representative Western blot showing efficient knockdown of MCL-1 protein using siRNA. **(H-J)** Axion MEA recordings were taken as in panels A-E. Baseline recordings were taken at 0 days (pre-transfection), and subsequent recordings were taken at days 1, 3, 4, and 7 over the course of the knockdown paradigm depicted in panel F (n = 3 replicate experiments). MCL-1 knockdown resulted in higher beat period irregularity **(H)**, higher maximum delay mean **(I)**, and shorter FPD mean **(J)** compared to non-targeting control siRNA. *$p < 0.05$, **$p < 0.01$. Graphs indicate mean ±SD. **(K)** Vehicle-treated hiPSC-CMs have organized myofibril structure as shown by maximum intensity projections. hiPSC-CMs treated with 2 μM AMG-176 or 2 μM AZD5991 have myofibrils that are unorganized and poorly defined Z-lines when compared to controls. Scale: 5 μm. Representative images are shown for all panels. Quantification of myofibril phenotypes is shown (n > 20 cells per condition from 3 separate experiments). Error bars indicate ±SD.

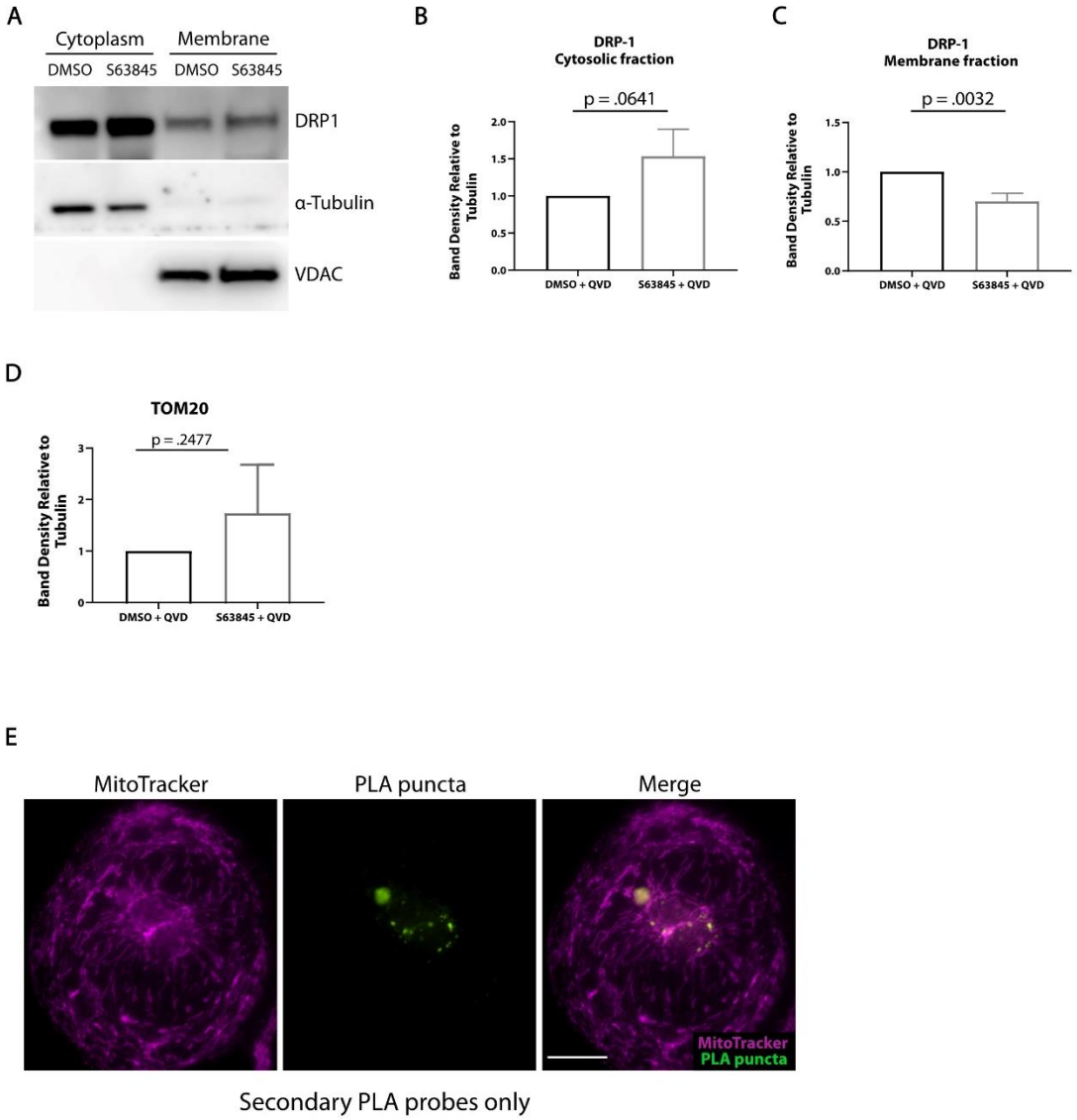
A
Cytoplasm
Membrane
DMSO
S63845
DMSO
S63845
DRP1
α-Tubulin
VDAC
B
DRP-1
Cytosolic fraction
p = .0641
Band Density Relative to Tubulin
DMSO + QVD
S63845 + QVD
C
DRP-1
Membrane fraction
p = .0032
Band Density Relative to Tubulin
DMSO + QVD
S63845 + QVD
D
TOM20
p = .2477
Band Density Relative to Tubulin
DMSO + QVD
S63845 + QVD
E
MitoTracker
PLA puncta
Merge
MitoTracker
PLA puncta
Secondary PLA probes only

Figure S3-3. (A) Representative Western blot showing cytosolic fraction and membrane fractions from hiPSC-CM protein lysates treated with vehicle or S63845 and QVD. Quantification of DRP-1 signal intensity normalized to either α-Tubulin for the cytosolic fraction **(B)** or VDAC for the membrane fraction **(C)**. Western blots from 3 independent experiments were quantified and graphs represent mean ±SD. **(D)** Quantification for TOM20 band density from the experiment shown in Figure 3C. Graph represents mean ±SD. **(E)** Representative image of secondary PLA probe control sample showing non-specific puncta in green. The area around the nucleus was avoided for all quantification purposes. Scale: 20 μm.

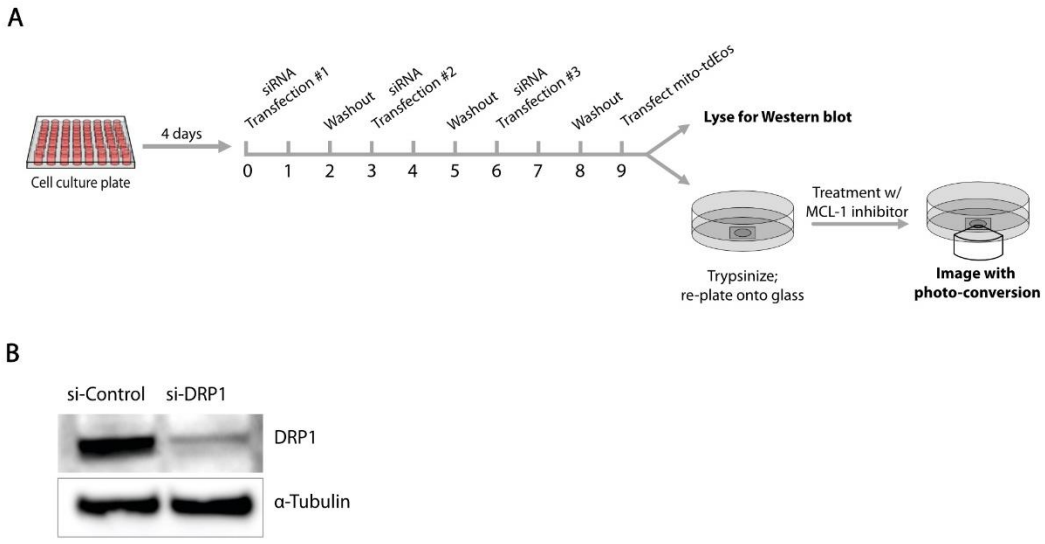

Figure S3-4. (A) Schematic of DRP-1 knockdown experiment followed by photo-conversion of mito-tdEos corresponding to Figure 4E-F. **(B)** Representative Western blot showing knockdown of DRP-1 compared to control siRNA corresponding to Figure 3-4E-F.

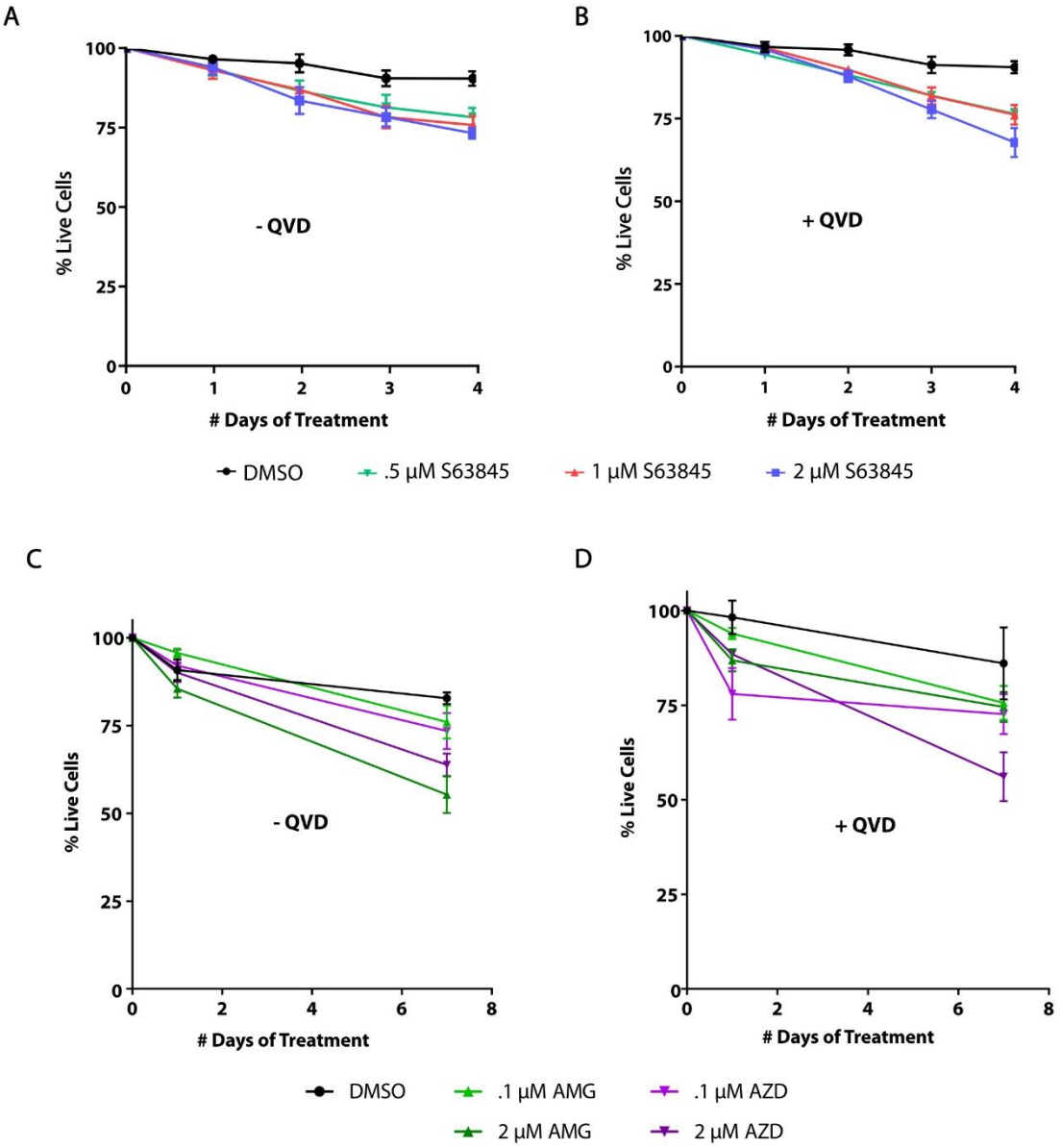
A
B
C
D
% Live Cells
# Days of Treatment
- QVD
+ QVD
DMSO
.5 µM S63845
1 µM S63845
2 µM S63845
.1 µM AMG
2 µM AMG
.1 µM AZD
2 µM AZD

Figure S3-5. hiPSC-CMs were treated with S63845 at the indicated concentrations and either vehicle DMSO **(A)** or with QVD **(B)**. Cell survival was measured over 4 days using an IncuCyte live cell imaging system. Representative images from each day of treatment were quantified and percentages of live cells are shown normalized to day 0 baseline. Graphs represent mean ±SEM and experiments were performed in 4 independent replicates. **(C-D)** hiPSC-CMs were treated with the indicated concentrations of AMG-176 or AZD5991 and vehicle DMSO **(C)** or QVD **(D)**. Cell survival was measured and quantified as in panels A-B. Graphs represent mean ±SEM and experiments were performed in 3 independent replicates.

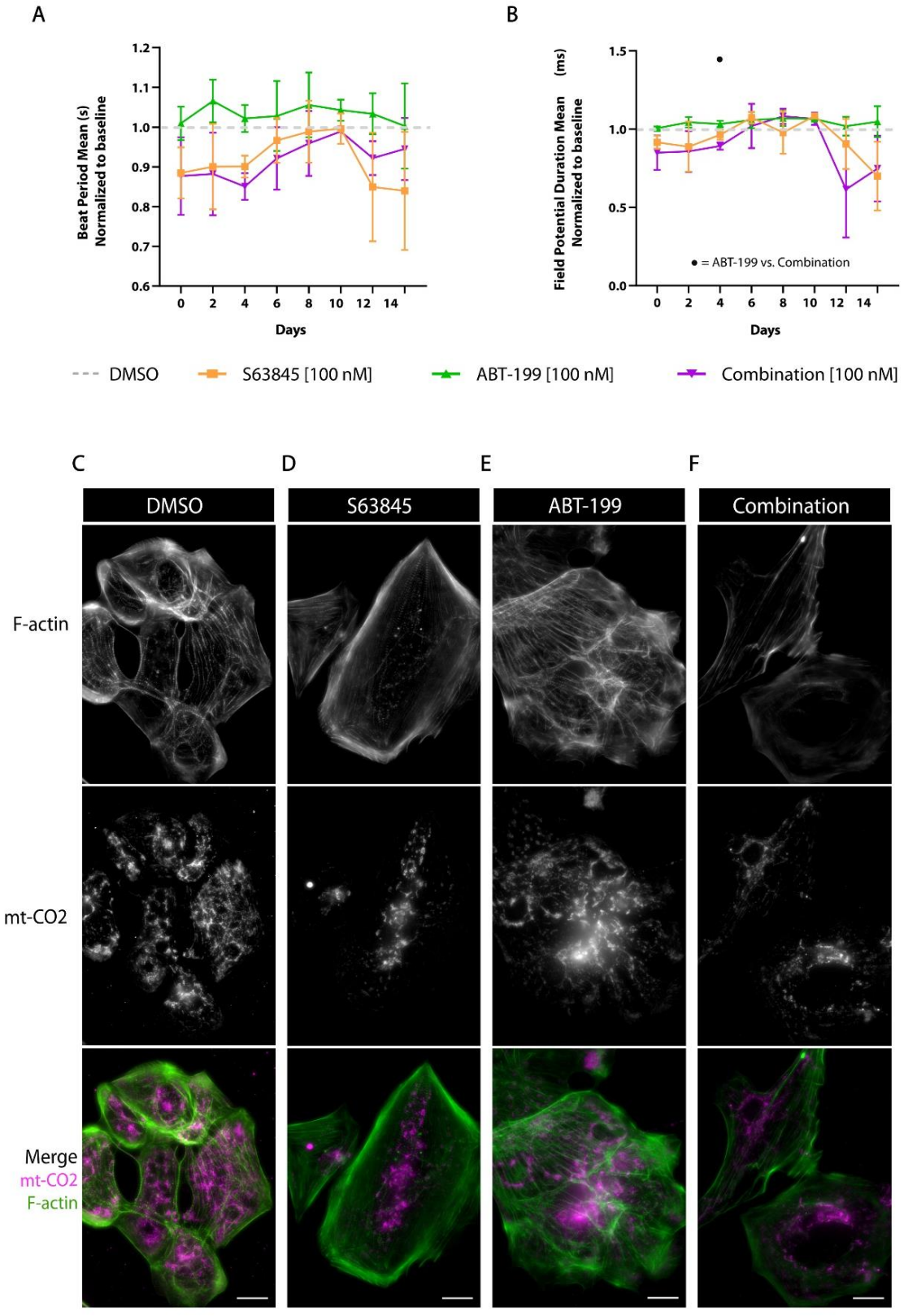
A
B
Beat Period Mean (s)
Normalized to baseline
Field Potential Duration Mean (ms)
Normalized to baseline
Days
Days
● = ABT-199 vs. Combination
DMSO
S63845 [100 nM]
ABT-199 [100 nM]
Combination [100 nM]
C
D
E
F
DMSO
S63845
ABT-199
Combination
F-actin
mt-CO2
Merge
mt-CO2
F-actin

Figure S3-6. Chronic inhibition of MCL-1, but not BCL-2, results in cardiac activity defects. hiPSC-CMs were treated every 2 days with DMSO, 100 nM MCL-1i (S63845 - orange), 100 nM BCL-2i (ABT-199 - green), or both inhibitors (magenta) for 14 days. MEA plate was recorded 2 hours following each treatment for 5 minutes and results were normalized to baseline recording for each respective well, followed by normalization to DMSO (gray dotted line). Results of recordings for beat period mean **(A)** and field potential duration mean **(B)** are shown. P-values were calculated by two-way ANOVA and show significance as follows: * = DMSO vs. S63845, † = DMSO vs. Combination, # = S63845 vs. ABT-199, ‡ = S63845 vs. Combination, ● = ABT-199 vs. Combination. One symbol indicates $p < 0.05$, two symbols indicate $p < 0.01$, three symbols indicate $p < 0.001$, and four symbols indicate $p < 0.0001$. Error bars indicate ±SEM. **(F-I)** Mitochondria and F-actin were imaged at the end of the treatment paradigm in Figure 3-6A-E. Representative SIM images are shown of cells treated with DMSO **(F)**, 100 nM S63845 **(G)**, 100 nM ABT-199 **(H)**, and 100 nM S63845 + 100 nM ABT-199 (Combination) **(I)**. Scale: 10 μm.

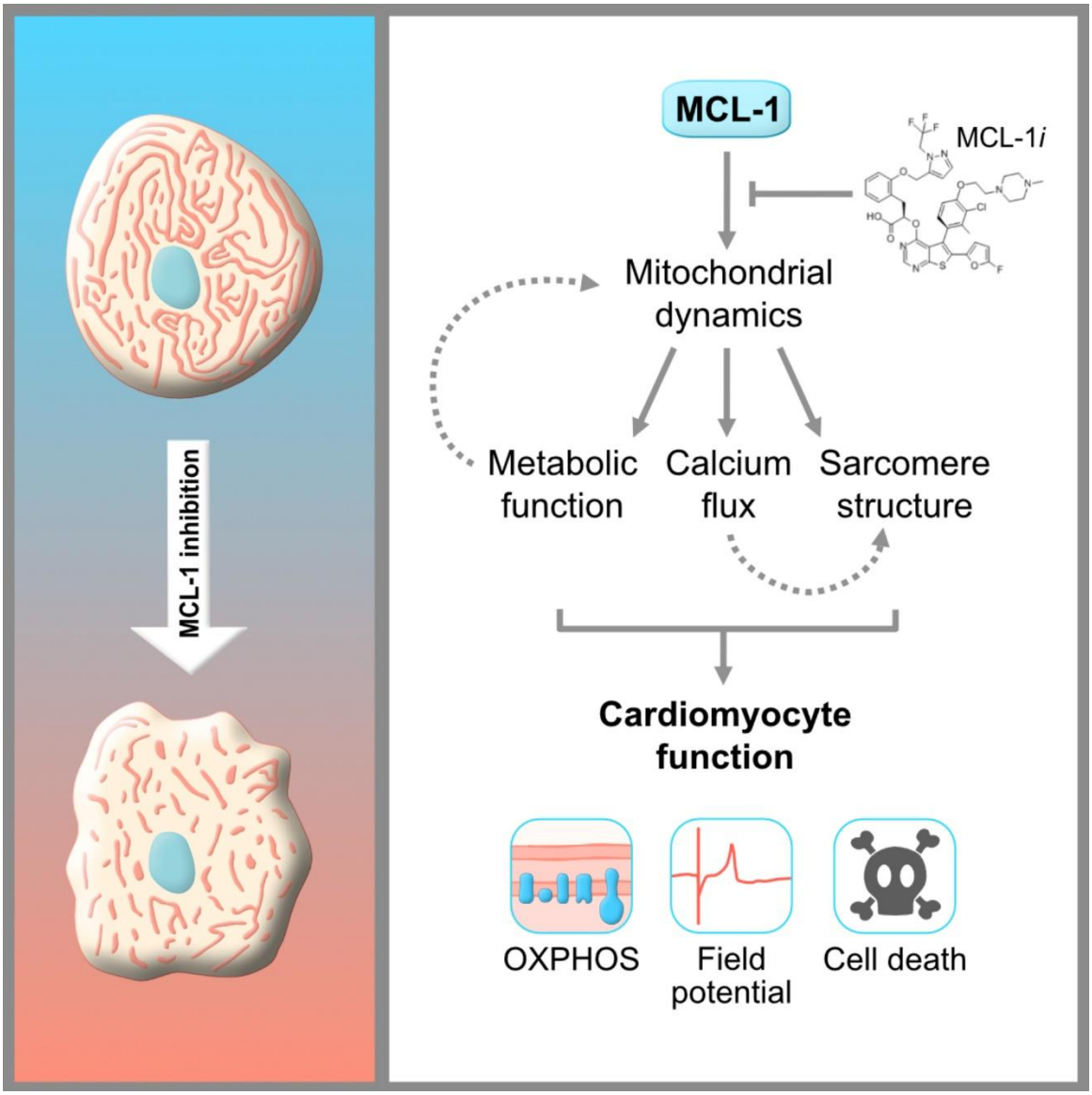

Figure S3-7: Model of main findings described in Chapter 3.

Chapter 4

FINAL DISCUSSION, CONCLUSIONS, AND FUTURE DIRECTIONS

Introduction

Pluripotent stem cells model the earliest stage of embryonic development, before cell specification and patterning occurs. During this vulnerable period, genetic integrity of these cells is especially important for assuring the survival and proper development of the organism. To prevent the dissemination of harmful mutations, stem cells are able to engage a rapid apoptotic response. While this response to DNA damage is p53-mediated, localization and function of p53 is not altered in hESCs in comparison to differentiated cells (Liu et al., 2013). Instead, hESC apoptotic sensitivity is mediated by a process termed mitochondrial "priming," in which levels of the pro-apoptotic (e.g. PUMA) and anti-apoptotic (e.g. BCL-2) members of the BCL-2 family are shifted to favor closer proximity to the apoptotic threshold (Liu et al., 2013). The property of mitochondrial priming has been applied to cancer cell therapeutic diagnosis, termed dynamic BH3 profiling, in which early drug-induced death signaling is measured to predict chemotherapy response across cancer types (Montero et al., 2015). While levels of pro- and anti-apoptotic proteins are important determinants of mitochondrial priming and cell death fate, specific tuning of apoptotic sensitivity likely depends on post-translational modifications, sub-cellular localization, and interactions with other proteins. Demonstrating this, another study showed the pro-apoptotic effector protein BAX,

which resides in an inactive cytosolic state in differentiated cells, was shown to be maintained in an active conformation localized at the Golgi in H9 hESCs (Dumitru and Gama et al., 2012). This conformation likely contributes to the primed mitochondrial state in which to rapidly engage cytochrome c release and caspase 3/7 cleavage in the event of DNA damage. Since PSCs also maintain fragmented mitochondrial networks that promote the pluripotent state, we hypothesized the highly expressed members of the BCL-2 family may contribute to mitochondrial phenotypes in these cells. Counterintuitively, the anti-apoptotic protein MCL-1 was found to have higher levels of expression in hESCs, which suggests MCL-1 is not a major factor for mitochondrial priming. The question remained as to why MCL-1 is so highly expressed in apoptosis-sensitive stem cells and whether this high expression confers dependence on MCL-1 for survival. The research presented in this dissertation has shed light onto the mechanisms by which MCL-1 maintains cell viability through its regulation of mitochondrial dynamics and function in stem and progenitor cells.

The major theme of the Gama laboratory is to understand the molecular mechanisms by which mitochondria control the fundamental properties of stem cell pluripotency and self-renewal. Here, I have described an unexpected, non-cell death function of MCL-1 in regulating mitochondrial dynamics and metabolism in PSCs and cardiomyocytes. We found that MCL-1 is induced upon reprogramming, and its depletion in PSCs induces changes to the mitochondrial network, as well as loss of key pluripotency transcription factors OCT4 and NANOG. Results from our studies show that MCL-1 localization at the mitochondrial matrix appears to be important for retaining self-renewal capacity. Mechanistically, we found MCL-1 to interact with DRP-1 and OPA1, two GTPases responsible for remodeling the

mitochondrial network. Depletion of MCL-1 compromised the levels and activity of these crucial regulators of mitochondrial dynamics. After these results were published, I became interested in whether these interactions between MCL-1 and the mitochondrial dynamics regulators are also maintained upon differentiation of PSCs to cardiomyocytes (hiPSC-CMs). In these cells, inhibition of MCL-1 by BH3 mimetics resulted in the disruption of mitochondrial morphology and dynamics as well as disorganization of the actin cytoskeleton. Interfering with MCL-1 function affected the homeostatic proximity of DRP-1 and MCL-1 at the outer mitochondrial membrane, resulting in decreased functionality of hiPSC-CMs. Cardiomyocytes displayed abnormal cardiac performance even after caspase inhibition, and instead committed to the necrotic cell death pathway. These results support the idea of non-apoptotic activity of MCL-1 in both PSC and hiPSC-CM survival and mitochondrial function. BH3 mimetics targeting MCL-1 are promising anti-tumor therapeutics, and progression toward using these drugs in patients depends on understanding not only MCL-1's canonical function in preventing apoptosis, but also in the maintenance of mitochondrial dynamics and metabolism. Further investigation into the relationship between cell death, mitochondrial dynamics, and the acquisition of pluripotency or a particular stem cell fate opens many exciting opportunities for future mechanistic studies centered on MCL-1. In the following sections, I will introduce some of the possible future directions and implications of MCL-1 research in stem and progenitor cells, focusing on non-canonical MCL-1 interactions at specific mitochondrial sub-compartments, MCL-1 in non-apoptotic cell death programs, MCL-1 connections to mitophagy processes, and the function of organelle contact sites at points of mitochondrial fission. This chapter aims to discuss potential molecular links that intricately connect MCL-1 to these fundamental mitochondrial signaling mechanisms and how they may contribute to human health and disease.

MCL-1 is a multifaceted anti-apoptotic protein

The work presented in this dissertation aimed to fill the gaps in knowledge between the molecular events that connect intrinsic cell death and mitochondrial dynamics in human stem and progenitor cells. Our work reveals MCL-1 as a crucial component of stem cell identity and is a likely interactor of GTPases DRP-1 and OPA1, which may modulate their activity in mitochondrial fission, fusion, and metabolism (Rasmussen et al., 2018, 2020b). However, the exact mechanisms behind the phenotypes that arise from disruption of MCL-1 and the mitochondrial dynamics machinery are still unknown. Mitochondria-nucleus crosstalk likely occurs downstream of MCL-1 in stem cells to regulate cell fate decisions at a transcriptional level (Khacho et al., 2016). MCL-1 regulation of mitochondrial dynamics is not only important in undifferentiated stem cells, but also for cells committed to a cardiac fate. Importantly, we show MCL-1 inhibition using small molecules can be damaging to the health of iPSC-derived cardiomyocytes, which depend highly on MCL-1 for proper mitochondrial function. This highlights the importance of basic science in drug development, and the necessity for testing early-phase cancer therapeutics in human iPSC-derived systems to reveal any potential toxicity before continuing with clinical trials. By studying the role of MCL-1 in mitochondrial dynamics, we can increase our understanding of the essential mechanisms governing pluripotency and self-renewal of stem cells, as well as the contribution of MCL-1 to the structure and function of the mitochondrial network in highly specialized cell types.

MCL-1 is essential for embryonic development and the survival of several cell lineages. Complete deletion of MCL-1 causes embryonic lethality before implantation (embryonic day 3.5) of the blastocyst (Rinkenberger et al., 2000). Likewise, conditional deletion of MCL-1 causes loss of hematopoietic stem and progenitor cells (Opferman et al., 2005), B cell and T cell progenitors (Opferman et al., 2003), activated B cells (Vikstrom et al., 2010), plasma cells required for antibody secretion (Peperzak et al., 2013), neuronal progenitor cells (Arbour et al., 2008) and cardiomyocytes (Thomas et al., 2013; Wang et al., 2013). Our work expands on these findings, identifying MCL-1 as a critical protein for viability of human PSCs and iPSC-derived cardiomyocytes (Rasmussen et al., 2018, 2020b). Still unknown, however, are the mechanisms by which specific cell depletion occurs, as it may be specific to species and cell type, especially considering the vast differences in mitochondrial network morphologies and metabolic properties in PSCs compared to differentiated cells such as neurons and cardiomyocytes. Much is yet to be discovered about why MCL-1 loss is so detrimental to the mitochondria, especially since most reported phenotypes are not due to unchecked apoptosis. Using iPSC-derived systems as a model may uncover new facets of MCL-1 regulation of mitochondrial homeostasis. For example, one future direction of the Gama laboratory is to use CRISPR/Cas9 gene-edited human fibroblasts which lack MCL-1 for the generation of iPSCs through reprogramming. Due to the inability of iPSCs to survive siRNA-mediated knockdown of MCL-1 (Rasmussen et al., 2018), we hypothesize that MCL-1 knockout (KO) cells would not fully reprogram into *bona fide* pluripotent stem cells. To dissect this issue further, we plan to express mutant forms of human MCL-1 based on the mouse constructs developed by the Opferman group (Perciavalle et al., 2012). If MCL-1^{Matrix} rescued the ability of MCL-1 KO fibroblasts to reprogram, this would complement our results shown in Figure 2-3E, in which MCL-1^{Matrix} expression prevented hESC

differentiation. It will be important to image mitochondria at different stages during reprogramming, since complete acquisition of the pluripotent state likely requires extensive remodeling of mitochondrial network morphology and metabolism, which could be mediated in part by MCL-1 activity.

MCL-1 at the OMM and the matrix

Mitochondria are highly motile and are constantly changing shape, having dynamic properties at both macro- and ultrastructural levels. Two distinct but associated membranes are found within the organelle, which are comprised mainly of phospholipids phosphatidylcholine (PC) and phosphatidylethanolamine (PE) (Dudek, 2017). Phosphatidic acid (PA) is a major precursor of cardiolipin (CL), a mitochondria-specific phospholipid, which is imported to the IMM from the ER. CL-deficient cells display abnormally large mitochondria with disorganized cristae (Xu et al., 2006; Acehan et al., 2007, 2009). Both PA and CL have been reported to inhibit and stimulate mitochondrial dynamics through interactions with the core proteins that regulate mitochondrial fission and fusion (i.e. Mitofusins, OPA1 and DRP-1). Specifically, PA stimulates the activity of Mitofusins, and CL has been shown to aid in the production and assembly of OPA1, both of which promote and are necessary for efficient mitochondrial fusion (Ban et al., 2017). CL is found at lower levels in the OMM, most likely in portions of the OMM that border cristae junctions and in areas of high membrane curvature since CL adopts a cone-like shape (Huang et al., 2006). The presence of CL-enriched "hot spots" in the OMM may provide a favorable local environment for mitochondrial division. CL aids in mitochondrial fission through the modulation of

DRP-1 and stimulates its oligomerization through interactions with DRP-1's variable domain (Stepanyants et al., 2015; Francy et al., 2017). Conversely, DRP-1 can also affect the organization of CL in the OMM, which may explain the role of DRP-1 puncta at the mitochondria even in the absence of active scission. DRP-1 regulation is complex, however, due to its lack of transmembrane domain and requirements for post-translational modifications as well as membrane receptor binding. Our studies show MCL-1^{OM} may interact with DRP-1 to help recruit it to the OMM or stabilize it along with its receptors to regulate fission. More complete insight into OMM lipid composition, especially CL content and localization, may help us understand the localization of MCL-1^{OM}, especially if there are two distinct pools of MCL-1 that perform different functions: one which prevents apoptosis by sequestering the BH3-only proteins from BAK/BAX, and one which participates in mitochondrial fission regulation through DRP-1.

Members of the BCL-2 family have been reported to interact with CL in the mitochondrial membrane. After the pro-apoptotic BH3-only protein BID is truncated and activated by caspase-8 (tBID), it docks at CL-rich sites on the OMM, which then allows it to bind and activate BAX (Lutter et al., 2000). Studies in mice have shown that loss of full-length BID can impair proper cristae formation in the absence of an apoptotic stimulus (Salisbury-Ruf et al., 2018). Many of the phenotypes reported in BID-null mice are similar to those in MCL-1 (i.e. cristae morphology defects, reduced ATP production, and cardiomyopathy). Immunoprecipitation experiments from this study showed BID also interacts with MCL-1^{Matrix}, and this interaction is mediated through α-helix-6 of BID, which includes the membrane-binding region. The association of BID with MCL-1^{Matrix} could explain the mitochondrial phenotypes

resulting from BID deletion. Deleting or mutating MCL-1 in this context and observing if these mutations phenocopy each other would be helpful to answer whether these two proteins work together to maintain mitochondrial homeostasis. Additionally, testing whether BID is at the matrix in human cells, especially cardiac myocytes, is also an important future direction. Since BID may interact with MCL-1 at the matrix, it could be hypothesized that BID aids in docking MCL-1 to the IMM and positioning MCL-1's hydrophobic BH3 region toward the matrix, facilitating interactions with other matrix proteins to organize the cristae. It would be interesting to test if this interaction occurs at CL-rich docking sites or at pools of key mitochondrial membrane lipids to enable MCL-1 regulation of matrix proteins such as OPA1 or the ETC components.

At the IMM and cristae, different states of remodeling occur during mitochondrial respiration and cell death signaling (Hackenbrock, 1966; Frank et al., 2001b; Cipolat et al., 2004; Germain et al., 2005; Youle and Bliek, 2012; Ramonet et al., 2013). This plasticity allows for the proper regulation of various cellular processes, including bioenergetics, cell death signaling, and calcium signaling. Not surprisingly, imbalance in flexibility of this response contributes to disruption of tissue homeostasis and the augmentation of disease phenotypes. Particularly during apoptosis, mitochondrial fission and cristae junction remodeling have been shown to occur with the activation of pro-apoptotic proteins BAK and BAX to assist in the release of cytochrome c pools (Frank et al., 2001b; Gao et al., 2001; Lee et al., 2004; Ow et al., 2008; Sheridan et al., 2008; Montessuit et al., 2010; Youle and Bliek, 2012; Sinibaldi et al., 2013). Cristae junctions, where the lamellar invaginations of the IMM are connected to IMM/OMM boundaries, are maintained by several proteins including F_1F_o-ATP synthase, OPA1, and the mitochondrial contact site

and cristae organizing system (MICOS) complex (Glytsou et al., 2016; Wollweber et al., 2017). Proper arrangement and function of OPA1 oligomers are required for cristae junction constriction, and stabilization of the cristae facilitates efficient respiration by coordination of the ETC (Frezza et al., 2006; Varanita et al., 2015; Pernas and Scorrano, 2016). Specifically, the more passive functions of OPA1 in structural maintenance of cristae membranes are performed by short OPA1 isoforms (OPA1-S), as opposed to long isoforms (OPA1-L), which mediate active IMM fusion (Del Dotto et al., 2017). The work shown in Chapter 2 identifies OPA1 as an interacting protein of MCL-1, and this interaction appears to be crucial for stem cell maintenance. However, the mechanisms by which MCL-1 executes this protection is less clear. Does MCL-1^{Matrix} support cristae morphology or ETC stability at the IMM through interactions with OPA1-S isoforms? It is also possible that MCL-1^{Matrix} performs these functions independent of OPA1; if so, it will be important to identify other interacting proteins at the IMM and matrix. One way to address these questions would be to elaborate on the MCL-1 mutant overexpression experiment outlined in the previous section. We could express tagged MCL-1 constructs (MCL-1^{OM} and MCL-1^{Matrix}) in an MCL-1-null cell line, followed by immunoprecipitation and mass spectrometry analysis to identify binding partners of MCL-1 at its specific localizations. To achieve these results in PSCs, this approach would depend on the ability of MCL-1 KO fibroblasts to reprogram while expressing only one form of MCL-1. While we hypothesize MCL-1^{Matrix}-expressing cells will reach the pluripotent state, it is possible that both forms of MCL-1 are required for complete reprogramming to iPSCs. Ultimately, however, only immunoprecipitation of the endogenous MCL-1^{OM} and MCL-1^{Matrix} forms will conclusively identify binding partners and the key residues which determine the interactions within each mitochondrial sub-compartment. This could be achieved using a CRISPR/Cas9 gene-editing approach

to modify *MCL-1*, but thus far it has not been possible to edit the *MCL-1* sequence and preserve only the matrix-residing form. Identification of the protease that post-translationally cleaves MCL-1 at its N-terminal region will also aid us in understanding MCL-1^{Matrix} structure and regulation. Combining these experiments in cells along with *in vitro* binding assays using recombinant MCL-1 mutants could confirm our findings that MCL-1 interacts with OPA1 and DRP-1 at the matrix and OMM, respectively, as well as identify new protein interactions which may support MCL-1's coordination of mitochondrial dynamics.

Another possibility is that MCL-1 ^{Matrix} is not directly involved in cristae/IMM structure but instead maintains mitochondrial bioenergetics. Supporting this idea in MEFs and murine livers, MCL-1^{Matrix} was shown to interact with very long-chain acyl-CoA dehydrogenase (VLCAD), a fundamental enzyme of the mitochondrial fatty acid β-oxidation pathway (Escudero et al., 2018). This interaction occurs through a modified configuration of the MCL-1 BH3 domain, in which the BH3 α-helix extends out of the hydrophobic binding pocket to engage with VLCAD. Blocking this interaction by MCL-1 deletion, or eliminating MCL-1^{Matrix} alone, led to uncontrolled long-chain fatty acid β-oxidation flux in response to nutrient deprivation. While VLCAD was not detected in any of our proteomics experiments as an interacting protein, it will be important to test if MCL-1^{Matrix} also interacts with VLCAD in undifferentiated stem cells. One explanation for why we could not detect VLCAD binding is that perhaps the modified conformation of the MCL-1 BH3 domain only occurs in differentiated cells to support higher dependence on fatty acid β-oxidation pathways. If the outward conformation of the MCL-1 BH3 domain is only present in differentiated cells, this could explain our results in iPSC-CMs in which the close proximity of MCL-1:OPA1 was not disrupted by S63845. Similarly, the VLCAD study also showed

S63845 treatment did not cause differences in the rate of long-chain fatty acid oxidation in MEFs, supporting the idea that small molecule inhibitors of MCL-1 may not block activity of the matrix form in differentiated cells.

MCL-1 as a potential necrosis-modulator

Results from Chapter 3 of this dissertation raise another interesting point about the downstream consequences of MCL-1 inhibition and the ultimate fate of the cell. Intrinsic apoptosis was described in detail in Chapter 1, but other forms of cell death may be activated by MCL-1 perturbations. Necrosis is characterized by cellular and organellar swelling, plasma membrane rupture, and spilling of cellular contents resulting in an inflammatory response (Grooten et al., 1993). While apoptosis and caspase activity do require some level of mitochondrial function to produce ATP, necrosis is ATP-independent and is marked by mitochondrial catastrophe (Skulachev, 2006). Deletion of MCL-1 has also been previously shown to cause necrosis, not apoptosis, in mouse cardiac muscle cells (Thomas et al., 2013). In our human cardiomyocyte studies, we observed impaired ATP production in the presence of the MCL-1 inhibitor, which was not improved by blocking caspase activity with QVD. While caspase 3/7 activity was present in a dose-dependent manner after MCL-1 inhibition, indicating the apoptotic pathway was triggered at some level, subsequent addition of QVD did not rescue cell viability. Instead, we found that IM-54, an anti-oxidant shown to prevent necrosis, rescued S63845-mediated cell death (Figure 3-5C). Follow up studies should be completed to confirm if this is a genuine, unregulated necrotic response, or if

these cells are actually resorting to another form of programmed cell death, such as necroptosis, pyroptosis, or ferroptosis, among others (Karch and Molkentin, 2015; Tang et al., 2019). Given the intricacies of mitochondrial control of cell death signaling pathways, it is possible that MCL-1 inhibition can trigger other types of regulated cell death besides apoptosis.

Overall, these results paired with the cytoskeletal defects seen in S63845-treated hiPSC-CMs could explain the phenotypes documented in the first MCL-1 KO mouse study published by the Korsmeyer group, in which deletion of MCL-1 resulted in implantation failure of the blastocyst (Rinkenberger et al., 2000). Since the ICM of these blastocysts showed no signs of apoptosis and could be cultured *in vitro*, the authors deduced the implantation defect was a result of MCL-1 depletion in the trophectoderm layer. In the 20 years since this discovery, data from several groups has supported the idea of MCL-1 non-apoptotic function, which have been discussed in previous chapters, but none have closely examined the trophoblast cells from MCL-1 null blastocysts. It would be interesting to measure the presence of potential necrotic phenotypes in these cells, which could explain the attachment defect. Our own data in PSCs and hiPSC-CMs lead us to hypothesize the implantation failure of MCL-1 null embryos is a result of necrosis caused by disrupted mitochondrial dynamics and actin organization in trophoblast cells lacking MCL-1.

Many intriguing implications could emerge from these studies. MCL-1 upregulation has mainly been associated with the onset of various cancers, and due to its importance in cellular survival, it has been extremely difficult to study its function in development. However, if a trophoblast model system could be deployed, we could uncover new mechanisms to explain the implantation issues found in the MCL-1 KO mouse model. Investigating the mitochondrial morphology, respiratory function, and cytoskeletal

maintenance of trophoblast cells will be important steps for identifying these issues. Microvilli, actin-based protrusions that extend from the trophoblast cells, are critical mediators of early blastocyst attachment (Staun-Ram and Shalev, 2005). If MCL-1 inhibition affects the actin cytoskeleton in trophoblast cells as it does in cardiomyocytes, then disorganization of actin filaments may prevent the proper formation of microvilli, leading to failed attachment. This could have broader implications for fertility issues in humans, as there may be potential MCL-1 mutations or upregulation in humans that result in failed pregnancies soon after fertilization. Future studies should focus on mapping MCL-1 mutations and single-nucleotide polymorphisms (SNPs) in patients who have had miscarriages or suffer from infertility, especially due to implantation defects. The use of MCL-1 inhibitors for the treatment of cancers may also prove to be challenging from this perspective and may present yet another roadblock for patients who hope to become pregnant after chemotherapy. However, by further elucidating the basic mechanisms by which MCL-1 promotes survival and mitochondrial function in trophoblasts, we can make more informed decisions on potential treatments and solutions for infertility.

Mitophagy regulation by the BCL-2 family

MCL-1 inhibition causes increased mitochondrial fragmentation through a DRP-1 dependent mechanism (Rasmussen et al., 2020b; Moyzis et al., 2020). The recruitment of DRP-1 to the mitochondria has been proposed to be a critical inducer of mitophagy, or the clearance of damaged mitochondria (Lee et al., 2011; Zhang, 2013; Kageyama et al., 2014; Burman et al., 2017). Mitophagy is

proposed to be an opposing process to apoptosis, and initiation of either pathway is dependent on signaling crosstalk and cell state (Pickles et al., 2018). Activation of PTEN-induced putative kinase 1 (PINK1) aids in the selective clearance of mitochondria through recruitment of the E3 ubiquitin ligase Parkin, which translocates to the mitochondria from the cytosol and targets mitochondrial membrane proteins for degradation by the autophagosome (Narendra et al., 2008). MFN1 and MFN2 are substrates for Parkin-mediated ubiquitination (Gegg et al., 2010). However, this modification targets them for proteasomal degradation rather than acting as a mitophagy signal, suggesting that elimination of mitochondrial fusion and a shift to fission occurs prior to mitophagy. This shift to fission initiated by DRP-1 activity may appear to be required for dividing defective sections of mitochondria from the rest of the network in order to be eliminated by mitophagy. It has instead been proposed that DRP-1-mediated mitochondrial fission protects healthy mitochondria from unhindered PINK1-Parkin activity (Burman et al., 2017). This hypothesis arises from the finding that DRP-1 KO cells display persistent recruitment of Parkin to mitochondria, resulting in increased mitophagy levels. It would be interesting to examine how MCL-1^{OM} may participate in regulation of mitophagy with respect to its interaction with DRP-1. Other anti-apoptotic family members, BCL-2 and BCL-xL, have been shown to negatively regulate mitophagy through inhibition of BECLIN-1 (also known as ATG6), a BH3 domain-containing protein that regulates formation of the phagophore (Pattingre et al., 2005; Maiuri et al., 2007; Fernández et al., 2018). Another study in HeLa cells showed that overexpression of any of the anti-apoptotic family members (BCL-2, BCL-xL, BCL-w, MCL-1, A1) prevented PINK1/Parkin-mediated mitophagy, but this block was independent of BECLIN-1 (Hollville et al., 2014). A drug screen to identify therapeutics for Alzheimer's disease revealed UMI-77, a BH3-mimetic targeting MCL-1, as a mitophagy activator (Cen

et al., 2020). This study also found MCL-1 binds to LC3A, a structural component of autophagosomal membranes. Thus, it is tempting to speculate that inhibition of MCL-1 causes excess clearing of mitochondria in PSCs and cardiomyocytes as well, either through direct interaction with mitophagy components or indirectly through mediation of DRP-1 activity.

Mitophagy can maintain cellular homeostasis and is also triggered by nutrient deprivation and other stressors; however, mitophagy can also be developmentally initiated (Pickles et al., 2018). In fact, decreased levels of mitophagy accompany increased mitochondrial fusion that occurs during stem cell differentiation, and increased mitophagy during somatic cell reprogramming promotes the switch in metabolism back to glycolytic dependence, as it reduces mitochondrial mass, mtDNA content, and ETC components that facilitate oxidative phosphorylation (Vazquez-Martin et al., 2012; Fu et al., 2019). Mitophagy is essential in post-mitotic cells, since they have lost their proliferative capacity and rely on maintaining a healthy pool of mitochondria (Zhang, 2013; Evans and Holzbaur, 2019). However, high levels of mitochondrial fission in stem cells would perhaps require high activation of mitophagy for quality control purposes (Naik et al., 2019). Supporting this, late-passage PINK1-deficient mouse iPSCs, while they expressed the pluripotency factors OCT4 and SOX2, were more prone to differentiation and showed accumulation of damaged mitochondria (Vazquez-Martin et al., 2016).

MCL-1 and inter-organelle contacts

Although we know that mitochondrial fragmentation and the protein machinery that coordinate this process are essential, details of how mitochondrial membrane integrity is disrupted, yet in a controlled manner, are not well understood. Structural analysis of DRP-1 discovered that the rings formed by DRP-1 oligomers are smaller in diameter (30-50 nm) than the average diameter of mitochondria (Ingerman et al., 2005; Mears et al., 2011), suggesting there are likely other constriction mechanisms involved. Recent work has illuminated the endoplasmic reticulum (ER) as well as the actin cytoskeleton as key players in mitochondrial dynamics (Lewis et al., 2016; Rehklau et al., 2017; Steffen and Koehler, 2018). ER tubules can be found at sites of fission, where they form contacts with the mitochondria through the ER-mitochondria encounter structure (ERMES) complex and initiated fission even before DRP-1 constriction (Elgass et al., 2015; Lewis et al., 2016; Yang and Svitkina, 2019). Following ER tubule encirclement of the mitochondria, it is proposed that INF2-induced actin polymerization occurs, triggering an initial constriction mechanism to facilitate DRP-1 recruitment, assembly, and final scission of the membrane (Korobova et al., 2013; Pon, 2013). Tethering of the ER to mitochondria, known as MERCs (mitochondria-ER contacts) (Copeland and Dalton, 1959; Csordás et al., 2006), might serve not only to facilitate mitochondrial fission, but also to regulate mitochondrial membrane biosynthesis, calcium signaling, and protein import (reviewed in (Kornmann and Walter, 2010)). The actin phenotypes caused by MCL-1 inhibition in cardiomyocytes described in Chapter 3 begs the question of whether the degradation of actin occurs due to a metabolic decrease in ATP and actin polymerization, or due to an unidentified method of direct mitochondria-to-actin crosstalk. Newly developed tools such as actin

chromobodies could help us answer some of these questions by revealing actin dynamics specifically at mitochondrial fission sites (Schiavon et al., 2020).

Other components such as lysosomes, calcium, and phospholipids have been implicated in mitochondrial division at various stages. Specifically, phosphatidylinositol 4-phosphate (PI(4)P), which is known to remodel membranes of the ER and the Golgi (Chung et al., 2015), was also shown to accumulate at mitochondrial fission sites (Nagashima et al., 2020). These pools of PI(4)P were contained within vesicles originating from the Golgi and helped to drive the final stages of division, an exciting and novel finding that adds to the complexity of the mitochondrial fission process. While the exact contribution of PI(4)P to the mitochondria during fission is unclear, it is possible that it aids in the recruitment of adaptor proteins necessary for actin polymerization (Nagashima et al., 2020). Mitochondrial membrane lipid content is also tightly regulated, as discussed earlier in this chapter, and PI(4)P deposits may induce increased membrane curvature, thus aiding DRP-1 at MERC sites. It will be interesting to determine if members of the BCL-2 family such as MCL-1 and BAK/BAX are involved in these regions of mitochondrial fission. It will also be important to study potential modifications to these processes in hESCs, where the balance of mitochondrial dynamics is shifted to favor high fission activity, and the Golgi has been identified as an origin for active BAX (Dumitru and Gama et al., 2012). It is intriguing to speculate that BAX may be shuttled to the mitochondria upon apoptotic stimuli via Golgi-derived vesicles.

MCL-1 has traditionally been thought of as a mitochondria-localized protein. Yet, some studies have reported that MCL-1 can be translocated to the nucleus in response to DNA damage, activating

Checkpoint kinase 1 (CHK1) and maintaining genome integrity (Jamil et al., 2008). Other studies report that MCL-1 acts with BCL-2 and BCL-xL to regulate transcription of pro-survival gene programs (Huang et al., 1997). While it is not understood how MCL-1 is shuttled to the nucleus during these responses, it is possible that newly identified mitochondria-nucleus contact sites may be involved. These contacts were discovered by combining biochemical studies with high-resolution Airyscan confocal imaging and electron microscopy, and tethering between the mitochondria and nucleus was shown to occur after stress response to promote survival (Desai et al., 2020). Future studies are needed to determine whether the phenotypes caused by disruption of MCL-1 are connected to MCL-1's potential protective role as a transcriptional regulator at the nucleus. These studies would be of particular interest in PSCs, where gene regulatory programs guiding self-renewal and differentiation are highly influenced by mitochondrial signaling. For example, acetyl-CoA and alpha-ketoglutarate, two metabolites of the tricarboxylic acid (TCA) cycle, have been shown to influence cell fate and pluripotency through epigenetic changes such as histone acetylation and demethylation, respectively (Moussaieff et al., 2015; Carey et al., 2015; Martínez-Reyes and Chandel, 2020). In conclusion, elucidating how the important cellular processes of mitochondrial signaling and crosstalk regulate function and quality control in stem and differentiated cells will certainly uncover new mechanisms underlying human development, health and disease.

References

Acehan, D., Khuchua, Z., Houtkooper, R.H., Malhotra, A., Kaufman, J., Vaz, F.M., Ren, M., Rockman, H.A., Stokes, D.L., Schlame, M., 2009. Distinct effects of tafazzin deletion in differentiated and undifferentiated mitochondria. Mitochondrion 9, 86–95. https://doi.org/10.1016/j.mito.2008.12.001

Acehan, D., Xu, Y., Stokes, D.L., Schlame, M., 2007. Comparison of lymphoblast mitochondria from normal subjects and patients with Barth syndrome using electron microscopic tomography. Lab. Invest. 87, 40–48. https://doi.org/10.1038/labinvest.3700480

Adams, J.M., Cory, S., 1998. The Bcl-2 Protein Family: Arbiters of Cell Survival. Science 281, 1322–1326. https://doi.org/10.1126/science.281.5381.1322

Alavi, M.V., Bette, S., Schimpf, S., Schuettauf, F., Schraermeyer, U., Wehrl, H.F., Ruttiger, L., Beck, S.C., Tonagel, F., Pichler, B.J., Knipper, M., Peters, T., Laufs, J., Wissinger, B., 2007. A splice site mutation in the murine Opa1 gene features pathology of autosomal dominant optic atrophy. Brain 130, 1029–1042. https://doi.org/10.1093/brain/awm005

Alexander, C., Votruba, M., Pesch, U.E.A., Thiselton, D.L., Mayer, S., Moore, A., Rodriguez, M., Kellner, U., Leo-Kottler, B., Auburger, G., Bhattacharya, S.S., Wissinger, B., 2000. OPA1 , encoding a dynamin-related GTPase, is mutated in autosomal dominant optic atrophy linked to chromosome 3q28. Nat. Genet. 26, 211–215. https://doi.org/10.1038/79944

Amita, M., Adachi, K., Alexenko, A.P., Sinha, S., Schust, D.J., Schulz, L.C., Roberts, R.M., Ezashi, T., 2013. Complete and unidirectional conversion of human embryonic stem cells to trophoblast by BMP4. Proc. Natl. Acad. Sci. 110, E1212–E1221. https://doi.org/10.1073/pnas.1303094110

Anand, R., Wai, T., Baker, M.J., Kladt, N., Schauss, A.C., Rugarli, E., Langer, T., 2014. The i-AAA protease YME1L and OMA1 cleave OPA1 to balance mitochondrial fusion and fission. J. Cell Biol. 204, 919–929. https://doi.org/10.1083/jcb.201308006

Andersen, J.L., Kornbluth, S., 2012. Mcl-1 rescues a glitch in the matrix. Nat. Cell Biol. 14, 563–565. https://doi.org/10.1038/ncb2511

Anderson, C.A., Blackstone, C., 2013. SUMO wrestling with Drp1 at mitochondria. EMBO J. 32, 1496–1498. https://doi.org/10.1038/emboj.2013.103

Antonny, B., Burd, C., De Camilli, P., Chen, E., Daumke, O., Faelber, K., Ford, M., Frolov, V.A., Frost, A., Hinshaw, J.E., Kirchhausen, T., Kozlov, M.M., Lenz, M., Low, H.H., McMahon, H., Merrifield, C., Pollard, T.D., Robinson, P.J., Roux, A., Schmid, S., 2016. Membrane fission by dynamin: what we know and what we need to know. EMBO J. 35, 2270–2284. https://doi.org/10.15252/embj.201694613

Arbour, N., Vanderluit, J.L., Grand, J.N.L., Jahani-Asl, A., Ruzhynsky, V.A., Cheung, E.C.C., Kelly, M.A., MacKenzie, A.E., Park, D.S., Opferman, J.T., Slack, R.S., 2008. Mcl-1 Is a Key Regulator of Apoptosis during CNS Development and after DNA Damage. J. Neurosci. 28, 6068–6078. https://doi.org/10.1523/JNEUROSCI.4940-07.2008

Archer, S.L., 2013. Mitochondrial Dynamics — Mitochondrial Fission and Fusion in Human Diseases. N. Engl. J. Med. 369, 2236–2251. https://doi.org/10.1056/NEJMra1215233

Ashkenazi, A., Dixit, V.M., 1998. Death Receptors: Signaling and Modulation. Science 281, 1305–1308. https://doi.org/10.1126/science.281.5381.1305

Assady, S., Maor, G., Amit, M., Itskovitz-Eldor, J., Skorecki, K.L., Tzukerman, M., 2001. Insulin Production by Human Embryonic Stem Cells. Diabetes 50, 1691–1697. https://doi.org/10.2337/diabetes.50.8.1691

Ban, T., Ishihara, T., Kohno, H., Saita, S., Ichimura, A., Maenaka, K., Oka, T., Mihara, K., Ishihara, N., 2017. Molecular basis of selective mitochondrial fusion by heterotypic action between OPA1 and cardiolipin. Nat. Cell Biol. 19, 856–863. https://doi.org/10.1038/ncb3560

Bereiter-Hahn, J., Vöth, M., 1994. Dynamics of mitochondria in living cells: Shape changes, dislocations, fusion, and fission of mitochondria. Microsc. Res. Tech. 27, 198–219. https://doi.org/10.1002/jemt.1070270303

Berman, S.B., Pineda, F.J., Hardwick, J.M., 2008. Mitochondrial fission and fusion dynamics: the long and short of it. Cell Death Differ. 15, 1147–1152. https://doi.org/10.1038/cdd.2008.57

Beroukhim, R., Mermel, C.H., Porter, D., Wei, G., Raychaudhuri, S., Donovan, J., Barretina, J., Boehm, J.S., Dobson, J., Urashima, M., Mc Henry, K.T., Pinchback, R.M., Ligon, A.H., Cho, Y.-J., Haery, L., Greulich, H., Reich, M., Winckler, W., Lawrence, M.S., Weir, B.A., Tanaka, K.E., Chiang, D.Y., Bass, A.J., Loo, A., Hoffman, C., Prensner, J., Liefeld, T., Gao, Q., Yecies, D., Signoretti, S., Maher, E., Kaye, F.J., Sasaki, H., Tepper, J.E., Fletcher, J.A., Tabernero, J.,

Baselga, J., Tsao, M.-S., Demichelis, F., Rubin, M.A., Janne, P.A., Daly, M.J., Nucera, C., Levine, R.L., Ebert, B.L., Gabriel, S., Rustgi, A.K., Antonescu, C.R., Ladanyi, M., Letai, A., Garraway, L.A., Loda, M., Beer, D.G., True, L.D., Okamoto, A., Pomeroy, S.L., Singer, S., Golub, T.R., Lander, E.S., Getz, G., Sellers, W.R., Meyerson, M., 2010. The landscape of somatic copy-number alteration across human cancers. Nature 463, 899–905. https://doi.org/10.1038/nature08822

Bigarella, C.L., Liang, R., Ghaffari, S., 2014. Stem cells and the impact of ROS signaling. Development 141, 4206–4218. https://doi.org/10.1242/dev.107086

Billard, C., 2013. BH3 Mimetics: Status of the Field and New Developments. Mol. Cancer Ther. 12, 1691–1700. https://doi.org/10.1158/1535-7163.MCT-13-0058

Bonizzi, G., Cicalese, A., Insinga, A., Pelicci, P.G., 2012. The emerging role of p53 in stem cells. Trends Mol. Med. 18, 6–12. https://doi.org/10.1016/j.molmed.2011.08.002

Brennan, M.S., Chang, C., Tai, L., Lessene, G., Strasser, A., Dewson, G., Kelly, G.L., Herold, M.J., 2018. Humanized Mcl-1 mice enable accurate preclinical evaluation of MCL-1 inhibitors destined for clinical use. Blood 132, 1573–1583. https://doi.org/10.1182/blood-2018-06-859405

Brooks, C., Wei, Q., Feng, L., Dong, G., Tao, Y., Mei, L., Xie, Z.-J., Dong, Z., 2007. Bak regulates mitochondrial morphology and pathology during apoptosis by interacting with mitofusins. Proc. Natl. Acad. Sci. 104, 11649–11654. https://doi.org/10.1073/pnas.0703976104

Buggisch, M., Ateghang, B., Ruhe, C., Strobel, C., Lange, S., Wartenberg, M., Sauer, H., 2007. Stimulation of ES-cell-derived cardiomyogenesis and neonatal cardiac cell proliferation by reactive oxygen species and NADPH oxidase. J. Cell Sci. 120, 885–894. https://doi.org/10.1242/jcs.03386

Burman, J.L., Pickles, S., Wang, C., Sekine, S., Vargas, J.N.S., Zhang, Z., Youle, A.M., Nezich, C.L., Wu, X., Hammer, J.A., Youle, R.J., 2017. Mitochondrial fission facilitates the selective mitophagy of protein aggregates. J. Cell Biol. 216, 3231–3247. https://doi.org/10.1083/jcb.201612106

Burté, F., Carelli, V., Chinnery, P.F., Yu-Wai-Man, P., 2015. Disturbed mitochondrial dynamics and neurodegenerative disorders. Nat. Rev. Neurol. 11, 11–24. https://doi.org/10.1038/nrneurol.2014.228

Caenepeel, S., Brown, S.P., Belmontes, B., Moody, G., Keegan, K.S., Chui, D., Whittington, D.A., Huang, X., Poppe, L., Cheng, A.C., Cardozo, M., Houze, J., Li, Y., Lucas, B., Paras, N.A., Wang, X., Taygerly, J.P., Vimolratana, M., Zancanella, M., Zhu, L., Cajulis, E., Osgood, T., Sun, J., Damon, L., Egan, R.K., Greninger, P., McClanaghan, J.D., Gong, J., Moujalled, D., Pomilio, G., Beltran, P., Benes, C.H., Roberts, A.W., Huang, D.C.S., Wei, A., Canon, J., Coxon, A., Hughes, P.E., 2018. AMG 176, a Selective MCL1 Inhibitor, is Effective in Hematological Cancer Models Alone and in Combination with Established Therapies. Cancer Discov. CD-18-0387. https://doi.org/10.1158/2159-8290.CD-18-0387

Carey, B.W., Finley, L.W.S., Cross, J.R., Allis, C.D., Thompson, C.B., 2015. Intracellular α-ketoglutarate maintains the pluripotency of embryonic stem cells. Nature 518, 413–416. https://doi.org/10.1038/nature13981

Cen, X., Chen, Y., Xu, X., Wu, R., He, F., Zhao, Q., Sun, Q., Yi, C., Wu, J., Najafov, A., Xia, H., 2020. Pharmacological targeting of MCL-1 promotes mitophagy and improves disease pathologies in an Alzheimer's disease mouse model. Nat. Commun. 11, 5731. https://doi.org/10.1038/s41467-020-19547-6

Certo, M., Moore, V.D.G., Nishino, M., Wei, G., Korsmeyer, S., Armstrong, S.A., Letai, A., 2006. Mitochondria primed by death signals determine cellular addiction to antiapoptotic BCL-2 family members. Cancer Cell 9, 351–365. https://doi.org/10.1016/j.ccr.2006.03.027

Chambers, S.M., Fasano, C.A., Papapetrou, E.P., Tomishima, M., Sadelain, M., Studer, L., 2009. Highly efficient neural conversion of human ES and iPS cells by dual inhibition of SMAD signaling. Nat. Biotechnol. 27, 275–280. https://doi.org/10.1038/nbt.1529

Chan, D.C., 2020. Mitochondrial Dynamics and Its Involvement in Disease. Annu. Rev. Pathol. Mech. Dis. 15, null. https://doi.org/10.1146/annurev-pathmechdis-012419-032711

Chan, D.C., 2012. Fusion and Fission: Interlinked Processes Critical for Mitochondrial Health. Annu. Rev. Genet. 46, 265–287. https://doi.org/10.1146/annurev-genet-110410-132529

Chan, D.C., 2007. Mitochondrial Dynamics in Disease. N. Engl. J. Med. 356, 1707–1709. https://doi.org/10.1056/NEJMp078040

Chang, C.-R., Blackstone, C., 2010. Dynamic regulation of mitochondrial fission through modification of the dynamin-related protein Drp1: Chang & Blackstone. Ann. N. Y. Acad. Sci. 1201, 34–39. https://doi.org/10.1111/j.1749-6632.2010.05629.x

Chappie, J.S., Acharya, S., Leonard, M., Schmid, S.L., Dyda, F., 2010. G domain dimerization controls dynamin's assembly-stimulated GTPase activity. Nature 465, 435–440. https://doi.org/10.1038/nature09032

Chaudhari, A.A., Seol, J.-W., Kim, S.-J., Lee, Y.-J., Kang, H., Kim, I., Kim, N.-S., Park, S.-Y., 2007. Reactive oxygen species regulate Bax translocation and mitochondrial transmembrane potential, a possible mechanism for enhanced TRAIL-induced apoptosis by CCCP. Oncol. Rep. 18, 71–76. https://doi.org/10.3892/or.18.1.71

Chavali, N.V., Kryshtal, D.O., Parikh, S.S., Wang, L., Glazer, A.M., Blackwell, D.J., Kroncke, B.M., Shoemaker, M.B., Knollmann, B.C., 2019. Patient-independent human induced pluripotent stem cell model: A new tool for rapid determination of genetic variant pathogenicity in long QT syndrome. Heart Rhythm 16, 1686–1695. https://doi.org/10.1016/j.hrthm.2019.04.031

Chen, B.-C., Legant, W.R., Wang, K., Shao, L., Milkie, D.E., Davidson, M.W., Janetopoulos, C., Wu, X.S., Hammer, J.A., Liu, Z., English, B.P., Mimori-Kiyosue, Y., Romero, D.P., Ritter, A.T., Lippincott-Schwartz, J., Fritz-Laylin, L., Mullins, R.D., Mitchell, D.M., Bembenek, J.N., Reymann, A.-C., Böhme, R., Grill, S.W., Wang, J.T., Seydoux, G., Tulu, U.S., Kiehart, D.P., Betzig, E., 2014. Lattice light-sheet microscopy: Imaging molecules to embryos at high spatiotemporal resolution. Science 346. https://doi.org/10.1126/science.1257998

Chen, H., Chan, D.C., 2017. Mitochondrial Dynamics in Regulating the Unique Phenotypes of Cancer and Stem Cells. Cell Metab. 26, 39–48. https://doi.org/10.1016/j.cmet.2017.05.016

Chen, H., Detmer, S.A., Ewald, A.J., Griffin, E.E., Fraser, S.E., Chan, D.C., 2003. Mitofusins Mfn1 and Mfn2 coordinately regulate mitochondrial fusion and are essential for embryonic development. J. Cell Biol. 160, 189–200. https://doi.org/10.1083/jcb.200211046

Chen, L., Willis, S.N., Wei, A., Smith, B.J., Fletcher, J.I., Hinds, M.G., Colman, P.M., Day, C.L., Adams, J.M., Huang, D.C.S., 2005. Differential Targeting of Prosurvival Bcl-2 Proteins by Their BH3-Only Ligands Allows Complementary Apoptotic Function. Mol. Cell 17, 393–403. https://doi.org/10.1016/j.molcel.2004.12.030

Chen, Y., Aon, M.A., Hsu, Y.-T., Soane, L., Teng, X., McCaffery, J.M., Cheng, W.-C., Qi, B., Li, H., Alavian, K.N., Dayhoff-Brannigan, M., Zou, S., Pineda, F.J., O'Rourke, B., Ko, Y.H., Pedersen, P.L., Kaczmarek, L.K., Jonas, E.A., Hardwick, J.M., 2011. Bcl-xL regulates mitochondrial energetics by stabilizing the inner membrane potential. J. Cell Biol. 195, 263–276. https://doi.org/10.1083/jcb.201108059

Chiappori, A.A., Schreeder, M.T., Moezi, M.M., Stephenson, J.J., Blakely, J., Salgia, R., Chu, Q.S., Ross, H.J., Subramaniam, D.S., Schnyder, J., Berger, M.S., 2012. A phase I trial of pan-Bcl-2 antagonist obatoclax administered as a 3-h or a 24-h infusion in combination with carboplatin and etoposide in patients with extensive-stage small cell lung cancer. Br. J. Cancer 106, 839–845. https://doi.org/10.1038/bjc.2012.21

Chipuk, J.E., Moldoveanu, T., Llambi, F., Parsons, M.J., Green, D.R., 2010. The BCL-2 Family Reunion. Mol. Cell 37, 299–310. https://doi.org/10.1016/j.molcel.2010.01.025

Chittenden, T., Flemington, C., Houghton, A.B., Ebb, R.G., Gallo, G.J., Elangovan, B., Chinnadurai, G., Lutz, R.J., 1995. A conserved domain in Bak, distinct from BH1 and BH2, mediates cell death and protein binding functions. EMBO J. 14, 5589–5596.

Cho, S.W., Park, J., Heo, H.J., Park, S., Song, S., Kim, I., Han, Y., Yamashita, J.K., Youm, J.B., Han, J., Koh, G.Y., 2014. Dual Modulation of the Mitochondrial Permeability Transition Pore and Redox Signaling Synergistically Promotes Cardiomyocyte Differentiation From Pluripotent Stem Cells. J. Am. Heart Assoc. 3. https://doi.org/10.1161/JAHA.113.000693

Chonghaile, T.N., Letai, A., 2008. Mimicking the BH3 domain to kill cancer cells. Oncogene 27, S149–S157. https://doi.org/10.1038/onc.2009.52

Chung, J., Torta, F., Masai, K., Lucast, L., Czapla, H., Tanner, L.B., Narayanaswamy, P., Wenk, M.R., Nakatsu, F., Camilli, P.D., 2015. PI4P/phosphatidylserine countertransport at ORP5- and ORP8-mediated ER–plasma membrane contacts. Science 349, 428–432. https://doi.org/10.1126/science.aab1370

Chung, S., Arrell, D.K., Faustino, R.S., Terzic, A., Dzeja, P.P., 2010. Glycolytic network restructuring integral to the energetics of embryonic stem cell cardiac differentiation. J. Mol. Cell. Cardiol. 48, 725–734. https://doi.org/10.1016/j.yjmcc.2009.12.014

Cipolat, S., Martins de Brito, O., Dal Zilio, B., Scorrano, L., 2004. OPA1 requires mitofusin 1 to promote mitochondrial fusion. Proc. Natl. Acad. Sci. U. S. A. 101, 15927–15932. https://doi.org/10.1073/pnas.0407043101

Clements, M., Thomas, N., 2014. High-Throughput Multi-Parameter Profiling of Electrophysiological Drug Effects in Human Embryonic Stem Cell Derived Cardiomyocytes Using Multi-Electrode Arrays. Toxicol. Sci. 140, 445–461. https://doi.org/10.1093/toxsci/kfu084

Cohen, N.A., Stewart, M.L., Gavathiotis, E., Tepper, J.L., Bruekner, S.R., Koss, B., Opferman, J.T., Walensky, L.D., 2012. A Competitive Stapled Peptide Screen Identifies a Selective Small Molecule that Overcomes MCL-1-Dependent Leukemia Cell Survival. Chem. Biol. 19, 1175–1186. https://doi.org/10.1016/j.chembiol.2012.07.018

Copeland, D.E., Dalton, A.J., 1959. An Association between Mitochondria and the Endoplasmic Reticulum in Cells of the Pseudobranch Gland of a Teleost. J. Biophys. Biochem. Cytol. 5, 393–396. https://doi.org/10.1083/jcb.5.3.393

Csordás, G., Renken, C., Várnai, P., Walter, L., Weaver, D., Buttle, K.F., Balla, T., Mannella, C.A., Hajnóczky, G., 2006. Structural and functional features and significance of the physical linkage between ER and mitochondria. J. Cell Biol. 174, 915–921. https://doi.org/10.1083/jcb.200604016

Davies, V.J., Hollins, A.J., Piechota, M.J., Yip, W., Davies, J.R., White, K.E., Nicols, P.P., Boulton, M.E., Votruba, M., 2007. Opa1 deficiency in a mouse model of autosomal dominant optic atrophy impairs mitochondrial morphology, optic nerve structure and visual function. Hum. Mol. Genet. 16, 1307–1318. https://doi.org/10.1093/hmg/ddm079

Del Dotto, V., Fogazza, M., Carelli, V., Rugolo, M., Zanna, C., 2018. Eight human OPA1 isoforms, long and short: What are they for? Biochim. Biophys. Acta BBA - Bioenerg. 1859, 263–269. https://doi.org/10.1016/j.bbabio.2018.01.005

Del Dotto, V., Mishra, P., Vidoni, S., Fogazza, M., Maresca, A., Caporali, L., McCaffery, J.M., Cappelletti, M., Baruffini, E., Lenaers, G., Chan, D., Rugolo, M., Carelli, V., Zanna, C., 2017. OPA1 Isoforms in the Hierarchical Organization of Mitochondrial Functions. Cell Rep. 19, 2557–2571. https://doi.org/10.1016/j.celrep.2017.05.073

Delettre, C., Lenaers, G., Griffoin, J.-M., Gigarel, N., Lorenzo, C., Belenguer, P., Pelloquin, L., Grosgeorge, J., Turc-Carel, C., Perret, E., Astarie-Dequeker, C., Lasquellec, L., Arnaud, B., Ducommun, B., Kaplan, J., Hamel, C.P., 2000. Nuclear gene OPA1 , encoding a mitochondrial dynamin-related protein, is mutated in dominant optic atrophy. Nat. Genet. 26, 207–210. https://doi.org/10.1038/79936

Desai, R., East, D.A., Hardy, L., Faccenda, D., Rigon, M., Crosby, J., Alvarez, M.S., Singh, A., Mainenti, M., Hussey, L.K., Bentham, R., Szabadkai, G., Zappulli, V., Dhoot, G.K., Romano, L.E., Xia, D., Coppens, I., Hamacher-Brady, A., Chapple, J.P., Abeti, R., Fleck, R.A., Vizcay-Barrena, G., Smith, K., Campanella, M., 2020. Mitochondria form contact sites with the nucleus to couple prosurvival retrograde response. Sci. Adv. 6, eabc9955. https://doi.org/10.1126/sciadv.abc9955

Dlasková, A., Engstová, H., Špaček, T., Kahancová, A., Pavluch, V., Smolková, K., Špačková, J., Bartoš, M., Hlavatá, L.P., Ježek, P., 2018. 3D super-resolution microscopy reflects mitochondrial cristae alternations and mtDNA nucleoid size and distribution. Biochim. Biophys. Acta BBA - Bioenerg., 20th European Bioenergetics Conference 1859, 829–844. https://doi.org/10.1016/j.bbabio.2018.04.013

Doi, D., Magotani, H., Kikuchi, T., Ikeda, M., Hiramatsu, S., Yoshida, K., Amano, N., Nomura, M., Umekage, M., Morizane, A., Takahashi, J., 2020. Pre-clinical study of induced pluripotent stem cell-derived dopaminergic progenitor cells for Parkinson's disease. Nat. Commun. 11, 3369. https://doi.org/10.1038/s41467-020-17165-w

Dorn, G.W., 2013. Mitochondrial dynamics in heart disease. Biochim. Biophys. Acta BBA - Mol. Cell Res. 1833, 233–241. https://doi.org/10.1016/j.bbamcr.2012.03.008

Dorn, G.W., Vega, R.B., Kelly, D.P., 2015. Mitochondrial biogenesis and dynamics in the developing and diseased heart. Genes Dev. 29, 1981–1991. https://doi.org/10.1101/gad.269894.115

Dudek, J., 2017. Role of Cardiolipin in Mitochondrial Signaling Pathways. Front. Cell Dev. Biol. 5. https://doi.org/10.3389/fcell.2017.00090

Dumitru, R., Gama, V., Fagan, B.M., Bower, J.J., Swahari, V., Pevny, L.H., Deshmukh, M., 2012. Human Embryonic Stem Cells Have Constitutively Active Bax at the Golgi and Are Primed to Undergo Rapid Apoptosis. Mol. Cell 46, 573–583. https://doi.org/10.1016/j.molcel.2012.04.002

Elgass, K.D., Smith, E.A., LeGros, M.A., Larabell, C.A., Ryan, M.T., 2015. Analysis of ER–mitochondria contacts using correlative fluorescence microscopy and soft X-ray tomography of mammalian cells. J. Cell Sci. 128, 2795–2804. https://doi.org/10.1242/jcs.169136

Elmore, S., 2007. Apoptosis: A Review of Programmed Cell Death. Toxicol. Pathol. 35, 495–516. https://doi.org/10.1080/01926230701320337

Escobar-Henriques, M., Joaquim, M., 2019. Mitofusins: Disease Gatekeepers and Hubs in Mitochondrial Quality Control by E3 Ligases. Front. Physiol. 10. https://doi.org/10.3389/fphys.2019.00517

Escudero, S., Zaganjor, E., Lee, S., Mill, C.P., Morgan, A.M., Crawford, E.B., Chen, J., Wales, T.E., Mourtada, R., Luccarelli, J., Bird, G.H., Steidl, U., Engen, J.R., Haigis, M.C., Opferman, J.T., Walensky, L.D., 2018. Dynamic Regulation of Long-Chain Fatty Acid Oxidation by a Noncanonical Interaction between the MCL-1 BH3 Helix and VLCAD. Mol. Cell 69, 729-743.e7. https://doi.org/10.1016/j.molcel.2018.02.005

Estaquier, J., Arnoult, D., 2007. Inhibiting Drp1-mediated mitochondrial fission selectively prevents the release of cytochrome c during apoptosis. Cell Death Differ. 14, 1086–1094. https://doi.org/10.1038/sj.cdd.4402107

Evans, C.S., Holzbaur, E.L.F., 2019. Quality Control in Neurons: Mitophagy and Other Selective Autophagy Mechanisms. J. Mol. Biol. https://doi.org/10.1016/j.jmb.2019.06.031

Evans, M.J., Kaufman, M.H., 1981. Establishment in culture of pluripotential cells from mouse embryos. Nature 292, 154–156. https://doi.org/10.1038/292154a0

Facucho-Oliveira, J.M., St. John, J.C., 2009. The Relationship Between Pluripotency and Mitochondrial DNA Proliferation During Early Embryo Development and Embryonic Stem Cell Differentiation. Stem Cell Rev. Rep. 5, 140–158. https://doi.org/10.1007/s12015-009-9058-0

Feaster, T.K., Cadar, A.G., Wang, L., Williams, C.H., Chun, Y.W., Hempel, J.E., Bloodworth, N., Merryman, W.D., Lim, C.C., Wu, J.C., Knollmann, B.C., Hong, C.C., 2015. Matrigel Mattress: A Method for the Generation of Single Contracting Human-Induced Pluripotent Stem Cell–Derived Cardiomyocytes. Circ. Res. 117, 995–1000. https://doi.org/10.1161/CIRCRESAHA.115.307580

Fernández, Á.F., Sebti, S., Wei, Y., Zou, Z., Shi, M., McMillan, K.L., He, C., Ting, T., Liu, Y., Chiang, W.-C., Marciano, D.K., Schiattarella, G.G., Bhagat, G., Moe, O.W., Hu, M.C., Levine, B., 2018. Disruption of the beclin 1–BCL2 autophagy regulatory complex promotes longevity in mice. Nature 558, 136–140. https://doi.org/10.1038/s41586-018-0162-7

Folmes, C.D., Ma, H., Mitalipov, S., Terzic, A., 2016. Mitochondria in pluripotent stem cells: stemness regulators and disease targets. Curr. Opin. Genet. Dev. 38, 1–7. https://doi.org/10.1016/j.gde.2016.02.001

Francy, C.A., Clinton, R.W., Fröhlich, C., Murphy, C., Mears, J.A., 2017. Cryo-EM Studies of Drp1 Reveal Cardiolipin Interactions that Activate the Helical Oligomer. Sci. Rep. 7, 1–12. https://doi.org/10.1038/s41598-017-11008-3

Frank, S., Gaume, B., Bergmann-Leitner, E.S., Leitner, W.W., Robert, E.G., Catez, F., Smith, C.L., Youle, R.J., 2001a. The Role of Dynamin-Related Protein 1, a Mediator of Mitochondrial Fission, in Apoptosis. Dev. Cell 1, 515–525. https://doi.org/10.1016/S1534-5807(01)00055-7

Frank, S., Gaume, B., Bergmann-Leitner, E.S., Leitner, W.W., Robert, E.G., Catez, F., Smith, C.L., Youle, R.J., 2001b. The Role of Dynamin-Related Protein 1, a Mediator of Mitochondrial Fission, in Apoptosis. Dev. Cell 1, 515–525. https://doi.org/10.1016/S1534-5807(01)00055-7

Frezza, C., Cipolat, S., Martins de Brito, O., Micaroni, M., Beznoussenko, G.V., Rudka, T., Bartoli, D., Polishuck, R.S., Danial, N.N., De Strooper, B., Scorrano, L., 2006. OPA1 controls apoptotic cristae remodeling independently from mitochondrial fusion. Cell 126, 177–189. https://doi.org/10.1016/j.cell.2006.06.025

Friedman, J.R., Nunnari, J., 2014. Mitochondrial form and function. Nature 505, 335–343. https://doi.org/10.1038/nature12985

Fu, W., Liu, Y., Yin, H., 2019. Mitochondrial Dynamics: Biogenesis, Fission, Fusion, and Mitophagy in the Regulation of Stem Cell Behaviors. Stem Cells Int. 2019. https://doi.org/10.1155/2019/9757201

Fuchs, Y., Steller, H., 2011. Programmed Cell Death in Animal Development and Disease. Cell 147, 742–758. https://doi.org/10.1016/j.cell.2011.10.033

Fujita, J., Crane, A.M., Souza, M.K., Dejosez, M., Kyba, M., Flavell, R.A., Thomson, J.A., Zwaka, T.P., 2008. Caspase Activity Mediates the Differentiation of Embryonic Stem Cells. Cell Stem Cell 2, 595–601. https://doi.org/10.1016/j.stem.2008.04.001

Galloway, C.A., Yoon, Y., 2015. Mitochondrial Dynamics in Diabetic Cardiomyopathy. Antioxid. Redox Signal. 22, 1545–1562. https://doi.org/10.1089/ars.2015.6293

Galluzzi, L., Vitale, I., Aaronson, S.A., Abrams, J.M., Adam, D., Agostinis, P., Alnemri, E.S., Altucci, L., Amelio, I., Andrews, D.W., Annicchiarico-Petruzzelli, M., Antonov, A.V., Arama, E., Baehrecke, E.H., Barlev, N.A., Bazan, N.G., Bernassola, F., Bertrand, M.J.M., Bianchi, K., Blagosklonny, M.V., Blomgren, K., Borner, C., Boya, P., Brenner, C., Campanella, M., Candi, E., Carmona-Gutierrez, D., Cecconi, F., Chan, F.K.-M., Chandel, N.S., Cheng, E.H., Chipuk, J.E., Cidlowski, J.A., Ciechanover, A., Cohen, G.M., Conrad, M., Cubillos-Ruiz, J.R., Czabotar, P.E., D'Angiolella, V., Dawson, T.M., Dawson, V.L., Laurenzi, V.D., Maria, R.D., Debatin, K.-M., DeBerardinis, R.J., Deshmukh, M., Daniele, N.D., Virgilio, F.D., Dixit, V.M., Dixon, S.J., Duckett, C.S., Dynlacht, B.D., El-Deiry, W.S., Elrod, J.W., Fimia, G.M., Fulda, S., García-Sáez, A.J., Garg, A.D., Garrido, C., Gavathiotis, E., Golstein, P., Gottlieb, E., Green, D.R., Greene, L.A., Gronemeyer, H., Gross, A., Hajnoczky, G., Hardwick, J.M., Harris, I.S., Hengartner, M.O., Hetz, C., Ichijo, H., Jäättelä, M., Joseph, B., Jost, P.J., Juin, P.P., Kaiser, W.J., Karin, M., Kaufmann, T., Kepp, O., Kimchi, A., Kitsis, R.N., Klionsky, D.J., Knight, R.A., Kumar, S., Lee, S.W., Lemasters, J.J., Levine, B., Linkermann, A., Lipton, S.A., Lockshin, R.A., López-Otín, C., Lowe, S.W., Luedde, T., Lugli, E., MacFarlane, M., Madeo, F., Malewicz, M., Malorni, W., Manic, G., Marine, J.-C., Martin, S.J., Martinou, J.-C., Medema, J.P., Mehlen, P., Meier, P., Melino, S., Miao, E.A., Molkentin, J.D., Moll, U.M., Muñoz-Pinedo, C., Nagata, S., Nuñez, G., Oberst, A., Oren, M., Overholtzer, M., Pagano, M., Panaretakis, T., Pasparakis, M., Penninger, J.M., Pereira, D.M., Pervaiz, S., Peter, M.E., Piacentini, M., Pinton, P., Prehn, J.H.M., Puthalakath, H., Rabinovich, G.A., Rehm, M., Rizzuto, R., Rodrigues, C.M.P., Rubinsztein, D.C., Rudel, T., Ryan, K.M., Sayan, E., Scorrano, L., Shao, F., Shi, Y., Silke, J., Simon, H.-U., Sistigu, A., Stockwell, B.R., Strasser, A., Szabadkai, G., Tait, S.W.G., Tang, D., Tavernarakis, N., Thorburn, A., Tsujimoto, Y., Turk, B., Berghe, T.V., Vandenabeele, P., Heiden, M.G.V., Villunger, A., Virgin, H.W., Vousden, K.H., Vucic, D., Wagner, E.F., Walczak, H., Wallach, D., Wang, Y., Wells, J.A., Wood, W., Yuan, J., Zakeri, Z., Zhivotovsky,

B., Zitvogel, L., Melino, G., Kroemer, G., 2018. Molecular mechanisms of cell death: recommendations of the Nomenclature Committee on Cell Death 2018. Cell Death Differ. 25, 486–541. https://doi.org/10.1038/s41418-017-0012-4

Gama, V., Deshmukh, M., 2012. Human embryonic stem cells: living on the edge. Cell Cycle Georget. Tex 11, 3905–3906. https://doi.org/10.4161/cc.22233

Ganesan, V., Willis, S.D., Chang, K.-T., Beluch, S., Cooper, K.F., Strich, R., 2019. Cyclin C directly stimulates Drp1 GTP affinity to mediate stress-induced mitochondrial hyperfission. Mol. Biol. Cell 30, 302–311. https://doi.org/10.1091/mbc.E18-07-0463

Gao, S., Malsburg, A. von der, Paeschke, S., Behlke, J., Haller, O., Kochs, G., Daumke, O., 2010. Structural basis of oligomerization in the stalk region of dynamin-like MxA. Nature 465, 502–506. https://doi.org/10.1038/nature08972

Gao, W., Pu, Y., Luo, K.Q., Chang, D.C., 2001. Temporal relationship between cytochrome c release and mitochondrial swelling during UV-induced apoptosis in living HeLa cells. J. Cell Sci. 114, 2855–2862.

Garcia-Pavia, P., Kim, Y., Restrepo-Cordoba, M.A., Lunde, I.G., Wakimoto, H., Smith, A.M., Toepfer, C.N., Getz, K., Gorham, J., Patel, P., Ito, K., Willcox, J.A., Arany, Z., Li, J., Owens, A.T., Govind, R., Nuñez, B., Mazaika, E., Bayes-Genis, A., Walsh, R., Finkelman, B., Lupon, J., Whiffin, N., Serrano, I., Midwinter, W., Wilk, A., Bardaji, A., Ingold, N., Buchan, R., Tayal, U., Pascual-Figal, D.A., de Marvao, A., Ahmad, M., Garcia-Pinilla, J.M., Pantazis, A., Dominguez, F., John Baksi, A., O'Regan, D.P., Rosen, S.D., Prasad, S.K., Lara-Pezzi, E., Provencio, M., Lyon, A.R., Alonso-Pulpon, L., Cook, S.A., DePalma, S.R., Barton, P.J.R., Aplenc, R., Seidman, J.G., Ky, B., Ware, J.S., Seidman, C.E., 2019. Genetic Variants Associated With Cancer Therapy–Induced Cardiomyopathy. Circulation 140, 31–41. https://doi.org/10.1161/CIRCULATIONAHA.118.037934

García-Sáez, A.J., Ries, J., Orzáez, M., Pérez-Payà, E., Schwille, P., 2009. Membrane promotes tBID interaction with BCL XL. Nat. Struct. Mol. Biol. 16, 1178–1185. https://doi.org/10.1038/nsmb.1671

Garrido, C., Galluzzi, L., Brunet, M., Puig, P.E., Didelot, C., Kroemer, G., 2006. Mechanisms of cytochrome c release from mitochondria. Cell Death Differ. 13, 1423–1433. https://doi.org/10.1038/sj.cdd.4401950

Gavathiotis, E., Suzuki, M., Davis, M.L., Pitter, K., Bird, G.H., Katz, S.G., Tu, H.-C., Kim, H., Cheng, E.H.-Y., Tjandra, N., Walensky, L.D., 2008. BAX Activation is Initiated at a Novel Interaction Site. Nature 455, 1076–1081. https://doi.org/10.1038/nature07396

Gegg, M.E., Cooper, J.M., Chau, K.-Y., Rojo, M., Schapira, A.H.V., Taanman, J.-W., 2010. Mitofusin 1 and mitofusin 2 are ubiquitinated in a PINK1/parkin-dependent manner upon induction of mitophagy. Hum. Mol. Genet. 19, 4861–4870. https://doi.org/10.1093/hmg/ddq419

Gentillon, C., Li, D., Duan, M., Yu, W.-M., Preininger, M.K., Jha, R., Rampoldi, A., Saraf, A., Gibson, G.C., Qu, C.-K., Brown, L.A., Xu, C., 2019. Targeting HIF-1α in combination with PPARα activation and postnatal factors promotes the metabolic maturation of human induced pluripotent stem cell-derived cardiomyocytes. J. Mol. Cell. Cardiol. 132, 120–135. https://doi.org/10.1016/j.yjmcc.2019.05.003

Germain, M., Mathai, J.P., McBride, H.M., Shore, G.C., 2005. Endoplasmic reticulum BIK initiates DRP1-regulated remodelling of mitochondrial cristae during apoptosis. EMBO J. 24, 1546–1556. https://doi.org/10.1038/sj.emboj.7600592

Glytsou, C., Calvo, E., Cogliati, S., Mehrotra, A., Anastasia, I., Rigoni, G., Raimondi, A., Shintani, N., Loureiro, M., Vazquez, J., Pellegrini, L., Enriquez, J.A., Scorrano, L., Soriano, M.E., 2016. Optic Atrophy 1 Is Epistatic to the Core MICOS Component MIC60 in Mitochondrial Cristae Shape Control. Cell Rep. 17, 3024–3034. https://doi.org/10.1016/j.celrep.2016.11.049

Goldstein, J.C., Waterhouse, N.J., Juin, P., Evan, G.I., Green, D.R., 2000. The coordinate release of cytochrome c during apoptosis is rapid, complete and kinetically invariant. Nat. Cell Biol. 2, 156–162. https://doi.org/10.1038/35004029

Goodell, M.A., Nguyen, H., Shroyer, N., 2015. Somatic stem cell heterogeneity: diversity in the blood, skin and intestinal stem cell compartments. Nat. Rev. Mol. Cell Biol. 16, 299–309. https://doi.org/10.1038/nrm3980

Goping, I.S., Gross, A., Lavoie, J.N., Nguyen, M., Jemmerson, R., Roth, K., Korsmeyer, S.J., Shore, G.C., 1998. Regulated Targeting of BAX to Mitochondria. J. Cell Biol. 143, 207–215. https://doi.org/10.1083/jcb.143.1.207

Green, D.R., Chipuk, J.E., 2008. APOPTOSIS: Stabbed in the BAX. Nature 455, 1047–1049. https://doi.org/10.1038/4551047a

Grooten, J., Goossens, V., Vanhaesebroeck, B., Fiers, W., 1993. Cell membrane permeabilization and cellular collapse, followed by loss of dehydrogenase activity: Early events in tumour necrosis factor-induced cytotoxicity. Cytokine 5, 546–555. https://doi.org/10.1016/S1043-4666(05)80003-1

Guo, L., Eldridge, S., Furniss, M., Mussio, J., Davis, M., 2018. Role of Mcl-1 in regulation of cell death in human induced pluripotent stem cell-derived cardiomyocytes in vitro. Toxicol. Appl. Pharmacol. 360, 88–98. https://doi.org/10.1016/j.taap.2018.09.041

Hackenbrock, C.R., 1966. ULTRASTRUCTURAL BASES FOR METABOLICALLY LINKED MECHANICAL ACTIVITY IN MITOCHONDRIA: I. Reversible Ultrastructural Changes with Change in Metabolic Steady State in Isolated Liver Mitochondria. J. Cell Biol. 30, 269–297. https://doi.org/10.1083/jcb.30.2.269

Hardwick, J.M., Soane, L., 2013. Multiple Functions of BCL-2 Family Proteins. Cold Spring Harb. Perspect. Biol. 5. https://doi.org/10.1101/cshperspect.a008722

Hinson, J.T., Chopra, A., Nafissi, N., Polacheck, W.J., Benson, C.C., Swist, S., Gorham, J., Yang, L., Schafer, S., Sheng, C.C., Haghighi, A., Homsy, J., Hubner, N., Church, G., Cook, S.A., Linke, W.A., Chen, C.S., Seidman, J.G., Seidman, C.E., 2015. Titin mutations in iPS cells define sarcomere insufficiency as a cause of dilated cardiomyopathy. Science 349, 982–986. https://doi.org/10.1126/science.aaa5458

Hird, A.W., Tron, A.E., 2019. Recent advances in the development of Mcl-1 inhibitors for cancer therapy. Pharmacol. Ther. 198, 59–67. https://doi.org/10.1016/j.pharmthera.2019.02.007

Hollville, E., Carroll, R.G., Cullen, S.P., Martin, S.J., 2014. Bcl-2 Family Proteins Participate in Mitochondrial Quality Control by Regulating Parkin/PINK1-Dependent Mitophagy. Mol. Cell 55, 451–466. https://doi.org/10.1016/j.molcel.2014.06.001

Hoppins, S., Edlich, F., Cleland, M.M., Banerjee, S., McCaffery, J.M., Youle, R.J., Nunnari, J., 2011. The Soluble Form of Bax Regulates Mitochondrial Fusion via MFN2 Homotypic Complexes. Mol. Cell 41, 150–160. https://doi.org/10.1016/j.molcel.2010.11.030

Hoppins, S., Lackner, L., Nunnari, J., 2007. The Machines that Divide and Fuse Mitochondria. Annu. Rev. Biochem. 76, 751–780. https://doi.org/10.1146/annurev.biochem.76.071905.090048

Hsu, Y.-H.R., Yogasundaram, H., Parajuli, N., Valtuille, L., Sergi, C., Oudit, G.Y., 2016. MELAS syndrome and cardiomyopathy: linking mitochondrial function to heart failure pathogenesis. Heart Fail. Rev. 21, 103–116. https://doi.org/10.1007/s10741-015-9524-5

Hsu, Y.-T., Youle, R.J., 1997. Nonionic Detergents Induce Dimerization among Members of the Bcl-2 Family. J. Biol. Chem. 272, 13829–13834. https://doi.org/10.1074/jbc.272.21.13829

Huang, D.C.S., O'Reilly, L.A., Strasser, A., Cory, S., 1997. The anti-apoptosis function of Bcl-2 can be genetically separated from its inhibitory effect on cell cycle entry. EMBO J. 16, 4628–4638. https://doi.org/10.1093/emboj/16.15.4628

Huang, K.C., Mukhopadhyay, R., Wingreen, N.S., 2006. A Curvature-Mediated Mechanism for Localization of Lipids to Bacterial Poles. PLOS Comput. Biol. 2, e151. https://doi.org/10.1371/journal.pcbi.0020151

Imahashi, K., Schneider, M.D., Steenbergen, C., Murphy, E., 2004. Transgenic Expression of Bcl-2 Modulates Energy Metabolism, Prevents Cytosolic Acidification During Ischemia, and Reduces Ischemia/Reperfusion Injury. Circ. Res. 95, 734–741. https://doi.org/10.1161/01.RES.0000143898.67182.4c

Ingerman, E., Perkins, E.M., Marino, M., Mears, J.A., McCaffery, J.M., Hinshaw, J.E., Nunnari, J., 2005. Dnm1 forms spirals that are structurally tailored to fit mitochondria. J. Cell Biol. 170, 1021–1027. https://doi.org/10.1083/jcb.200506078

Inoue, S., Browne, G., Melino, G., Cohen, G.M., 2009. Ordering of caspases in cells undergoing apoptosis by the intrinsic pathway. Cell Death Differ. 16, 1053–1061. https://doi.org/10.1038/cdd.2009.29

Ishihara, N., Nomura, M., Jofuku, A., Kato, H., Suzuki, S.O., Masuda, K., Otera, H., Nakanishi, Y., Nonaka, I., Goto, Y., Taguchi, N., Morinaga, H., Maeda, M., Takayanagi, R., Yokota, S.,

Mihara, K., 2009. Mitochondrial fission factor Drp1 is essential for embryonic development and synapse formation in mice. Nat. Cell Biol. 11, 958–966. https://doi.org/10.1038/ncb1907

Itoh, K., Nakamura, K., Iijima, M., Sesaki, H., 2013. Mitochondrial dynamics in neurodegeneration. Trends Cell Biol. 23, 64–71. https://doi.org/10.1016/j.tcb.2012.10.006

Jahani-Asl, A., Germain, M., Slack, R.S., 2010. Mitochondria: Joining forces to thwart cell death. Biochim. Biophys. Acta BBA - Mol. Basis Dis., Mitochondrial Dysfunction 1802, 162–166. https://doi.org/10.1016/j.bbadis.2009.09.006

Jain, A.K., Barton, M.C., 2018. p53: emerging roles in stem cells, development and beyond. Development 145, dev158360. https://doi.org/10.1242/dev.158360

Jamil, S., Mojtabavi, S., Hojabrpour, P., Cheah, S., Duronio, V., 2008. An essential role for MCL-1 in ATR-mediated CHK1 phosphorylation. Mol. Biol. Cell 19, 3212–3220. https://doi.org/10.1091/mbc.e07-11-1171

Johnson, L.V., Walsh, M.L., Bockus, B.J., Chen, L.B., 1981. Monitoring of relative mitochondrial membrane potential in living cells by fluorescence microscopy. J. Cell Biol. 88, 526–535. https://doi.org/10.1083/jcb.88.3.526

Kageyama, Y., Hoshijima, M., Seo, K., Bedja, D., Sysa-Shah, P., Andrabi, S.A., Chen, W., Höke, A., Dawson, V.L., Dawson, T.M., Gabrielson, K.L., Kass, D.A., Iijima, M., Sesaki, H., 2014. Parkin-independent mitophagy requires Drp1 and maintains the integrity of mammalian heart and brain. EMBO J. 33, 2798–2813. https://doi.org/10.15252/embj.201488658

Kale, J., Osterlund, E.J., Andrews, D.W., 2018. BCL-2 family proteins: changing partners in the dance towards death. Cell Death Differ. 25, 65–80. https://doi.org/10.1038/cdd.2017.186

Kalkavan, H., Green, D.R., 2018. MOMP, cell suicide as a BCL-2 family business. Cell Death Differ. 25, 46–55. https://doi.org/10.1038/cdd.2017.179

Karbassi, E., Fenix, A., Marchiano, S., Muraoka, N., Nakamura, K., Yang, X., Murry, C.E., 2020. Cardiomyocyte maturation: advances in knowledge and implications for regenerative medicine. Nat. Rev. Cardiol. 1–19. https://doi.org/10.1038/s41569-019-0331-x

Karbowski, M., Lee, Y.-J., Gaume, B., Jeong, S.-Y., Frank, S., Nechushtan, A., Santel, A., Fuller, M., Smith, C.L., Youle, R.J., 2002. Spatial and temporal association of Bax with mitochondrial fission

sites, Drp1, and Mfn2 during apoptosis. J. Cell Biol. 159, 931–938. https://doi.org/10.1083/jcb.200209124

Karbowski, M., Norris, K.L., Cleland, M.M., Jeong, S.-Y., Youle, R.J., 2006. Role of Bax and Bak in mitochondrial morphogenesis. Nature 443, 658–662. https://doi.org/10.1038/nature05111

Karch, J., Molkentin, J., 2015. Regulated Necrotic Cell Death. Circ. Res. 116, 1800–1809. https://doi.org/10.1161/CIRCRESAHA.116.305421

Kasahara, A., Cipolat, S., Chen, Y., Dorn, G.W., Scorrano, L., 2013. Mitochondrial Fusion Directs Cardiomyocyte Differentiation via Calcineurin and Notch Signaling. Science 342, 734–737. https://doi.org/10.1126/science.1241359

Kasahara, A., Scorrano, L., 2014. Mitochondria: from cell death executioners to regulators of cell differentiation. Trends Cell Biol. 24, 761–770. https://doi.org/10.1016/j.tcb.2014.08.005

Kawamura, T., Suzuki, J., Wang, Y.V., Menendez, S., Morera, L.B., Raya, A., Wahl, G.M., Belmonte, J.C.I., 2009. Linking the p53 tumour suppressor pathway to somatic cell reprogramming. Nature 460, 1140–1144. https://doi.org/10.1038/nature08311

Kerr, J.F.R., Wyllie, A.H., Currie, A.R., 1972. Apoptosis: A Basic Biological Phenomenon with Wideranging Implications in Tissue Kinetics. Br. J. Cancer 26, 239–257. https://doi.org/10.1038/bjc.1972.33

Khacho, M., Clark, A., Svoboda, D.S., Azzi, J., MacLaurin, J.G., Meghaizel, C., Sesaki, H., Lagace, D.C., Germain, M., Harper, M.-E., Park, D.S., Slack, R.S., 2016. Mitochondrial Dynamics Impacts Stem Cell Identity and Fate Decisions by Regulating a Nuclear Transcriptional Program. Cell Stem Cell 19, 232–247. https://doi.org/10.1016/j.stem.2016.04.015

Kim, H.-E., Du, F., Fang, M., Wang, X., 2005. Formation of apoptosome is initiated by cytochrome c-induced dATP hydrolysis and subsequent nucleotide exchange on Apaf-1. Proc. Natl. Acad. Sci. 102, 17545–17550. https://doi.org/10.1073/pnas.0507900102

Kluck, R.M., Bossy-Wetzel, E., Green, D.R., Newmeyer, D.D., 1997. The Release of Cytochrome c from Mitochondria: A Primary Site for Bcl-2 Regulation of Apoptosis. Science 275, 1132–1136. https://doi.org/10.1126/science.275.5303.1132

Kluck, R.M., Esposti, M.D., Perkins, G., Renken, C., Kuwana, T., Bossy-Wetzel, E., Goldberg, M., Allen, T., Barber, M.J., Green, D.R., Newmeyer, D.D., 1999. The Pro-Apoptotic Proteins, Bid and Bax, Cause a Limited Permeabilization of the Mitochondrial Outer Membrane That Is Enhanced by Cytosol. J. Cell Biol. 147, 809–822. https://doi.org/10.1083/jcb.147.4.809

Kornmann, B., Walter, P., 2010. ERMES-mediated ER-mitochondria contacts: molecular hubs for the regulation of mitochondrial biology. J. Cell Sci. 123, 1389–1393. https://doi.org/10.1242/jcs.058636

Korobova, F., Ramabhadran, V., Higgs, H.N., 2013. An actin-dependent step in mitochondrial fission mediated by the ER-associated formin INF2. Science 339, 464–467. https://doi.org/10.1126/science.1228360

Kotschy, A., Szlavik, Z., Murray, J., Davidson, J., Maragno, A.L., Le Toumelin-Braizat, G., Chanrion, M., Kelly, G.L., Gong, J.-N., Moujalled, D.M., Bruno, A., Csekei, M., Paczal, A., Szabo, Z.B., Sipos, S., Radics, G., Proszenyak, A., Balint, B., Ondi, L., Blasko, G., Robertson, A., Surgenor, A., Dokurno, P., Chen, I., Matassova, N., Smith, J., Pedder, C., Graham, C., Studeny, A., Lysiak-Auvity, G., Girard, A.-M., Gravé, F., Segal, D., Riffkin, C.D., Pomilio, G., Galbraith, L.C.A., Aubrey, B.J., Brennan, M.S., Herold, M.J., Chang, C., Guasconi, G., Cauquil, N., Melchiore, F., Guigal-Stephan, N., Lockhart, B., Colland, F., Hickman, J.A., Roberts, A.W., Huang, D.C.S., Wei, A.H., Strasser, A., Lessene, G., Geneste, O., 2016. The MCL1 inhibitor S63845 is tolerable and effective in diverse cancer models. Nature 538, 477–482. https://doi.org/10.1038/nature19830

Kozopas, K.M., Yang, T., Buchan, H.L., Zhou, P., Craig, R.W., 1993. MCLI, a gene expressed in programmed myeloid cell differentiation, has sequence similarity to BCL2. Proc Natl Acad Sci USA 5.

Kruse, J.-P., Gu, W., 2009. Modes of p53 Regulation. Cell 137, 609–622. https://doi.org/10.1016/j.cell.2009.04.050

Kumar, R.M., Cahan, P., Shalek, A.K., Satija, R., DaleyKeyser, Aj., Li, H., Zhang, J., Pardee, K., Gennert, D., Trombetta, J.J., Ferrante, T.C., Regev, A., Daley, G.Q., Collins, J.J., 2014. Deconstructing transcriptional heterogeneity in pluripotent stem cells. Nature 516, 56–61. https://doi.org/10.1038/nature13920

Kuwana, T., Mackey, M.R., Perkins, G., Ellisman, M.H., Latterich, M., Schneiter, R., Green, D.R., Newmeyer, D.D., 2002. Bid, Bax, and Lipids Cooperate to Form Supramolecular Openings in the Outer Mitochondrial Membrane. Cell 111, 331–342. https://doi.org/10.1016/S0092-8674(02)01036-X

Kuznetsov, A.V., Hermann, M., Saks, V., Hengster, P., Margreiter, R., 2009. The cell-type specificity of mitochondrial dynamics. Int. J. Biochem. Cell Biol., Mitochondrial Dynamics and Function in Biology and Medicine 41, 1928–1939. https://doi.org/10.1016/j.biocel.2009.03.007

Labbé, K., Murley, A., Nunnari, J., 2014. Determinants and Functions of Mitochondrial Behavior. Annu. Rev. Cell Dev. Biol. 30, 357–391. https://doi.org/10.1146/annurev-cellbio-101011-155756

Leber, B., Lin, J., Andrews, D., 2010. Still embedded together binding to membranes regulates Bcl-2 protein interactions. Oncogene 29, 5221–5230. https://doi.org/10.1038/onc.2010.283

Leber, B., Lin, J., Andrews, D.W., 2007. Embedded Together: The Life and Death Consequences of Interaction of the Bcl-2 Family with Membranes. Apoptosis Int. J. Program. Cell Death 12, 897–911. https://doi.org/10.1007/s10495-007-0746-4

Lee, M.R., Mantel, C., Lee, S.A., Moon, S.-H., Broxmeyer, H.E., 2016. MiR-31/SDHA Axis Regulates Reprogramming Efficiency through Mitochondrial Metabolism. Stem Cell Rep. 7, 1–10. https://doi.org/10.1016/j.stemcr.2016.05.012

Lee, Y., Jeong, S.-Y., Karbowski, M., Smith, C.L., Youle, R.J., 2004. Roles of the Mammalian Mitochondrial Fission and Fusion Mediators Fis1, Drp1, and Opa1 in Apoptosis. Mol. Biol. Cell 15, 5001–5011. https://doi.org/10.1091/mbc.e04-04-0294

Lee, Y., Lee, H.-Y., Hanna, R.A., Gustafsson, Å.B., 2011. Mitochondrial autophagy by Bnip3 involves Drp1-mediated mitochondrial fission and recruitment of Parkin in cardiac myocytes. Am. J. Physiol. - Heart Circ. Physiol. 301, H1924–H1931. https://doi.org/10.1152/ajpheart.00368.2011

Legant, W.R., Shao, L., Grimm, J.B., Brown, T.A., Milkie, D.E., Avants, B.B., Lavis, L.D., Betzig, E., 2016. High-density three-dimensional localization microscopy across large volumes. Nat. Methods 13, 359–365. https://doi.org/10.1038/nmeth.3797

Legros, F., Lombès, A., Frachon, P., Rojo, M., 2002. Mitochondrial Fusion in Human Cells Is Efficient, Requires the Inner Membrane Potential, and Is Mediated by Mitofusins. Mol. Biol. Cell 13, 4343–4354. https://doi.org/10.1091/mbc.e02-06-0330

Letai, A., 2016. S63845, an MCL-1 Selective BH3 Mimetic: Another Arrow in Our Quiver. Cancer Cell 30, 834–835. https://doi.org/10.1016/j.ccell.2016.11.016

Letai, A., Bassik, M.C., Walensky, L.D., Sorcinelli, M.D., Weiler, S., Korsmeyer, S.J., 2002. Distinct BH3 domains either sensitize or activate mitochondrial apoptosis, serving as prototype cancer therapeutics. Cancer Cell 2, 183–192. https://doi.org/10.1016/S1535-6108(02)00127-7

Lewis, M.R., Lewis, W.H., 1914. Mitochondria in Tissue Culture. Science 39, 330–333. https://doi.org/10.1126/science.39.1000.330

Lewis, S.C., Uchiyama, L.F., Nunnari, J., 2016. ER-mitochondria contacts couple mtDNA synthesis with mitochondrial division in human cells. Science 353, aaf5549. https://doi.org/10.1126/science.aaf5549

Li, F., He, Z., Shen, J., Huang, Q., Li, W., Liu, X., He, Y., Wolf, F., Li, C.-Y., 2010. Apoptotic Caspases Regulate Induction of iPSCs from Human Fibroblasts. Cell Stem Cell 7, 508–520. https://doi.org/10.1016/j.stem.2010.09.003

Li, H., Chen, Y., Jones, A.F., Sanger, R.H., Collis, L.P., Flannery, R., McNay, E.C., Yu, T., Schwarzenbacher, R., Bossy, B., Bossy-Wetzel, E., Bennett, M.V.L., Pypaert, M., Hickman, J.A., Smith, P.J.S., Hardwick, J.M., Jonas, E.A., 2008. Bcl-xL induces Drp1-dependent synapse formation in cultured hippocampal neurons. Proc. Natl. Acad. Sci. 105, 2169–2174. https://doi.org/10.1073/pnas.0711647105

Li, Y., Feng, H., Gu, H., Lewis, D.W., Yuan, Y., Zhang, L., Yu, H., Zhang, P., Cheng, H., Miao, W., Yuan, W., Cheng, S.-Y., Gollin, S.M., Cheng, T., 2013. The p53–PUMA axis suppresses iPSC generation. Nat. Commun. 4, 1–9. https://doi.org/10.1038/ncomms3174

Liu, J.C., Guan, X., Ryan, J.A., Rivera, A.G., Mock, C., Agarwal, V., Letai, A., Lerou, P.H., Lahav, G., 2013. High Mitochondrial Priming Sensitizes hESCs to DNA-Damage-Induced Apoptosis. Cell Stem Cell 13, 483–491. https://doi.org/10.1016/j.stem.2013.07.018

Llambi, F., Moldoveanu, T., Tait, S.W.G., Bouchier-Hayes, L., Temirov, J., McCormick, L.L., Dillon, C.P., Green, D.R., 2011. A unified model of mammalian BCL-2 protein family interactions at the mitochondria. Mol. Cell 44, 517–531. https://doi.org/10.1016/j.molcel.2011.10.001

Llambi, F., Wang, Y.-M., Victor, B., Yang, M., Schneider, D.M., Gingras, S., Parsons, M.J., Zheng, J.H., Brown, S.A., Pelletier, S., Moldoveanu, T., Chen, T., Green, D.R., 2016. BOK Is a Non-Canonical BCL-2 Family Effector of Apoptosis Regulated by ER-Associated Degradation. Cell 165, 421–433. https://doi.org/10.1016/j.cell.2016.02.026

Lutter, M., Fang, M., Luo, X., Nishijima, M., Xie, X., Wang, X., 2000. Cardiolipin provides specificity for targeting of tBid to mitochondria. Nat. Cell Biol. 2, 754–756. https://doi.org/10.1038/35036395

Machiraju, P., Greenway, S.C., 2019. Current methods for the maturation of induced pluripotent stem cell-derived cardiomyocytes. World J. Stem Cells 11, 33–43. https://doi.org/10.4252/wjsc.v11.i1.33

MacVicar, T., Langer, T., 2016. OPA1 processing in cell death and disease – the long and short of it. J. Cell Sci. 129, 2297–2306. https://doi.org/10.1242/jcs.159186

Madden, D.T., Davila-Kruger, D., Melov, S., Bredesen, D.E., 2011. Human Embryonic Stem Cells Express Elevated Levels of Multiple Pro-Apoptotic BCL-2 Family Members. PLoS ONE 6. https://doi.org/10.1371/journal.pone.0028530

Maiuri, M.C., Le Toumelin, G., Criollo, A., Rain, J.-C., Gautier, F., Juin, P., Tasdemir, E., Pierron, G., Troulinaki, K., Tavernarakis, N., Hickman, J.A., Geneste, O., Kroemer, G., 2007. Functional and physical interaction between Bcl-XL and a BH3-like domain in Beclin-1. EMBO J. 26, 2527–2539. https://doi.org/10.1038/sj.emboj.7601689

Mandai, M., Watanabe, A., Kurimoto, Y., Hirami, Y., Morinaga, C., Daimon, T., Fujihara, M., Akimaru, H., Sakai, N., Shibata, Y., Terada, M., Nomiya, Y., Tanishima, S., Nakamura, M., Kamao, H., Sugita, S., Onishi, A., Ito, T., Fujita, K., Kawamata, S., Go, M.J., Shinohara, C., Hata, K., Sawada, M., Yamamoto, M., Ohta, S., Ohara, Y., Yoshida, K., Kuwahara, J., Kitano, Y., Amano, N., Umekage, M., Kitaoka, F., Tanaka, A., Okada, C., Takasu, N., Ogawa, S., Yamanaka, S., Takahashi, M., 2017. Autologous Induced Stem-Cell–Derived Retinal Cells for

Macular Degeneration. N. Engl. J. Med. 376, 1038–1046. https://doi.org/10.1056/NEJMoa1608368

Martin, G.R., 1981. Isolation of a pluripotent cell line from early mouse embryos cultured in medium conditioned by teratocarcinoma stem cells. Proc. Natl. Acad. Sci. U. S. A. 78, 7634–7638.

Martínez-Reyes, I., Chandel, N.S., 2020. Mitochondrial TCA cycle metabolites control physiology and disease. Nat. Commun. 11, 102. https://doi.org/10.1038/s41467-019-13668-3

Martinou, J.-C., Youle, R.J., 2011. Mitochondria in Apoptosis: Bcl-2 family Members and Mitochondrial Dynamics. Dev. Cell 21, 92–101. https://doi.org/10.1016/j.devcel.2011.06.017

Mears, J.A., Lackner, L.L., Fang, S., Ingerman, E., Nunnari, J., Hinshaw, J.E., 2011. Conformational changes in Dnm1 support a contractile mechanism for mitochondrial fission. Nat. Struct. Mol. Biol. 18, 20–26. https://doi.org/10.1038/nsmb.1949

Meeusen, S., McCaffery, J.M., Nunnari, J., 2004. Mitochondrial Fusion Intermediates Revealed in Vitro. Science 305, 1747–1752. https://doi.org/10.1126/science.1100612

Meglei, G., McQuibban, G.A., 2009. The Dynamin-Related Protein Mgm1p Assembles into Oligomers and Hydrolyzes GTP To Function in Mitochondrial Membrane Fusion. Biochemistry 48, 1774–1784. https://doi.org/10.1021/bi801723d

Mehlen, P., Bredesen, D.E., 2011. Dependence Receptors: From Basic Research to Drug Development. Sci. Signal. 4, mr2–mr2. https://doi.org/10.1126/scisignal.2001521

Mishra, P., Carelli, V., Manfredi, G., Chan, D.C., 2014. Proteolytic Cleavage of Opa1 Stimulates Mitochondrial Inner Membrane Fusion and Couples Fusion to Oxidative Phosphorylation. Cell Metab. 19, 630–641. https://doi.org/10.1016/j.cmet.2014.03.011

Moldoveanu, T., Czabotar, P.E., 2019. BAX, BAK, and BOK: A Coming of Age for the BCL-2 Family Effector Proteins. Cold Spring Harb. Perspect. Biol. https://doi.org/10.1101/cshperspect.a036319

Montero, J., Letai, A., 2016. Dynamic BH3 profiling-poking cancer cells with a stick. Mol. Cell. Oncol. 3, e1040144. https://doi.org/10.1080/23723556.2015.1040144

Montero, J., Sarosiek, K.A., DeAngelo, J.D., Maertens, O., Ryan, J., Ercan, D., Piao, H., Horowitz, N.S., Berkowitz, R.S., Matulonis, U., Jänne, P.A., Amrein, P.C., Cichowski, K., Drapkin, R.,

Letai, A., 2015. Drug-Induced Death Signaling Strategy Rapidly Predicts Cancer Response to Chemotherapy. Cell 160, 977–989. https://doi.org/10.1016/j.cell.2015.01.042

Montessuit, S., Somasekharan, S.P., Terrones, O., Lucken-Ardjomande, S., Herzig, S., Schwarzenbacher, R., Manstein, D.J., Bossy-Wetzel, E., Basañez, G., Meda, P., Martinou, J.-C., 2010. Membrane Remodeling Induced by the Dynamin-Related Protein Drp1 Stimulates Bax Oligomerization. Cell 142, 889–901. https://doi.org/10.1016/j.cell.2010.08.017

Morciano, G., Giorgi, C., Balestra, D., Marchi, S., Perrone, D., Pinotti, M., Pinton, P., 2016a. Mcl-1 involvement in mitochondrial dynamics is associated with apoptotic cell death. Mol. Biol. Cell 27, 20–34. https://doi.org/10.1091/mbc.E15-01-0028

Morciano, G., Pedriali, G., Sbano, L., Iannitti, T., Giorgi, C., Pinton, P., 2016b. Intersection of mitochondrial fission and fusion machinery with apoptotic pathways: Role of Mcl-1: Mcl-1 in mitochondrial dynamics. Biol. Cell 108, 279–293. https://doi.org/10.1111/boc.201600019

Moussaieff, A., Rouleau, M., Kitsberg, D., Cohen, M., Levy, G., Barasch, D., Nemirovski, A., Shen-Orr, S., Laevsky, I., Amit, M., Bomze, D., Elena-Herrmann, B., Scherf, T., Nissim-Rafinia, M., Kempa, S., Itskovitz-Eldor, J., Meshorer, E., Aberdam, D., Nahmias, Y., 2015. Glycolysis-mediated changes in acetyl-CoA and histone acetylation control the early differentiation of embryonic stem cells. Cell Metab. 21, 392–402. https://doi.org/10.1016/j.cmet.2015.02.002

Moyzis, A.G., Lally, N.S., Liang, W., Leon, L.J., Najor, R.H., Orogo, A.M., Gustafsson, Å.B., 2020. Mcl-1-mediated mitochondrial fission protects against stress but impairs cardiac adaptation to exercise. J. Mol. Cell. Cardiol. 146, 109–120. https://doi.org/10.1016/j.yjmcc.2020.07.009

Murray, T.V.A., Ahmad, A., Brewer, A.C., 2014. Reactive oxygen at the heart of metabolism. Trends Cardiovasc. Med. 24, 113–120. https://doi.org/10.1016/j.tcm.2013.09.003

Murriel, C.L., Churchill, E., Inagaki, K., Szweda, L.I., Mochly-Rosen, D., 2004. Protein Kinase Cδ Activation Induces Apoptosis in Response to Cardiac Ischemia and Reperfusion Damage A MECHANISM INVOLVING BAD AND THE MITOCHONDRIA. J. Biol. Chem. 279, 47985–47991. https://doi.org/10.1074/jbc.M405071200

Nagashima, S., Tábara, L.-C., Tilokani, L., Paupe, V., Anand, H., Pogson, J.H., Zunino, R., McBride, H.M., Prudent, J., 2020. Golgi-derived PI(4)P-containing vesicles drive late steps of mitochondrial division. Science 367, 1366–1371. https://doi.org/10.1126/science.aax6089

Naik, P.P., Birbrair, A., Bhutia, S.K., 2019. Mitophagy-driven metabolic switch reprograms stem cell fate. Cell. Mol. Life Sci. 76, 27–43. https://doi.org/10.1007/s00018-018-2922-9

Narendra, D., Tanaka, A., Suen, D.-F., Youle, R.J., 2008. Parkin is recruited selectively to impaired mitochondria and promotes their autophagy. J. Cell Biol. 183, 795–803. https://doi.org/10.1083/jcb.200809125

Nascimento, A., Lannigan, J., Kashatus, D., 2016. High-Throughput Detection and Quantification of Mitochondrial Fusion Through Imaging Flow Cytometry. Cytom. Part J. Int. Soc. Anal. Cytol. 89, 708–719. https://doi.org/10.1002/cyto.a.22891

Nishimura, A., Shimauchi, T., Tanaka, T., Shimoda, K., Toyama, T., Kitajima, N., Ishikawa, T., Shindo, N., Numaga-Tomita, T., Yasuda, S., Sato, Y., Kuwahara, K., Kumagai, Y., Akaike, T., Ide, T., Ojida, A., Mori, Y., Nishida, M., 2018. Hypoxia-induced interaction of filamin with Drp1 causes mitochondrial hyperfission–associated myocardial senescence. Sci. Signal. 11, eaat5185. https://doi.org/10.1126/scisignal.aat5185

Nunnari, J., Marshall, W.F., Straight, A., Murray, A., Sedat, J.W., Walter, P., 1997. Mitochondrial transmission during mating in Saccharomyces cerevisiae is determined by mitochondrial fusion and fission and the intramitochondrial segregation of mitochondrial DNA. Mol. Biol. Cell 8, 1233–1242. https://doi.org/10.1091/mbc.8.7.1233

Odorico, J.S., Kaufman, D.S., Thomson, J.A., 2001. Multilineage Differentiation from Human Embryonic Stem Cell Lines. STEM CELLS 19, 193–204. https://doi.org/10.1634/stemcells.19-3-193

Oltersdorf, T., Elmore, S.W., Shoemaker, A.R., Armstrong, R.C., Augeri, D.J., Belli, B.A., Bruncko, M., Deckwerth, T.L., Dinges, J., Hajduk, P.J., Joseph, M.K., Kitada, S., Korsmeyer, S.J., Kunzer, A.R., Letai, A., Li, C., Mitten, M.J., Nettesheim, D.G., Ng, S., Nimmer, P.M., O'Connor, J.M., Oleksijew, A., Petros, A.M., Reed, J.C., Shen, W., Tahir, S.K., Thompson, C.B., Tomaselli, K.J., Wang, B., Wendt, M.D., Zhang, H., Fesik, S.W., Rosenberg, S.H., 2005. An inhibitor of Bcl-2 family proteins induces regression of solid tumours. Nature 435, 677–681. https://doi.org/10.1038/nature03579

Oltval, Z.N., Milliman, C.L., Korsmeyer, S.J., 1993. Bcl-2 heterodimerizes in vivo with a conserved homolog, Bax, that accelerates programed cell death. Cell 74, 609–619. https://doi.org/10.1016/0092-8674(93)90509-O

Ong, S.-B., Kalkhoran, S.B., Hernández-Reséndiz, S., Samangouei, P., Ong, S.-G., Hausenloy, D.J., 2017. Mitochondrial-Shaping Proteins in Cardiac Health and Disease – the Long and the Short of It! Cardiovasc. Drugs Ther. 31, 87–107. https://doi.org/10.1007/s10557-016-6710-1

Opferman, J.T., 2016. Attacking Cancer's Achilles Heel: Antagonism of Anti-Apoptotic BCL-2 Family Members. FEBS J. 283, 2661–2675. https://doi.org/10.1111/febs.13472

Opferman, J.T., Iwasaki, H., Ong, C.C., Suh, H., Mizuno, S., Akashi, K., Korsmeyer, S.J., 2005. Obligate Role of Anti-Apoptotic MCL-1 in the Survival of Hematopoietic Stem Cells. Science 307, 1101–1104. https://doi.org/10.1126/science.1106114

Opferman, J.T., Letai, A., Beard, C., Sorcinelli, M.D., Ong, C.C., Korsmeyer, S.J., 2003. Development and maintenance of B and T lymphocytes requires antiapoptotic MCL-1. Nature 426, 671–676. https://doi.org/10.1038/nature02067

Ow, Y.-L.P., Green, D.R., Hao, Z., Mak, T.W., 2008. Cytochrome c: functions beyond respiration. Nat. Rev. Mol. Cell Biol. 9, 532–542. https://doi.org/10.1038/nrm2434

Parikh, S.S., Blackwell, D.J., Gomez-Hurtado, N., Frisk, M., Wang, L., Kim, K., Dahl, C.P., Fiane, A., Tønnessen, T., Kryshtal, D.O., Louch, W.E., Knollmann, B.C., 2017. Thyroid and Glucocorticoid Hormones Promote Functional T-Tubule Development in Human-Induced Pluripotent Stem Cell–Derived Cardiomyocytes. Circ. Res. 121, 1323–1330. https://doi.org/10.1161/CIRCRESAHA.117.311920

Pattingre, S., Tassa, A., Qu, X., Garuti, R., Liang, X.H., Mizushima, N., Packer, M., Schneider, M.D., Levine, B., 2005. Bcl-2 Antiapoptotic Proteins Inhibit Beclin 1-Dependent Autophagy. Cell 122, 927–939. https://doi.org/10.1016/j.cell.2005.07.002

Peperzak, V., Vikström, I., Walker, J., Glaser, S.P., LePage, M., Coquery, C.M., Erickson, L.D., Fairfax, K., Mackay, F., Strasser, A., Nutt, S.L., Tarlinton, D.M., 2013. Mcl-1 is essential for the survival of plasma cells. Nat. Immunol. 14, 290–297. https://doi.org/10.1038/ni.2527

Perciavalle, R.M., Opferman, J.T., 2013. Delving Deeper: MCL-1's Contributions to Normal and Cancer Biology. Trends Cell Biol. 23, 22–29. https://doi.org/10.1016/j.tcb.2012.08.011

Perciavalle, R.M., Stewart, D.P., Koss, B., Lynch, J., Milasta, S., Bathina, M., Temirov, J., Cleland, M.M., Pelletier, S., Schuetz, J.D., Youle, R.J., Green, D.R., Opferman, J.T., 2012. Anti-apoptotic MCL-1 localizes to the mitochondrial matrix and couples mitochondrial fusion to respiration. Nat. Cell Biol. 14, 575–583. https://doi.org/10.1038/ncb2488

Pernas, L., Scorrano, L., 2016. Mito-Morphosis: Mitochondrial Fusion, Fission, and Cristae Remodeling as Key Mediators of Cellular Function. Annu. Rev. Physiol. 78, 505–531. https://doi.org/10.1146/annurev-physiol-021115-105011

Pickles, S., Vigié, P., Youle, R.J., 2018. Mitophagy and Quality Control Mechanisms in Mitochondrial Maintenance. Curr. Biol. 28, R170–R185. https://doi.org/10.1016/j.cub.2018.01.004

Pon, L.A., 2013. Mitochondrial Fission: Rings around the Organelle. Curr. Biol. 23, R279–R281. https://doi.org/10.1016/j.cub.2013.02.042

Praefcke, G.J.K., McMahon, H.T., 2004. The dynamin superfamily: universal membrane tubulation and fission molecules? Nat. Rev. Mol. Cell Biol. 5, 133–147. https://doi.org/10.1038/nrm1313

Prieto, J., León, M., Ponsoda, X., Sendra, R., Bort, R., Ferrer-Lorente, R., Raya, A., López-García, C., Torres, J., 2016. Early ERK1/2 activation promotes DRP1-dependent mitochondrial fission necessary for cell reprogramming. Nat. Commun. 7, 11124. https://doi.org/10.1038/ncomms11124

Prigione, A., Hossini, A.M., Lichtner, B., Serin, A., Fauler, B., Megges, M., Lurz, R., Lehrach, H., Makrantonaki, E., Zouboulis, C.C., Adjaye, J., 2011. Mitochondrial-Associated Cell Death Mechanisms Are Reset to an Embryonic-Like State in Aged Donor-Derived iPS Cells Harboring Chromosomal Aberrations. PLoS ONE 6. https://doi.org/10.1371/journal.pone.0027352

Purvis, J.E., Karhohs, K.W., Mock, C., Batchelor, E., Loewer, A., Lahav, G., 2012. p53 Dynamics Control Cell Fate. Science 336, 1440–1444. https://doi.org/10.1126/science.1218351

Ramalho-Santos, M., Yoon, S., Matsuzaki, Y., Mulligan, R.C., Melton, D.A., 2002. "Stemness": Transcriptional Profiling of Embryonic and Adult Stem Cells. Science 298, 597–600. https://doi.org/10.1126/science.1072530

Ramirez, M.L.G., Salvesen, G.S., 2018. A primer on caspase mechanisms. Semin. Cell Dev. Biol., SI: Nuclear positioning 82, 79–85. https://doi.org/10.1016/j.semcdb.2018.01.002

Ramonet, D., Perier, C., Recasens, A., Dehay, B., Bové, J., Costa, V., Scorrano, L., Vila, M., 2013. Optic atrophy 1 mediates mitochondria remodeling and dopaminergic neurodegeneration linked to complex I deficiency. Cell Death Differ. 20, 77–85. https://doi.org/10.1038/cdd.2012.95

Rasmussen, M.L., Kline, L.A., Park, K.P., Ortolano, N.A., Romero-Morales, A.I., Anthony, C.C., Beckermann, K.E., Gama, V., 2018. A Non-apoptotic Function of MCL-1 in Promoting Pluripotency and Modulating Mitochondrial Dynamics in Stem Cells. Stem Cell Rep. 10, 684–692. https://doi.org/10.1016/j.stemcr.2018.01.005

Rasmussen, M.L., Robertson, G.L., Gama, V., 2020a. Break on Through: Golgi-Derived Vesicles Aid in Mitochondrial Fission. Cell Metab. 31, 1047–1049. https://doi.org/10.1016/j.cmet.2020.05.010

Rasmussen, M.L., Taneja, N., Neininger, A.C., Wang, L., Robertson, G.L., Riffle, S.N., Shi, L., Knollmann, B.C., Burnette, D.T., Gama, V., 2020b. MCL-1 Inhibition by Selective BH3 Mimetics Disrupts Mitochondrial Dynamics Causing Loss of Viability and Functionality of Human Cardiomyocytes. iScience 23, 101015. https://doi.org/10.1016/j.isci.2020.101015

Rastogi, A., Joshi, P., Contreras, E., Gama, V., 2019. Remodeling of mitochondrial morphology and function: an emerging hallmark of cellular reprogramming. Cell Stress 3, 181–194. https://doi.org/10.15698/cst2019.06.189

Rehklau, K., Hoffmann, L., Gurniak, C.B., Ott, M., Witke, W., Scorrano, L., Culmsee, C., Rust, M.B., 2017. Cofilin1-dependent actin dynamics control DRP1-mediated mitochondrial fission. Cell Death Dis. 8, e3063. https://doi.org/10.1038/cddis.2017.448

Reynolds, J.E., Li, J., Craig, R.W., Eastman, A., 1996. BCL-2 and MCL-1 Expression in Chinese Hamster Ovary Cells Inhibits Intracellular Acidification and Apoptosis Induced by Staurosporine. Exp. Cell Res. 225, 430–436. https://doi.org/10.1006/excr.1996.0194

Rinkenberger, J.L., Horning, S., Klocke, B., Roth, K., Korsmeyer, S.J., 2000. Mcl-1 deficiency results in peri-implantation embryonic lethality. Genes Dev. 6.

Rizzuto, R., Brini, M., Giorgi, F.D., Rossi, R., Heim, R., Tsien, R.Y., Pozzan, T., 1996. Double labelling of subcellular structures with organelle-targeted GFP mutants in vivo. Curr. Biol. 6, 183–188. https://doi.org/10.1016/S0960-9822(02)00451-7

Salisbury-Ruf, C.T., Bertram, C.C., Vergeade, A., Lark, D.S., Shi, Q., Heberling, M.L., Fortune, N.L., Okoye, G.D., Jerome, W.G., Wells, Q.S., Fessel, J., Moslehi, J., Chen, H., Roberts, L.J., Boutaud, O., Gamazon, E.R., Zinkel, S.S., 2018. Bid maintains mitochondrial cristae structure and function and protects against cardiac disease in an integrative genomics study. eLife 7, e40907. https://doi.org/10.7554/eLife.40907

Sarosiek, K.A., Fraser, C., Muthalagu, N., Bhola, P.D., Chang, W., McBrayer, S.K., Cantlon, A., Fisch, S., Golomb-Mello, G., Ryan, J.M., Deng, J., Jian, B., Corbett, C., Goldenberg, M., Madsen, J.R., Liao, R., Walsh, D., Sedivy, J., Murphy, D.J., Carrasco, D.R., Robinson, S., Moslehi, J., Letai, A., 2017. Developmental regulation of mitochondrial apoptosis by c-Myc governs age- and tissue-specific sensitivity to cancer therapeutics. Cancer Cell 31, 142–156. https://doi.org/10.1016/j.ccell.2016.11.011

Schiavon, C.R., Zhang, T., Zhao, B., Moore, A.S., Wales, P., Andrade, L.R., Wu, M., Sung, T.-C., Dayn, Y., Feng, J.W., Quintero, O.A., Shadel, G.S., Grosse, R., Manor, U., 2020. Actin chromobody imaging reveals sub-organellar actin dynamics. Nat. Methods 17, 917–921. https://doi.org/10.1038/s41592-020-0926-5

Schindelin, J., Arganda-Carreras, I., Frise, E., Kaynig, V., Longair, M., Pietzsch, T., Preibisch, S., Rueden, C., Saalfeld, S., Schmid, B., Tinevez, J.-Y., White, D.J., Hartenstein, V., Eliceiri, K., Tomancak, P., Cardona, A., 2012. Fiji: an open-source platform for biological-image analysis. Nat. Methods 9, 676–682. https://doi.org/10.1038/nmeth.2019

Senichkin, V.V., Streletskaia, A.Y., Zhivotovsky, B., Kopeina, G.S., 2019. Molecular Comprehension of Mcl-1: From Gene Structure to Cancer Therapy. Trends Cell Biol. 29, 549–562. https://doi.org/10.1016/j.tcb.2019.03.004

Shamas-Din, A., Kale, J., Leber, B., Andrews, D.W., 2013. Mechanisms of action of Bcl-2 family proteins. Cold Spring Harb. Perspect. Biol. 5, a008714. https://doi.org/10.1101/cshperspect.a008714

Sharp, W.W., Simpson, D.G., Borg, T.K., Samarel, A.M., Terracio, L., 1997. Mechanical forces regulate focal adhesion and costamere assembly in cardiac myocytes. Am. J. Physiol.-Heart Circ. Physiol. 273, H546–H556. https://doi.org/10.1152/ajpheart.1997.273.2.H546

Sheridan, C., Delivani, P., Cullen, S.P., Martin, S.J., 2008. Bax- or Bak-Induced Mitochondrial Fission Can Be Uncoupled from Cytochrome c Release. Mol. Cell 31, 570–585. https://doi.org/10.1016/j.molcel.2008.08.002

Simpson, D.G., Decker, M.L., Clark, W.A., Decker, R.S., 1993. Contractile activity and cell-cell contact regulate myofibrillar organization in cultured cardiac myocytes. J. Cell Biol. 123, 323–336. https://doi.org/10.1083/jcb.123.2.323

Sinibaldi, F., Howes, B.D., Droghetti, E., Polticelli, F., Piro, M.C., Di Pierro, D., Fiorucci, L., Coletta, M., Smulevich, G., Santucci, R., 2013. Role of Lysines in Cytochrome c–Cardiolipin Interaction. Biochemistry 52, 4578–4588. https://doi.org/10.1021/bi400324c

Skulachev, V.P., 2006. Bioenergetic aspects of apoptosis, necrosis and mitoptosis. Apoptosis 11, 473–485. https://doi.org/10.1007/s10495-006-5881-9

Smirnova, E., Griparic, L., Shurland, D.-L., van der Bliek, A.M., 2001. Dynamin-related Protein Drp1 Is Required for Mitochondrial Division in Mammalian Cells. Mol. Biol. Cell 12, 2245–2256.

Smith, R.C., Tabar, V., 2019. Constructing and Deconstructing Cancers using Human Pluripotent Stem Cells and Organoids. Cell Stem Cell 24, 12–24. https://doi.org/10.1016/j.stem.2018.11.012

Song, M., Franco, A., Fleischer, J.A., Zhang, L., Dorn, G.W., 2017. Abrogating Mitochondrial Dynamics in Mouse Hearts Accelerates Mitochondrial Senescence. Cell Metab. 26, 872-883.e5. https://doi.org/10.1016/j.cmet.2017.09.023

Souers, A.J., Leverson, J.D., Boghaert, E.R., Ackler, S.L., Catron, N.D., Chen, J., Dayton, B.D., Ding, H., Enschede, S.H., Fairbrother, W.J., Huang, D.C.S., Hymowitz, S.G., Jin, S., Khaw, S.L., Kovar, P.J., Lam, L.T., Lee, J., Maecker, H.L., Marsh, K.C., Mason, K.D., Mitten, M.J., Nimmer, P.M., Oleksijew, A., Park, C.H., Park, C.-M., Phillips, D.C., Roberts, A.W., Sampath, D., Seymour, J.F., Smith, M.L., Sullivan, G.M., Tahir, S.K., Tse, C., Wendt, M.D., Xiao, Y., Xue, J.C., Zhang, H., Humerickhouse, R.A., Rosenberg, S.H., Elmore, S.W., 2013. ABT-199, a potent and selective BCL-2 inhibitor, achieves antitumor activity while sparing platelets. Nat. Med. 19, 202–208. https://doi.org/10.1038/nm.3048

Staun-Ram, E., Shalev, E., 2005. Human trophoblast function during the implantation process. Reprod. Biol. Endocrinol. RBE 3, 56. https://doi.org/10.1186/1477-7827-3-56

Steffen, J., Koehler, C.M., 2018. ER–mitochondria contacts: Actin dynamics at the ER control mitochondrial fission via calcium release. J. Cell Biol. 217, 15–17. https://doi.org/10.1083/jcb.201711075

Stepanyants, N., Macdonald, P.J., Francy, C.A., Mears, J.A., Qi, X., Ramachandran, R., 2015. Cardiolipin's propensity for phase transition and its reorganization by dynamin-related protein 1 form a basis for mitochondrial membrane fission. Mol. Biol. Cell 26, 3104–3116. https://doi.org/10.1091/mbc.E15-06-0330

Stephan, T., Roesch, A., Riedel, D., Jakobs, S., 2019. Live-cell STED nanoscopy of mitochondrial cristae. Sci. Rep. 9, 12419. https://doi.org/10.1038/s41598-019-48838-2

Sugioka, R., Shimizu, S., Tsujimoto, Y., 2004. Fzo1, a Protein Involved in Mitochondrial Fusion, Inhibits Apoptosis. J. Biol. Chem. 279, 52726–52734. https://doi.org/10.1074/jbc.M408910200

Taguchi, N., Ishihara, N., Jofuku, A., Oka, T., Mihara, K., 2007. Mitotic Phosphorylation of Dynamin-related GTPase Drp1 Participates in Mitochondrial Fission. J. Biol. Chem. 282, 11521–11529. https://doi.org/10.1074/jbc.M607279200

Takahashi, K., Tanabe, K., Ohnuki, M., Narita, M., Ichisaka, T., Tomoda, K., Yamanaka, S., 2007. Induction of Pluripotent Stem Cells from Adult Human Fibroblasts by Defined Factors. Cell 131, 861–872. https://doi.org/10.1016/j.cell.2007.11.019

Takahashi, K., Yamanaka, S., 2015. A developmental framework for induced pluripotency. Development 142, 3274–3285. https://doi.org/10.1242/dev.114249

Takahashi, K., Yamanaka, S., 2006. Induction of pluripotent stem cells from mouse embryonic and adult fibroblast cultures by defined factors. Cell 126, 663–676. https://doi.org/10.1016/j.cell.2006.07.024

Tanaka, A., Youle, R.J., 2008. A Chemical Inhibitor of DRP1 Uncouples Mitochondrial Fission and Apoptosis. Mol. Cell 29, 409–410. https://doi.org/10.1016/j.molcel.2008.02.005

Tang, D., Kang, R., Berghe, T.V., Vandenabeele, P., Kroemer, G., 2019. The molecular machinery of regulated cell death. Cell Res. 29, 347–364. https://doi.org/10.1038/s41422-019-0164-5

Taylor, R.C., Cullen, S.P., Martin, S.J., 2008. Apoptosis: controlled demolition at the cellular level. Nat. Rev. Mol. Cell Biol. 9, 231–241. https://doi.org/10.1038/nrm2312

Thomas, R.L., Roberts, D.J., Kubli, D.A., Lee, Y., Quinsay, M.N., Owens, J.B., Fischer, K.M., Sussman, M.A., Miyamoto, S., Gustafsson, Å.B., 2013. Loss of MCL-1 leads to impaired autophagy and rapid development of heart failure. Genes Dev. 27, 1365–1377. https://doi.org/10.1101/gad.215871.113

Thomson, J.A., Itskovitz-Eldor, J., Shapiro, S.S., Waknitz, M.A., Swiergiel, J.J., Marshall, V.S., Jones, J.M., 1998. Embryonic Stem Cell Lines Derived from Human Blastocysts. Science 282, 1145–1147. https://doi.org/10.1126/science.282.5391.1145

Todt, F., Cakir, Z., Reichenbach, F., Emschermann, F., Lauterwasser, J., Kaiser, A., Ichim, G., Tait, S.W., Frank, S., Langer, H.F., Edlich, F., 2015. Differential retrotranslocation of mitochondrial Bax and Bak. EMBO J. 34, 67–80. https://doi.org/10.15252/embj.201488806

Tron, A.E., Belmonte, M.A., Adam, A., Aquila, B.M., Boise, L.H., Chiarparin, E., Cidado, J., Embrey, K.J., Gangl, E., Gibbons, F.D., Gregory, G.P., Hargreaves, D., Hendricks, J.A., Johannes, J.W., Johnstone, R.W., Kazmirski, S.L., Kettle, J.G., Lamb, M.L., Matulis, S.M., Nooka, A.K., Packer, M.J., Peng, B., Rawlins, P.B., Robbins, D.W., Schuller, A.G., Su, N., Yang, W., Ye, Q., Zheng, X., Secrist, J.P., Clark, E.A., Wilson, D.M., Fawell, S.E., Hird, A.W., 2018. Discovery of Mcl-1-specific inhibitor AZD5991 and preclinical activity in multiple myeloma and acute myeloid leukemia. Nat. Commun. 9, 1–14. https://doi.org/10.1038/s41467-018-07551-w

Trounson, A., DeWitt, N.D., 2016. Pluripotent stem cells progressing to the clinic. Nat. Rev. Mol. Cell Biol. 17, 194–200. https://doi.org/10.1038/nrm.2016.10

Tsujimoto, Y., Finger, L.R., Yunis, J., Nowell, P.C., Croce, C.M., 1984. Cloning of the chromosome breakpoint of neoplastic B cells with the t(14;18) chromosome translocation. Science 226, 1097–1099. https://doi.org/10.1126/science.6093263

Upton, J.-P., Valentijn, A.J., Zhang, L., Gilmore, A.P., 2007. The N-terminal conformation of Bax regulates cell commitment to apoptosis. Cell Death Differ. 14, 932–942. https://doi.org/10.1038/sj.cdd.4402092

van der Bliek, A.M., Payne, G.S., 2010. Dynamin Subunit Interactions Revealed. Dev. Cell 18, 687–688. https://doi.org/10.1016/j.devcel.2010.05.001

Varanita, T., Soriano, M.E., Romanello, V., Zaglia, T., Quintana-Cabrera, R., Semenzato, M., Menabò, R., Costa, V., Civiletto, G., Pesce, P., Viscomi, C., Zeviani, M., Di Lisa, F., Mongillo, M., Sandri, M., Scorrano, L., 2015. The Opa1-Dependent Mitochondrial Cristae Remodeling Pathway Controls Atrophic, Apoptotic, and Ischemic Tissue Damage. Cell Metab. 21, 834–844. https://doi.org/10.1016/j.cmet.2015.05.007

Vazquez-Martin, A., Cufí, S., Corominas-Faja, B., Oliveras-Ferraros, C., Vellon, L., Menendez, J.A., 2012. Mitochondrial fusion by pharmacological manipulation impedes somatic cell reprogramming to pluripotency: New insight into the role of mitophagy in cell stemness. Aging 4, 393–401.

Vazquez-Martin, A., Van den Haute, C., Cufí, S., Corominas-Faja, B., Cuyàs, E., Lopez-Bonet, E., Rodriguez-Gallego, E., Fernández-Arroyo, S., Joven, J., Baekelandt, V., Menendez, J.A., 2016. Mitophagy-driven mitochondrial rejuvenation regulates stem cell fate. Aging 8, 1330–1349. https://doi.org/10.18632/aging.100976

Vikstrom, I., Carotta, S., Lüthje, K., Peperzak, V., Jost, P.J., Glaser, S., Busslinger, M., Bouillet, P., Strasser, A., Nutt, S.L., Tarlinton, D.M., 2010. Mcl-1 is Essential for Germinal Center Formation and B cell Memory. Science 330, 1095–1099. https://doi.org/10.1126/science.1191793

Wai, T., Langer, T., 2016. Mitochondrial Dynamics and Metabolic Regulation. Trends Endocrinol. Metab. 27, 105–117. https://doi.org/10.1016/j.tem.2015.12.001

Walensky, L.D., 2012. Stemming Danger with Golgified BAX. Mol. Cell 46, 554–556. https://doi.org/10.1016/j.molcel.2012.05.034

Wanet, A., Arnould, T., Najimi, M., Renard, P., 2015. Connecting Mitochondria, Metabolism, and Stem Cell Fate. Stem Cells Dev. 24, 1957–1971. https://doi.org/10.1089/scd.2015.0117

Wang, L., Kim, K., Parikh, S., Cadar, A.G., Bersell, K.R., He, H., Pinto, J.R., Kryshtal, D.O., Knollmann, B.C., 2018. Hypertrophic cardiomyopathy-linked mutation in troponin T causes myofibrillar disarray and pro-arrhythmic action potential changes in human iPSC cardiomyocytes. J. Mol. Cell. Cardiol. 114, 320–327. https://doi.org/10.1016/j.yjmcc.2017.12.002

Wang, Ping, Wang, Peiguo, Liu, B., Zhao, J., Pang, Q., Agrawal, S.G., Jia, L., Liu, F.-T., 2015. Dynamin-related protein Drp1 is required for Bax translocation to mitochondria in response to

irradiation-induced apoptosis. Oncotarget 6, 22598–22612. https://doi.org/10.18632/oncotarget.4200

Wang, X., Bathina, M., Lynch, J., Koss, B., Calabrese, C., Frase, S., Schuetz, J.D., Rehg, J.E., Opferman, J.T., 2013. Deletion of MCL-1 causes lethal cardiac failure and mitochondrial dysfunction. Genes Dev. 27, 1351–1364. https://doi.org/10.1101/gad.215855.113

Waterham, H.R., Koster, J., van Roermund, C.W.T., Mooyer, P.A.W., Wanders, R.J.A., Leonard, J.V., 2007. A Lethal Defect of Mitochondrial and Peroxisomal Fission. N. Engl. J. Med. 356, 1736–1741. https://doi.org/10.1056/NEJMoa064436

Weber, A., Boger, R., Vick, B., Urbanik, T., Haybaeck, J., Zoller, S., Teufel, A., Krammer, P., Opferman, J., Galle, P., Schuchmann, M., Heikenwalder, M., Schulze-Bergkamen, H., 2010. Hepatocyte-specific deletion of the anti-apoptotic protein Mcl-1 triggers proliferation and hepatocarcinogenesis in mice. Hepatol. Baltim. Md 51, 1226–1236. https://doi.org/10.1002/hep.23479

Wegel, E., Göhler, A., Lagerholm, B.C., Wainman, A., Uphoff, S., Kaufmann, R., Dobbie, I.M., 2016. Imaging cellular structures in super-resolution with SIM, STED and Localisation Microscopy: A practical comparison. Sci. Rep. 6, 27290. https://doi.org/10.1038/srep27290

Westermann, B., 2010. Mitochondrial fusion and fission in cell life and death. Nat. Rev. Mol. Cell Biol. 11, 872–884. https://doi.org/10.1038/nrm3013

Wollweber, F., von der Malsburg, K., van der Laan, M., 2017. Mitochondrial contact site and cristae organizing system: A central player in membrane shaping and crosstalk. Biochim. Biophys. Acta BBA - Mol. Cell Res., Membrane Contact Sites 1864, 1481–1489. https://doi.org/10.1016/j.bbamcr.2017.05.004

Wolter, K.G., Hsu, Y.-T., Smith, C.L., Nechushtan, A., Xi, X.-G., Youle, R.J., 1997. Movement of Bax from the Cytosol to Mitochondria during Apoptosis. J. Cell Biol. 139, 1281–1292. https://doi.org/10.1083/jcb.139.5.1281

Wright, K.M., Deshmukh, M., 2006. Restricting Apoptosis for Postmitotic Cell Survival and its Relevance to Cancer. Cell Cycle 5, 1616–1620. https://doi.org/10.4161/cc.5.15.3129

Xu, Y., Condell, M., Plesken, H., Edelman-Novemsky, I., Ma, J., Ren, M., Schlame, M., 2006. A Drosophila model of Barth syndrome. Proc. Natl. Acad. Sci. 103, 11584–11588. https://doi.org/10.1073/pnas.0603242103

Yang, C., Svitkina, T.M., 2019. Ultrastructure and dynamics of the actin–myosin II cytoskeleton during mitochondrial fission. Nat. Cell Biol. 21, 603–613. https://doi.org/10.1038/s41556-019-0313-6

Yang, T., Buchan, H.L., Townsend, K.J., Craig, R.W., 1996. MCL-1, a member of the BCL-2 family, is induced rapidly in response to signals for cell differentiation or death, but not to signals for cell proliferation. J. Cell. Physiol. 166, 523–536. https://doi.org/10.1002/(SICI)1097-4652(199603)166:3<523::AID-JCP7>3.0.CO;2-R

Youle, R.J., Bliek, A.M. van der, 2012. Mitochondrial Fission, Fusion, and Stress. Science 337, 1062–1065. https://doi.org/10.1126/science.1219855

Zhang, J., 2013. Autophagy and mitophagy in cellular damage control. Redox Biol. 1, 19–23. https://doi.org/10.1016/j.redox.2012.11.008

Zhang, J., Nuebel, E., Daley, G.Q., Koehler, C.M., Teitell, M.A., 2012. Metabolic Regulation in Pluripotent Stem Cells during Reprogramming and Self-Renewal. Cell Stem Cell 11, 589–595. https://doi.org/10.1016/j.stem.2012.10.005

Züchner, S., Mersiyanova, I.V., Muglia, M., Bissar-Tadmouri, N., Rochelle, J., Dadali, E.L., Zappia, M., Nelis, E., Patitucci, A., Senderek, J., Parman, Y., Evgrafov, O., Jonghe, P.D., Takahashi, Y., Tsuji, S., Pericak-Vance, M.A., Quattrone, A., Battologlu, E., Polyakov, A.V., Timmerman, V., Schröder, J.M., Vance, J.M., 2004. Mutations in the mitochondrial GTPase mitofusin 2 cause Charcot-Marie-Tooth neuropathy type 2A. Nat. Genet. 36, 449–451. https://doi.org/10.1038/ng1341

Appendix

MATERIALS AND METHODS

Cell Culture

Human embryonic stem cell line H9 (WA09) used in Chapter 2 was obtained from WiCell Research Institute (Wisconsin). Cells were seeded as undifferentiated colonies on plates coated with Matrigel (Corning), maintained at 37˚C and 5% CO_2, and fed daily with mTeSR (Stem Cell Technologies). Differentiation of hESCs into embryoid bodies was induced by plating 4-day-old colonies onto non-adherent plates without Matrigel.

Mouse ES cells (mESCs) used in Chapter 2 were kindly provided by Guang Hu (NIEHS). Briefly, mESCs were maintained on gelatin-coated plates in the ESGRO complete plus clonal grade medium (Millipore). Human foreskin fibroblast cell lines (BJ-1), were received from ATCC and maintained and cultured as recommended by the supplier in Minimum Essential Medium (MEM) supplemented with 10% FBS. Cells were maintained at 37˚C and 5% CO^2.

Human induced pluripotent stem cell-derived cardiomyocytes (iCell Cardiomyocytes^2) used in Chapter 3 were obtained from Cellular Dynamics International (#CMC-100-012-000.5). Cells were thawed according the manufacturer protocol in iCell Plating medium. Briefly, cells were thawed and plated on 0.1% gelatin at 50,000 cells/well in 96-well plates. Cells were maintained at 37˚C and 5% CO_2 and fed every other day with iCell Cardiomyocyte Maintenance medium (Cellular Dynamics International

#M1003). For knockdown experiments, wells were coated with 5 μg/mL fibronectin (Corning #354008) 1 hour prior to plating. For functional experiments using the Axion bioanalyzer, cells were plated on 50 μg/mL fibronectin in a 48-well CytoView MEA plate (Axion Biosystems #M768-tMEA-48B). For imaging experiments, cells were re-plated on glass-bottom 35 mm dishes (Cellvis #D35C4-20-1.5-N) coated with 10 μg/mL fibronectin. For live-cell imaging, cells were maintained at 37˚C with 5% CO_2 in a stage top incubator (Tokai Hit). To account for batch effects, at least two different vials of iCell Cardiomyocytes[2] were used to replicate each experiment.

Human induced pluripotent stem cells (hiPSC) used in Chapter 3 were generated from human fibroblasts as previously described (Wang et al., 2018). hiPSCs were maintained on growth factor-reduced Matrigel (Corning) coated plates in home-made E8 medium. hiPSCs were passaged every 4 days using 0.5 mM EDTA for 10 minutes at room temperature. hiPSCs were maintained at 37 ˚C at 5% CO_2 and received fresh medium daily.

hiPSC-derived cardiomyocytes (hiPSC-CMs) used in Figure 3-6 were generated using the small molecules CHIR 99021 (Selleck Chemicals) and IWR-1 (Sigma). Cardiac differentiation media were defined as M1 (RPMI 1640 with glucose with B27 minus insulin), M2 (RPMI 1640 minus glucose with B27 minus insulin), and M3 (RPMI 1640 with glucose with B27). hiPSCs were cultured until they reached 60% confluence, at which point cardiac differentiation was initiated (day 0). At day 0, hiPSCs were supplemented in M1 with 6 μM CHIR99021. On day 2, the media was changed to M1. On day 3, cells were treated with 5 μM IWR-1 in M1. Metabolic selection was started at day 10 and cells were treated with M2 from day 10 to 16. On day 16, cells were transitioned to M3 with or without 0.1 μM triiodo-L-thyronine hormone (Sigma) and 1 μM Dexamethasone (Cayman) (Parikh et al., 2017). Media

was changed every other day until day 30. For experiments in Figure 3-6, data was collected from at least three separate differentiations.

Cell Treatments

All treatments in Chapter 2 were performed on day 2-3 for hESCs or at 80% confluency for fibroblasts. The pan-caspase inhibitor Q-VD-OPh (QVD) (SM Biochemicals #SMPH001) was added to cells at a concentration of 25 μM. The small molecule inhibitor of MCL-1 (MIM-1) was acquired from from Loren Walensky (Cohen et al. 2012). The stock solutions were prepared in DMSO and the peptides were added directly into medium (final concentration: 10 μM) at 37 °C. Commercially available GX15, MDVI and ABT-737 were purchased from Selleck Chemicals LLC (Houston TX, USA) and stock solutions were prepared in DMSO. BMP4 was diluted in HCl and used at 100ng/mL for 7 days. All experiments were repeated at least 3 times in duplicate and error bars indicate standard deviation.

All treatments for Chapter 3 were added directly to cells in maintenance medium. The pan-caspase inhibitor QVD was added to cells at a concentration of 25μM. The small molecule MCL-1 inhibitor derivative (S63845) was a gift from Joseph Opferman (St. Jude's Children Hospital). ABT-199 was purchased from Active Biochemicals (#A-1231). AMG-176 (#CT-AMG176) and AZD5991 (#CT-A5991) were purchased from ChemieTek. The necrosis inhibitor IM-54 (#SC222053A) was purchased from Santa Cruz Technologies and added to cells at a concentration of 10 μM. All stock solutions were prepared in DMSO. H_2O_2 solution (#H1009) was purchased from Sigma and added to cells at 10 μM in sterile water.

Lentiviral Transduction

To generate lentiviral-mediated knockdown lines of hESCs in Chapter 2, 3-day-old colonies were transduced with *MCL-1* lentiviral shRNA purchased from Open Biosystems (clone TRCN0000005517). After 10 hours, the cells were allowed to recover for 12-14 hours in mTeSR. Selection with puromycin (10 μg/ml; Sigma) was started 24 hours after transduction and was continued for 2 days, with replacement of the conditioned medium and puromycin daily. Transduction efficiency was validated by Western blot for recovered hESC colonies.

Reprogramming of fibroblasts was induced by transduction with CytoTune™-iPS Sendai Reprogramming Kit (Thermo Fisher Scientific) according to the manufacturer protocol.

RNAi and Plasmid Transfection

To generate transient knockdowns of MCL-1 in hESCs for Chapter 2, commercially available siRNA (Thermo Fisher Scientific). Cells were seeded at 100,000 cells per well in a 6-well dish coated with Matrigel. Once cells reached 30-40% confluency, they were transfected as per the manufacturer protocol using Lipofectamine RNAiMax (Thermo Fisher Scientific #13778075) in mTeSR containing 25 μM QVD. To increase knockdown efficiency, the transfection was repeated 24 hours later. Cells were left to recover for an additional 24 hours in fresh mTeSR containing 25 μM QVD. Cells were collected or fixed for analysis by Western blot, immunofluorescence, or EM following recovery. To generate transient knockdowns in hiPSC-CMs in Chapter 3, commercially available siRNAs targeting DRP-1 (DNM1L) (Thermo Fisher Scientific #AM51331, ID19561) and MCL-1 (Thermo Fisher Scientific #4390824, IDs8583) were used. Cells were seeded at 50,000 cells per well in a 96-well plate coated with 5 μg/mL

fibronectin. Cells were transfected as per the manufacturer protocol using either TransIT-TKO Transfection Reagent (Mirus Bio #MIR2154) or RNAiMax (Thermo Fisher Scientific) in iCell maintenance media containing 25uM Q-VD-OPh. To increase knockdown efficiency, the transfection was repeated 48 and 96 hours later. Cells were left to recover for an additional 24 hours in fresh media containing 25 μM QVD. Cells were lysed for Western blot or re-plated on glass-bottom 35 mm dishes and fixed for analysis by immunofluorescence. The siRNA oligo sequence for MCL-1 (s8583) is as follows: CCAGUAUACUUCUUAGAAAttt. Silencer Select Negative Control No. 1 (Thermo Fisher Scientific #4390843) was used as a control for all knockdown experiments.

Plasmids encoding MCL-1, GFP-tagged MCL-1, and DsRed-mito proteins were transfected using FuGene (Promega) at ratio 3:1 as described in the manufacturer protocol. Plasmids encoding mito-tdEos (Addgene #57644) or GCaMP5G (Addgene #31788) were transfected using ViaFect (Promega #E4981) as described in the manufacturer protocol. Cells were maintained until optimal transfection efficiency was reached before cells were lysed for Western blot or fixed in 4% paraformaldehyde (PFA) for imaging.

Immunofluorescence

For immunofluorescence experiments in Chapter 2, cells were fixed with 4% PFAfor 30 min at 4°C and permeabilized in 0.3% Triton X-100 for 1 hr at room temperature. After blocking, cells were treated with primary and secondary antibodies using standard methods. For high-resolution imaging, cells were fixed with 4% paraformaldehyde for 20 min and permeabilized in 1% Triton-X-100 for 10 min at room temperature. After blocking in 10% BSA, cells were treated with primary and secondary antibodies using

standard methods. See Table 1 for antibodies used in Chapter 2. Cells were mounted in Vectashield (Vector Laboratories #H-1000) prior to imaging.

For immunofluorescence experiments in Chapter 3, cells were fixed with 4% PFA for 20 min and permeabilized in 1% Triton-X-100 for 5 min at room temperature. After blocking in 10% BSA, cells were treated with primary and secondary antibodies using standard methods. Cells were mounted in Vectashield (Vector Laboratories #H-1000) prior to imaging. Primary antibodies used include Alexa Fluor-488 Phalloidin (Thermo Fisher Scientific #A12379), mouse anti-mtCO2 (Abcam #ab110258), and mouse anti-Mitochondria (Abcam #ab92824). For Incucyte experiments, nuclei were visualized using NucLight Rapid Red Reagent (Essen Bioscience #4717). Alexa Fluor-488 (Thermo Fisher Scientific #A11008) and Alexa Fluor-568 (Thermo Fisher Scientific #A11011) were used as secondary antibodies. MitoTracker Red CMXRos (Thermo Fisher Scientific #M7512) added at 100 nM was used to visualize mitochondria in PLA experiments.

Immunoprecipitation

Immunoprecipitation experiments in Chapter 2 were performed by incubating whole-cell or mitochondrial lysates with 50% slurry Dynabeads (Invitrogen) for 1 hr at 4°C, then incubating with MCL-1 Y37 antibody (Abcam) for 1 hr at 4°C. Beads were separated by magnet and washed in 1% Triton. Protein was eluted and incubated with LDS/BME sample buffer at 95°C for 5 min. For mitochondrial purifications, instructions were followed per the Mitochondria Isolation Kit for Cultured Cells (Abcam #ab110170).

Image acquisition

For experiments in Chapter 2, Images were acquired using a Hamamatsu ORCA-ER digital B/W CCD camera mounted on a Leica inverted fluorescence microscope (DMIRE 2). The software used for image acquisition was Metamorph version 5.0 (Universal Imaging Corporation). Co-localization images were acquired using a Zeiss 880 LSM microscope with an AiryScan detector. The software used for AiryScan image processing was ZEN Black (Zeiss). Super-resolution images were acquired using an Andor DU-897 EMCCD camera mounted on a Nikon structured illumination microscope (SIM). The software used for image acquisition and reconstruction was NIS-Elements Viewer (Nikon).

Samples for transmission electron microscopy (TEM) in Chapter 2 were fixed in 2.5% Glutamine in 0.1M sodium cacodylate buffer for 1 hr at room temperature, then prepared, sectioned and stained by the Vanderbilt CISR EM core. TEM images were acquired using a side mounted 2k x 2k AMT CCD camera system and a bottom-mounted 2k by 2k Gatan CCD camera system mounted on a Philips/FEI T-12 high resolution transmission electron microscope.

Super-resolution images in Chapter 3 for Figures 3-1 and 3-2 were acquired using a GE DeltaVision OMX microscope equipped with a 1.42 NA 60X Oil objective and a sCMOS camera. Super-resolution images for Figures 3-1, 3-2, 3-7, S3-2 and S3-6 were acquired using a Nikon SIM microscope equipped with a 1.49 NA 100x Oil objective an Andor DU-897 EMCCD camera. Images for Figures 3-4, S3-3 and S3-6 were acquired on a Nikon Eclipse Ti inverted widefield microscope equipped with a 1.45 NA 100X Oil or 1.40 NA 60X Oil objective. Image processing and quantification was performed using Fiji. Measurement of cell number to assay cell death was performed on a Incucyte S3 live cell imaging system (Essen Bioscience) equipped with a 10X objective. Images for the PLA experiments were acquired on a

Nikon Eclipse Ti-E spinning disk confocal microscope equipped with a 1.40 NA 60X Oil objective and an Andor DU-897 EMCCD camera.

Mass Spectrometry

All MS/MS samples were analyzed using Sequest (Thermo Fisher Scientific, San Jose, CA, USA; version 27, rev. 12). Sequest was set up to search the uniprot_kb_human_swissprot_20120610_rev database (40720 entries) assuming the digestion enzyme trypsin. Sequest was searched with a fragment ion mass tolerance of 0.00 Da and a parent ion tolerance of 2.5 Da. Oxidation of methionine and carbamidomethyl of cysteine were specified in Sequest as variable modifications. Charge state deconvolution and deisotoping were not performed on the extracted tandem mass spectra. Scaffold (version Scaffold_4.7.2, Proteome Software Inc., Portland, OR) was used to validate MS/MS based peptide and protein identifications. Peptide identifications were accepted if they could be established at greater than 95.0% probability by the Peptide Prophet algorithm (Keller, A et al Anal. Chem. 2002;74(20):5383-92). Protein identifications were accepted if they could be established at greater than 99.0% probability and contained at least 2 identified peptides. Protein probabilities were assigned by the Protein Prophet algorithm (Nesvizhskii, Al et al Anal. Chem. 2003;75(17):4646-58). Proteins that contained similar peptides and could not be differentiated based on MS/MS analysis alone were grouped to satisfy the principles of parsimony.

Proximity Ligation Assay

For PLA experiments in Chapter 2, hESCs were seeded onto Matrigel-coated 8-chamber MatTek glass slides (#CCS-8) at 10,000 cells/chamber. When cells reached ~50% confluency they were fixed in 4%

PFA for 20 min and permeabilized in 1% Triton for 10 min at room temperature. Following fixation, the DuoLink proximity ligation assay (PLA) was performed as per manufacturer protocol (Sigma). The primary antibodies were incubated for 1.5 hours at room temperature and are as follows: MCL-1 (Proteintech) + pDRP-1 S616 (Cell Signaling), MCL-1 (Proteintech) + OPA1 (Cell Signaling), MCL-1 (Proteintech) + BIM (Cell Signaling), and control containing no primary antibody. Images were acquired on a Nikon spinning disk confocal microscope and quantified using NIS-Elements software. Background noise levels were subtracted, and puncta were normalized to the number of nuclei in each image. At least 300 nuclei were counted for each condition in duplicate.

For PLA experiments in Chapter 3, hiPSC-CMs were plated onto fibronectin-coated 8-chamber MatTek glass slides at 10,000 cells/chamber. After treatments, cells were fixed in 4% PFA for 20 min and permeabilized in 1% Triton-100-X for 10 min at room temperature. Following fixation, the DuoLink proximity ligation assay (Sigma #DUO92014) was performed as per manufacturer protocol. The primary antibodies were incubated overnight at 4˚C and are as follows: mouse anti-MCL-1 (Proteintech # 66026-1-Ig), rabbit anti-DRP-1 (Cell Signaling Technologies #8570S), rabbit anti-OPA1 (Cell Signaling Technologies #67589S), and control containing no primary antibody.

Membrane fractionation

For the crude membrane fractionation experiments in Chapter 3, hiPSC-CMs were lysed in 1X CHAPS (Sigma #C5070-5G) containing protease and phosphatase inhibitors for 20 mins on ice while vortexing, followed by centrifugation at 14,000 rpm for 20 mins. The supernatant was collected (cytosolic fraction)

and the pellet was resuspended in the same volume of 1X CHAPS buffer containing protease and phosphatase inhibitors. Lysates were then prepared for gel electrophoresis and Western blot as described.

Western blot

Gel samples were prepared by mixing cell lysates with LDS sample buffer (Life Technologies, #NP0007) and 2-Mercaptoethanol (BioRad #1610710) and boiled at 95˚C for 5 minutes. Samples were resolved on 4-20% Mini-PROTEAN TGX precast gels (BioRad #4561096) and transferred onto PVDF membrane (BioRad #1620177). Antibodies used for Chapter 2 are described in Table 1. Antibodies used for Western blotting in Chapter 3 are as follows: DRP-1 (Cell Signaling Technologies #8570S), pDRP-1 S616 (Cell Signaling Technologies #4494), OPA1 (Cell Signaling Technologies #67589S), MCL-1 (Cell Signaling Technologies #94296S), TOM20 (Cell Signaling Technologies # 42406S), VDAC (Cell Signaling Technologies #4866T) and α-Tubulin (Sigma # 05-829).

Impedance assays

The Axion Biosystems analyzer was used to measure contractility and impedance in hiPSC-CMs for Chapter 3. Cells were plated on 48-well CytoView MEA plates and maintained for 10 days before treatment and recordings. Recordings were taken for 5 minutes approximately two hours after media change at 37˚C and 5% CO_2. Cells were assayed using the standard cardiac analog mode setting with 12.5 kHz sampling frequency to measure spontaneous cardiac beating. The Axion instrument was controlled using Maestro Pro firmware version 1.5.3.4. Cardiac beat detector settings are as follows:

Beat Detection Threshold	300 μV
Min. Beat Period	250 ms
Max. Beat Period	5 s

Synchronized Beat Maximum Propagation Delay	30 ms
Minimum Active Channels Ratio	50.00%
Running Average Beat Count	10

Recordings for the hormone-matured hiPSC-CMs in Figure 3-6 were obtained using a CardioExcyte96 instrument (Nanion Technologies). Cell preparation, data acquisition, and data processing were completed as described previously (Chavali et al., 2019).

Calcium imaging

Cells were transfected with GCaMP5G probe in 96-well plates and protein expression was allowed to stabilize for 48 hours. Cells were maintained on the microscope stage incubator for 30 minutes prior to imaging on a Nikon Eclipse Ti inverted microscope equipped with a 10X .30 NA objective. For each biological replicate, three technical replicates of a 10-second time-lapse recording were collected for each well. Baseline recordings were taken 24 hours prior to treatment. Subsequent recordings were taken 2 hours post treatment. Calcium intake was quantified in Fiji. Briefly, background fluorescence was first measured for intensity correction. A kymograph was then created using the Multiple Kymograph tool in Fiji using a 25-pixel thick line drawn across the entire cell. Calcium intake was measured as the ratio of the mean intensity of the brightest frame to the mean intensity of the darkest frame in the kymograph.

Plate-reader assays (CaspaseGlo 3/7 and CellTiter-Blue)

Cells were plated onto 1% gelatin-coated white round-bottomed 96-well plates at 20,000 cells/well. At least two duplicate wells were used per condition. At the end of inhibitor treatments, media was aspirated

from the wells and a 1:1 ratio of CaspaseGlo 3/7 reagent (Promega #8091) and fresh media was added. The plates were incubated at room temperature for 1 hr in the dark and analyzed in a Promega GloMax luminometer according to manufacturer instructions. For the cell viability assay in Figure 3-5C, hiPSC-CMs were plated onto 1% gelatin-coated black clear-bottomed 96-well plates at 20,000 cells/well. Three replicate wells were used per condition. Cells were pre-treated with indicated inhibitors for 24 hours, followed by addition of fresh media and inhibitors or H_2O_2 for an additional 24 hours. 10% Triton-X-100 was added to untreated wells as a blank for normalization. CellTiter-Blue reagent was added to wells (20 μL) and plates were incubated at 37°C and 5% CO_2 for 2 hrs. Plates were analyzed in a POLARstar Omega plate-reader (BMG LabTech) according to manufacturer instructions.

Seahorse Mito Stress Test

hiPSC-CMs were plated from thaw onto 1% gelatin-coated Seahorse XF96 V3 PS cell culture microplates 7 days before the assay at 20,000 cells per well. 24 hours prior to the assay, inhibitor treatments were added to triplicate wells in maintenance media. One hour prior to the assay, media was switched to XF DMEM media containing 1 mM pyruvate, 2 mM glutamine, and 10 mM glucose. Oxygen consumption rate (OCR) was measured sequentially after addition of 1.0 μM oligomycin, 0.5 μM FCCP, and 0.5 μM rotenone.

Photoconversion experiments

Mitochondrial network connectivity and fusion was assayed using photo-conversion of mitochondria tagged with mito-tdEos (Addgene #57644). Photo-conversion was performed on a Nikon Eclipse Ti

inverted widefield microscope equipped with a 1.45 NA 100X Oil objective. Briefly, a stimulation region was closing down the field diaphragm and using the filter to shine 405 nm light for 6 seconds. Images for the converted (TxRed) and unconverted (FITC) were acquired before and after stimulation. The TxRed image before stimulation was used to subtract background from the post-stimulation images, followed by thresholding and automated measurement in Fiji (Schindelin et al., 2012). The initial converted area immediately after stimulation was used as a measure of connectivity, while the spread of the converted signal after 20 minutes was used as a measure of fusion/motility. The initial converted area (TxRed channel) was normalized to the total unconverted area (FITC channel) to account for any initial variation in the total mitochondrial area.

Statistical Analysis

All experiments were performed with a minimum of 3 biological replicates. Statistical significance was determined by unpaired, two-tailed Student's t-test or by one- or two-way ANOVA as appropriate for each experiment. GraphPad Prism v8.1.2 was used for all statistical analysis and data visualization.

Error bars in all bar graphs represent standard error of the mean or standard deviation as described for each figure, while Tukey plots were represented with boxes (with median, Q1, Q3 percentiles), whiskers (minimum and maximum values within 1.5 times interquartile range) and solid circles (outliers). No outliers were removed from the analyses.

For MEA experiments, means from triplicate biological replicates (each with 2-3 technical replicate wells) for each measurement were plotted and significance was determined by two-way ANOVA. 20 hour data

was excluded for two-way ANOVA in Figure 3-2B-C and E-F, since this time-point was not recorded for ABT-199; likewise, ABT-199 was excluded from analysis in Figure 3-2D.

For PLA experiments in Chapter 2, images were quantified using Fiji. Briefly, background noise levels were subtracted, and number of puncta per ROI was normalized to mitochondrial area. ROIs in at least 5 cells per condition were quantified in three independent experiments.

Quantification of mitochondrial morphology was performed in NIS-Elements (Nikon); briefly, we segmented mitochondria in 3D and performed skeletonization of the resulting 3D mask. Skeleton major axis and sphericity measurements were exported into Excel, and the data was filtered and analyzed in MatLab. Quantification of actin organization was performed in a blinded fashion and percentages of each category are displayed. Cell viability measured using the Incucyte live cell imaging system was performed by automatic segmentation of nuclei in Fiji, followed by subtraction of dead cells as indicated by fragmented nuclei and rounded phenotype detected by phase contrast.

Table 1. List of primary antibodies used in Chapter 2

Antibody	Manufacturer	Catalog	Dilution	Application
BAX	Santa Cruz	sc-493	1:500	Western blot
BCL-2	Cell Sig. Tech.	4223	1:1000	Western blot
BCL-XL	Cell Sig. Tech.	2764	1:1000	Western blot
MCL-1 (Y37)	Abcam	ab32087	1ug/1mg	Immunoprecipitation
MCL-1	Cell Sig. Tech.	94296	1:1000	Western blot
OCT4	Abcam	ab19857	1:1000	Western blot
OCT4	STEMCELL Tech.	60093	1:200	Immunostaining
NANOG	Abcam	ab109250	1:500; 1:200	Western blot; Immunostaining
α-Tubulin	Sigma	05-829	1:2000	Western blot
β-actin	Sigma	A1978	1:10,000	Western blot
SIRT2	Abnova	H00022933-M01	1:500	Western blot
SOX2	STEMCELL Tech.	60055.1	1:500	Immunostaining
tGFP	OriGene	TA150041	1:200	Immunostaining
GFP	Abcam	ab13970	1:200	Immunostaining
RFP	Invitrogen	R10367	1:200	Immunostaining
Cyt c	BD Biosciences	556432	1:200	Immunostaining
p-DRP-1 (S616)	Cell Sig. Tech.	4494	1:500	Western blot
DRP-1	Cell Sig. Tech.	8570	1:500	Western blot
mT-CO2 (Cox2)	Abcam	ab110258	1:1000; 1:100	Western blot; Immunostaining
OPA1	Abcam	ab119685	1:1000	Western blot
TOM20	Santa Cruz	sc-17764	1:200	Immunostaining

Table 2: shRNA sequences used in Chapter 2

Construct	TRC ID	Sequence
sh*MCL-1* (1)	TRCN0000005517	GCTAAACACTTGAAGACCATA
sh*MCL-1* (2)	TRCN0000197024	GAGCTGGTTTGGCATATCTAA
sh*MCL-1* (3)	TRCN0000196390	GCCTAGTTTATCACCAATAAT